AD

USAAVLABS TECHNICAL REPORT 70-71A

ANALYSIS OF HELICOPTER STRUCTURAL CRASHWORTHINESS

VOLUME I

MATHEMATICAL SIMULATION AND EXPERIMENTAL VERIFICATION FOR HELICOPTER CRASHWORTHINESS

By

Clifford I. Gatlin

Donald E. Goebel

Stuart E. Larsen

January 1971

EUSTIS DIRECTORATE

U. S. ARMY AIR MOBILITY RESEARCH AND DEVELOPMENT LABORATORY

FORT EUSTIS, VIRGINIA

CONTRACT DAAJ02-69-C-0030

DYNAMIC SCIENCE (THE AvSER FACILITY)

A DIVISION OF MARSHALL INDUSTRIES

PHOENIX, ARIZONA

160

DISCLAIMER NOTICE

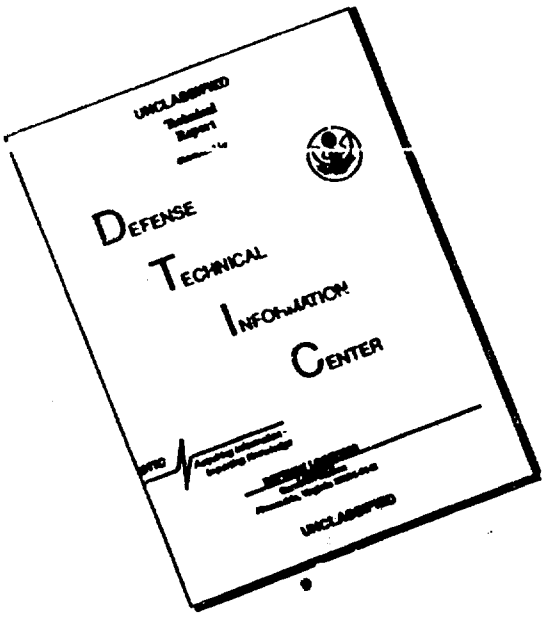

THIS DOCUMENT IS BEST QUALITY AVAILABLE. THE COPY FURNISHED TO DTIC CONTAINED A SIGNIFICANT NUMBER OF PAGES WHICH DO NOT REPRODUCE LEGIBLY.

Disclaimers

The findings in this report are not to be construed as an official Department of the Army position unless so designated by other authorized documents.

When Government drawings, specifications, or other data are used for any purpose other than in connection with a definitely related Government procurement operation, the United States Government thereby incurs no responsibility nor any obligation whatsoever; and the fact that the Government may have formulated, furnished, or in any way supplied the said drawings, specifications, or other data is not to be regarded by implication or otherwise as in any manner licensing the holder or any other person or corporation, or conveying any rights or permission, to manufacture, use, or sell any patented invention that may in any way be related thereto.

Disposition Instructions

Destroy this report when no longer needed. Do not return it to the originator.

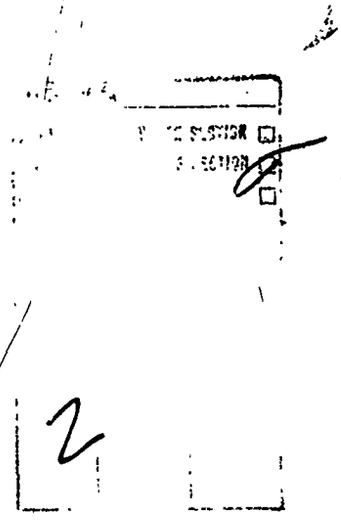

DEPARTMENT OF THE ARMY
EUSTIS DIRECTORATE
U.S. ARMY AIR MOBILITY RESEARCH AND DEVELOPMENT LABORATORY
FORT EUSTIS, VIRGINIA 23604

This report was prepared by Dynamic Science (The AvSER Facility), A Division of Marshall Industries, under the terms of Contract DAAJ02-69-C-0030.

The purpose of this effort was to (1) document and classify the most hazardous factors concerning airframe crashworthiness, (2) seek methods of reducing vertical decelerations at the floor level in potentially survivable crashes, and (3) seek design methods for maintaining the "protective shell" around the occupants in an accident. The contractor achieved these objectives by conducting a study of 43 major accidents involving the UH-1D/H aircraft to determine what types of structural failure were contributing to injuries in helicopter accidents and by developing, programming, and verifying a 23-degree-of-freedom, nonlinear lumped mass mathematical model. This model was then used in a parametric study of the UH-1D/H aircraft to evaluate potential areas of crashworthiness improvement. This report contains a description of the accident data study, mathematical model, parametric study, full-scale drop test, and the results obtained.

The conclusions and recommendations submitted by the contractor are considered to be valid; however, the mathematical model developed has definite limitations, the most critical limitation being that the model considers only vertical impact loads and therefore does not consider the longitudinal and lateral components that are usually also present in the helicopter crash environment. A second limitation is that it would be extremely difficult to use this approach to model and analytically study the crashworthiness of future aircraft designs with any confidence. This is due to the problems that would be encountered in attempting to predict the necessary weight data to apply to the lumped mass simulation and the spring constant data necessary to apply to the various springs that connect the masses of the model.

It is the intent of this Command to expand this mathematical model to include dynamic response to combined crash loading; i.e., crash loads which possess vertical, longitudinal, and lateral components, thereby developing a more realistic and useful analytical tool.

This report is divided into two volumes. Volume I contains a description of the accident data study, mathematical model, parametric study, full-scale drop test, and the results obtained. Volume II is a user manual for the computer program developed.

Project 1F162203A529
Contract DAAJ02-69-C-0030
USAAVLABS Technical Report 70-71A
January 1971

ANALYSIS OF HELICOPTER STRUCTURAL CRASHWORTHINESS

VOLUME I. MATHEMATICAL SIMULATION AND EXPERIMENTAL VERIFICATION FOR HELICOPTER CRASHWORTHINESS

Final Report

AvSER Report 1520-70-30

By

Clifford I. Gatlin
Donald E. Goebel
Stuart E. Larsen

Prepared by

Dynamic Science (The AvSER Facility)
A Division of Marshall Industries
Phoenix, Arizona

for

EUSTIS DIRECTORATE
U. S. ARMY AIR MOBILITY RESEARCH AND DEVELOPMENT LABORATORY
FORT EUSTIS, VIRGINIA

SUMMARY

This report describes the development of a mathematical model that will simulate the response of a UH-1D/H helicopter airframe to vertical crash loading and the full-scale crash test performed to verify the validity of the model.

In the initial phase of the model development, a study was made of 43 major accidents involving the UH-1D/H aircraft to determine what types of structural failure were contributing to injuries in helicopter accidents.

Based on the results of this accident study, a nonlinear lumped-mass model of 23 degrees of freedom was developed and programmed for computer solution. This model was then used in a parametric study of the UH-1D/H to evaluate potential areas of crashworthiness improvement.

At the conclusion of the parametric study, a full-scale, instrumented drop test of a UH-1D/H airframe was conducted. The data generated in this test were correlated with the model data to determine the ability of the model to predict airframe accelerations and deflections under crash conditions.

The results of this program indicate that:

- The structural weaknesses contributing to most impact injuries in UH-1D/H helicopter accidents are lack of resistance to failure in lateral roll-over and lack of energy-absorbing capability to reduce vertical accelerations;
- The mathematical model is capable of accurately predicting the floor and engine accelerations and deflections;
- In its present form, the model does not accurately predict the transmission accelerations and deflections.

Further research in the field of mathematical modeling for structural crashworthiness is recommended.

FOREWORD

The major portion of the data contained in this report was taken from U. S. Army sponsored research in aircraft crashworthiness conducted during the period February 1968 to July 1970.

The research effort detailed in this report is a major contributive element to a U. S. Army program being conducted to develop crash survival design criteria. The work is authorized by DA Project 1F162203A529. Results of the program are used to update and/or refine data contained in the Crash Survival Design Guide, USAAVLABS Technical Report 70-22.

Appreciation is extended to the following organizations for providing accident case histories upon which the crashworthiness analysis of survivable UH-1 helicopter accidents was based:

1. U. S. Army Board for Aviation Accident Research, Fort Rucker, Alabama.

2. U. S. Air Force Directorate of Aerospace Safety, Norton Air Force Base, California.

Additional credit is due Mr. Joseph L. Haley, Jr., for his contribution to the program. Mr. Haley performed the crashworthiness analysis of survivable UH-1 helicopter accidents.

TABLE OF CONTENTS

TABLE OF CONTENTS (Cont'd)

TABLE OF CONTENTS (Cont'd)

LIST OF ILLUSTRATIONS

LIST OF TABLES

LIST OF SYMBOLS

M(n)	Mass (n)
CM(n)	Weight of Mass (n)
CI(n)	Moment of Inertia of Mass (n)
d	Dimension
FS(n)	Force in Coupled Spring (n)
FD(n)	Force in Coupled Damper (n)
FTS(n)	Force in Torsional Spring (n)
FTD(n)	Force in Torsional Damper (n)
fns	Load-Deflection Characteristics of Coupled Spring (n)
fnd	Load-Deflection Characteristics of Coupled Damper (n)
fnts	Load-Deflection Characteristics of Torsional Spring (n)
fntd	Load-Deflection Characteristics of Torsional Damper (n)
L(n)	Half-Length of Mass (n)
X(n)	Coordinate Location of Centriod of Mass (n)
$\theta(n)$	Rotational Angle (n)
$\dot{X}(n)$, $\dot{\theta}(n)$	First Derivative (Velocity) of X(n) or $\theta(n)$
$\ddot{X}(n)$, $\ddot{\theta}(n)$	Second Derivative (Acceleration) of X(n) or $\theta(n)$

INTRODUCTION

Although the personnel restraint systems of Army aircraft have been improved in the past several years, accident records indicate a significant number of crashes in which the seats remain attached to the structure while the seated occupants continue to receive serious injuries. Several of the factors contributing to these serious injuries are listed below:

- Inadequate energy-absorbing structure below the fuselage floor, permitting the transmission of excessive decelerative forces to the seated occupant.
- Inadequate fuselage strength to maintain a protective shell in a lateral "roll-over" accident.
- Inadequate structural strength to resist inward and upward crushing of the lower forward fuselage in nose-down longitudinal impacts.
- Inadequate floor ductility to prevent seats located over floor fracture points from tearing away.

The concept of designing aircraft structures to sustain "crash" loads is still in its infancy. Some consideration has been given to the concept in the form of increased component tie-down strength in helicopters. For example, the rotor mast of early helicopters was restrained to a level of 4-6G forward, 4-6G vertical, and 2-3G lateral, depending upon the philosophy of the designer. Some current helicopter rotor masts are being restrained to withstand 15-20G forward, 15-20G vertical, and 10G lateral loads. The greater retention strength of these helicopter rotor masts undoubtedly results in fewer injuries to aircraft occupants.

Some key questions, however, remained unanswered. Which of the above factors was the primary cause of fatalities in aircraft accidents? Should methods for elimination of the primary cause of fatalities be sought first? Or would methods of eliminating a secondary cause of fatalities provide tools needed to attack the primary cause?

To provide additional insight into these problems, Dynamic Science has conducted a three-phase Airframe Structural Crashworthiness Study for USAAVLABS. In Phase I of this project, some 240 major accidents involving the UH-1D/H helicopter were reviewed to obtain data to be used in relating contact injuries to structural weaknesses. The results of this study indicated that the fuselage structural design features needing improvement were, in order of priority, as follows:

- Structural integrity and energy-absorbing mechanisms to protect personnel in lateral impacts.

- Energy-absorbing mechanisms to protect personnel from severe decelerative forces in vertical impacts.

- Fuselage strength and continuity to provide livable volume during forward or sideways "roll-over" accidents.

- Sufficient transmission mounting strength to preclude penetration of the crew compartment.

Comparison of these necessary design changes with both the analytical tools available for their solution and the overall benefit to be derived from such solutions led to a decision to attack first the problems of providing protection from severe vertical impacts and transmission intrusion into the crew compartment simultaneously. The tools employed and the experience gained would then be applied to the solution of the remaining problems.

In Phase II, therefore, a mathematical model of a helicopter was developed employing the lumped mass concept. This model was responsive primarily to simulated vertical loading, although small variations in pitch attitude at impact could be simulated. A sufficient number of individual masses were employed so that the model could simulate large twin-rotor cargo helicopters as well as small single-rotor observation helicopters.

The model was programmed for computer solution and, with appropriate input data, was used to simulate the structural response of the UH-1D helicopter. Following this, the response characteristics of various portions of the simulated UH-1D were altered and trial runs performed to determine the effect of introducing energy-absorbing capability into the airframe.

To verify the ability of the model to analytically predict the response of the UH-1D airframe, a full-scale drop test of a UH-1D was conducted in Phase III. The data recorded during this test indicated that, although the model was indeed capable of predicting the nature of the response, the peak accelerations of certain portions of the airframe determined analytically were higher than the test results indicate.

This report presents the results of the work accomplished in the three phases just discussed.

CRASHWORTHINESS ANALYSIS OF SURVIVABLE UH-1 HELICOPTER ACCIDENTS

OBJECTIVE

At the beginning of this project, it was known that improved airframe structural crashworthiness* was necessary to improve the survival rate in severe helicopter crashes. An adequate airframe structure provides the following protection in a crash:

- Enough crushable structure between the outer skin and the occupiable volume liner to absorb the energy of the moving fuselage without transmitting decelerative forces in excess of human tolerance.
- Enough stiffness to prevent crushing the occupants.
- Enough structural continuity to prevent a fracture large enough to permit partial or complete ejection of occupants.
- A continuous keel or slide surface along the fuselage belly to permit sliding over soft terrain without causing excessive longitudinal deceleration.
- Maximum protection possible for all flammable fluid systems.
- Adequate emergency exits.

Although all of the desirable features above were believed to be necessary for optimum airframe structural crashworthiness, the priority to be placed on the development of these features in production aircraft was not known. This accident study was conducted to relate the cause of impact injuries to specific structural weaknesses in the airframe.

DATA SOURCES

The weekly accident summaries prepared by the U. S. Army Board for Aviation Accident Research (USABAAR), Fort Rucker, Alabama, were reviewed to pinpoint the accidents pertinent to this study. The Directorate of Aerospace Safety, Norton Air Force

*Airframe Structural Crashworthiness: The ability of airframe structure to maintain a protective shell around occupants during a crash and to minimize accelerations applied to the occupiable portion of the aircraft during crash impacts.

Base, California, was also asked to retrieve pertinent UH-1F helicopter accident cases.

The data needed to fulfill the study objectives could not be obtained at either facility by routine retrieval methods, primarily because much of the information desired was recorded only in the case files. Visits were made to both USABAAR and Norton Air Force Base to review/study case files, since it was necessary to study the original file for each accident in detail in order to estimate the most probable causes of injuries to personnel.

In addition to the review of accident files, a visit was also made to the U. S. Army Aeronautical Depot Maintenance Center (ARADMAC), Corpus Christi, Texas, to inspect all types of severely damaged aircraft, including the UH-1. This review of more than 150 crash-damaged aircraft was helpful in estimating the impact forces and injuries indicated in the accident case reviews. It was not possible, however, to correlate the damaged helicopters at ARADMAC with many of the accident reports at USABAAR since most of the accident reports reviewed at USABAAR were of UH-1D and UH-1H helicopters that sustained nonrepairable damage and, therefore, were not sent to ARADMAC.

RESULTS

Thirty-seven Army accident cases for the period July 1967 through December 1968 were studied. The results from studying Air Force accident cases that occurred during the period January 1966 through April 1968 are included. Thus, the results from 43 case studies were used in this analysis. During the time period for the Army accidents (July 1967 through December 1968), approximately 240 UH-1D/H major accidents (survivable and nonsurvivable) occurred. Thus, the 37 Army accident cases included represent about 15 percent of the total accidents. Although 240 UH-1D/H accidents were reviewed, only 37 were studied. The remainder were eliminated for one or more of the following reasons:

- The accident did not result in major injuries to any personnel.
- No personnel survived the accident.
- Insufficient information was available in the accident file.

The data on each accident case was recorded on individual worksheets. A typical worksheet in shown in Figure 1.

U. S. ARMY HELICOPTER ACCIDENTS

Case Number 31 Date Data Collected Aug 69

GENERAL
USABAAR Code No. _____
Aircraft Identity UH-1D
Accident Date _____

IMPACT DATA
Flight Path Vel. Prior to Impact 25-35 fps
Crash Path Dist. _____
Flight Path Angle 90°
Terrain Angle Flat
Pitch Angle _____
Roll Angle _____
Yaw Angle _____

Vertical Stop Distance
Aircraft _____
Earth _____
Total _____
V_v 25-35 fps
V_h 0
V_l Unk.

Horizontal Stop Distance
Aircraft _____
Earth _____
Total _____

Lateral Stop Distance
Aircraft _____
Earth _____
Total _____

QUESTIONS

1. Was inadequate containerization cause of personnel injury? Yes _____ No ✓
2. What specific fuselage structural weakness caused injury?
   List: a. Lack of vertical energy absorption capability
   b.
   c.
3. Did helicopter roll laterally? Yes _____ No ✓
4. Did helicopter roll over forward completely? Yes _____ No ✓
5. Did helicopter impact inverted? Yes _____ No ✓
6. Injury Data

Total No. aboard	Type of injury	FATAL	MAJOR	MINOR	NONE
8		☐	7	1	☐

PERSONNEL	INJURY DEGREE	INJURY CAUSE
PILOT	Major	Excessive Vertical G
COPILOT	Major	Excessive Vertical G
CREW CHIEF	Minor	
CREW		
PASSENGER	Major	Excessive Vertical G
PASSENGER	Major	Excessive Vertical G
PASSENGER	Major	Excessive Vertical G
PASSENGER	Major	Excessive Vertical G
PASSENGER	Major	Excessive Vertical G
PASSENGER		

7. Postcrash fire Yes _____ No ✓
8. Remarks: Transmission retained. A/C impacted nose high in a rice paddy while in a flat spin to the left.

Figure 1. Accident Data Collection Worksheet.

The data on each case is summarized in Table I. Thirty-six UH-1D and UH-1H Army aircraft, 1 UH-1C aircraft, and 6 U. S. Air Force UH-1F helicopters (very similar to the Army UH-1B) are included. Each accident case is numerically identified in Column 1. Columns 2 through 5 present key kinematics information, and the remaining 10 columns contain data concerning personnel injuries and fuselage containerization. Each column is explained below:

Column 2, Aircraft Rolled Sideward - Denotes whether or not the helicopter impacted on its side at some time during the crash.

Column 3, Aircraft Rolled Forward - Denotes whether or not the helicopter rolled end over about its (X) pitch axis during the crash sequence.

Column 4, Aircraft "Plowed" Soil - Denotes whether or not the helicopter nose and belly tended to "plow" or push soil or water ahead of the aircraft during the crash sequence.

Column 5, Aircraft Impacted Inverted - Denotes whether or not the aircraft initially impacted in an inverted attitude.

Column 6, Fatalities - Denotes the total number of fatalities among personnel on board the helicopter during the accident.

Column 7, Major Injuries - Denotes the total number of personnel aboard the helicopter who sustained injuries requiring more than 5 days' hospitalization. The severity of personnel injuries are listed in both Army and Air Force report forms as follows:

/none/ /minor/ /major/ /fatal/

Column 8, None or Minor Injuries - Denotes the number of personnel aboard the helicopter who sustained no injuries or injuries of a degree less than major.

Note: Columns 6, 7, and 8 may be added to obtain total personnel on board.

Column 9, Personnel With High Vertical G - Denotes number of on-board personnel who received injuries due to upward decelerative forces. These injuries are caused by inadequate energy-absorbing structure in the occupant seats and in the area below the helicopter floor level.

TABLE I. KINEMATIC AND INJURY DATA FROM 43 SURVIVABLE UH-1 HELICOPTER ACCIDENTS

1 Accident Identity	2 Aircraft Rolled Sideward	3 Aircraft Rolled Forward	4 Aircraft "Plowed" Soil	5 Aircraft Impacted Inverted	6 Fatalities	7 Major Injuries	8 None or Minor Injuries	9 Personnel With High Vertical G	10 Personnel Thrown out	11 Personnel Crushed by Fuselage	12 Transmission Penetrated Troop Area	13 Rotor Blade Penetrated Cockpit	14 Postcrash Fire	15 Remarks
1	No	No	No	No	0	4	3	0	2	1	No	No	No	Left cockpit area crushed aft by impact into 12 inch tree to cause copilot injury
2	No	No	Unknown	No	0	2	3	2	No	None	No	No	Yes	
3	No	No	Slight	No	0	4	1	3	No	None	No	No	No	Sand beach impact.
4	No	No	Unknown	No	3	5	0	0	*2	1	Unknown	No	Yes	50 kt impact at flat impact angle. *2 passengers ejected did not use lap belt.
5	Yes	No	No	No	0	9	2	0	1	1	Unknown	Unknown	No	Aircraft rolled more than twice down a mountain slope. Copilot crushed by roof.
6	Yes	No	Slight	No	0	3	3	0	3	Unknown	Unknown	Unknown	Yes	Impact angle = 11° Impact Velocity = 60-80 kts Crashpath = 300' Landing gear and transmission separated.
7	No	No	No	No	3	1	0	Unknown	No	Unknown	Unknown	Unknown	Yes	Impact angle = 55° Impact velocity = Unknown Crashpath = 5°-10' Massive and immediate fire.
8	No	No	Unknown	No	3	*1	0	Unknown	No	2 or 3	Yes	Unknown	Yes	Impact angle = 15°-30° Impact velocity = 50-70 kts Nose crushed aft and trapped crew. *Died several hours later.
9	Yes	Unknown	Unknown	No	0	1	0	0	No	None	No	No	Yes	Injury caused by arm impact into injurious environment.
10	No	No	No	No	0	4	0	2	No	None	No	No	Yes	Severe vertical impact thru trees. Main cargo doors would not open.
11	Yes	No	No	No	0	4	2	1	1	None	No	No	No	Vertical impact thru trees.
12	Yes	No	Unknown	No	0	2	9	Unknown	No	None	No	No	No	Cross tubes displaced sideward about 2 inches.
13	Yes	No	Unknown	No	3	7	0	0	2 or 3	1(Pilot)	Unknown	No	No	Aircraft rolled approximately 140' down 50 degree slope.
14	No	No	Unknown	No	3	1	0	0	No	Unknown	Unknown	No	No	Aircraft crashed into large trees up to 6" diameter.
15	Yes	No	No	No	0	6	4	0	No	Unknown	No	No	No	Flare too high, aircraft fell thru and struck on left side.
16	No	No	No	No	0	4	3	0	No	1 (Copilot)	Unknown	Unknown	No	Hoist cable snagged in 150' trees causing tail rotor loss in tree top. Aircraft spiralled down.
17	No	No	No	No	0	4	0	2	No	No	No	No	No	Photos indicate 5°-10° nose down impact.

TABLE I. Continued

1 Accident Identity	2 Aircraft Rolled Sideward	3 Aircraft Rolled Forward	4 Aircraft "Plowed" Soil	5 Aircraft Impacted Inverted	6 Fatalities	7 Major Injuries	8 None or Minor Injuries	9 Personnel With High Vertical G	10 Personnel Thrown Out	11 Personnel Crushed by Fuselage	12 Transmission Penetrated Troop Area	13 Rotor Blade Penetrated Cockpit	14 Postcrash Fire	15 Remarks
18	Yes	No	No	No	0	4	0	2	No	*1 (Pilot)	No	No	Yes	*Crush injury to pilot's leg caused by wedging between rudder pedals and console.
19	Yes	No	No	No	1	5	5	1	No	1 (Copilot)	No	No	No	Engine failure, aircraft struck, bounced, hit skid and rolled to right.
20	Yes, Pure Lateral Impact	No	No	No	9	2	0	0	No	4 or 5	Yes	No	No	Aircraft dropped from 100' tall trees. Struck ground on side. All restraints broke on lower side. Pilot's seat also broke free.
21	No	No	Unknown	No	1	4	4	0	*2	1	Yes	No	Yes	Transmission displaced forward and sideward and trapped crew chief in fire. *Lap belts not used.
22	Yes, to Right	No	No	No	2	7	0	1	No	2	No	No	Yes	Poor restraint and lack of doors caused 2 fatalities to be trapped and burned. Fire became intense in 3 minutes.
23	Yes, Pure Lateral Impact	No	No	No	0	4	0	0	No	0	No	No	No	Main rotor blade struck 8 inch tree at 15' height above ground and helicopter fell through on side.
24	No	No	No	No	0	4	*9	4	No	1 (Pilot)	No	**Yes	No	*Injuries to these nine passengers were not reported. ** Main rotor blade struck roof and crushed it down.
25	Yes, After Impact	No	Yes, Plowed Water	No	0	3	1	0	*1	0	No	No	No	* Ejected because of intentional belt release after initial impact in river.
26	Yes, After Impact	No	Yes, Plowed Water	No	0	9	0	0	3-6	*2	No	No	No	* Passenger and Copilot injured by rearward movement of instrument panel. Shallow river impact.
27	No	No	Unknown	No	0	9	0	0	*Unknown	Unknown	Unknown	No	Yes	*Details missing in very brief report. Aircraft settled, with inadequate power.
28	No	Yes	*Yes	No	0	6	0	0	No	Unknown	*No	No	No	*Transmission completely severed from fuselage during water impact. Figures 7 and 8 indicate probable "end-over" impact.
29	Yes	No	No	No	3	3	0	0	1	*2	No	No	Yes	*Gunner and passenger trapped and crushed by lack of door on right side.
30	Yes	No	No	No	1	*9	1	0	2	No	No	No	Yes	*7 injuries caused primarily by failure to use restraint (includes the 2 personnel thrown out).
31	No	No	No	No	0	7	1	*7	No	No	No	No	No	*Primarily vertical impact in rice paddy.

TABLE I. Continued

1 Accident Identity	2 Aircraft Rolled Sideward	3 Aircraft Rolled Forward	4 Aircraft "Plowed" Soil	5 Aircraft Impacted Inverted	6 Fatalities	7 Major Injuries	8 None or Minor Injuries	9 Personnel With High Vertical G	10 Personnel Thrown Out	11 Personnel Crushed by Fuselage	12 Transmission Penetrated Troop Area	13 Rotor Blade Penetrated Cockpit	14 Postcrash Fire	15 Remarks
32	No	Prob-able	Probable	No	*2	4	0	No	Unknown	*2	Yes	No	Yes	*2 fatalities caused by inability to exit from pinned position between transmission and terrain.
33	Yes, After Initial Impact	Prob-able	No	No	0	2	2		No	1	Yes	*Yes	No	Rice paddy (water) impact. *1'-2' on pilot side.
34	No	No	No	No	1	0	3	3	No	No	Yes	No	No	UH-1C aircraft, Primarily vertical impact.
35	Yes	No	No	Yes	0	1	1	0	No	Unknown	Yes	No	No	Mild impact, aircraft lifted off asphalt and rolled in air, struck on back.
36	Yes	No	No	Yes	0	0	2	0	0	0	*Yes	No	No	Meager data in report, A/C rolled rapidly to right at lift off. *3' downward.
37	Yes	No	*Yes	No	1	2	2	1	1	Unknown	No	No	**No	*Nose crushed aft about 1' by possible soil plowing as shown in Figure 9. ** Fuel spilled in crash.
Fuselage Integrity and Personnel Injuries in UH-1F (Air Force) Helicopters														
38	No	No	No	No	Unknown	Unknown	Unknown	Unknown	No	No	No	No	No	Test aircraft. Entire crash sequence covered by Fairchild camera. Rear cross tube punctured fuel tank.
39	Yes	Yes	Yes	No	0	1	3	No	No	No	*No	*No	Yes	*Transmission completely severed from aircraft.
40	Yes, After Initial Impact	No	Unknown	No	*3	0	0	No	2	Unknown	No	Unknown	No	*Copilot survived and tried to stop leg bleed by tourniquet; he expired due to loss of blood.
41	Yes, After Initial Impact	Unknown	Unknown	No	0	5	0	3	No	*No	No	No	No	*Roof displaced forward and down, but did not cause injuries.
42	Yes	Unknown	Unknown	*Yes	0	2	1	No	No	*No	No	No	Yes	*Roof structure displaced downward on opposite side of crew chief and could have struck head of an occupant.
43	No	No	No	No	0	7	1	*7	No	No	No	No	No	*Severe vertical impact. seat legs penetrated floor. Fuel spilled out aft end of right tank, but no fire.

Column 10, Personnel Thrown Out - Denotes on-board personnel who were ejected from the helicopter during the crash sequence.

Column 11, Personnel Crushed by Fuselage - Denotes personnel who received injuries or were "trapped" by inward displacement of structure.

Column 12, Transmission Penetrated Troop Area - Denotes sufficient displacement of the transmission mass to constitute a hazard to on-board personnel.

Column 13, Rotor Blade Penetrated Cockpit - Denotes sufficient intrusion of the rotor blade into the cockpit to constitute a hazard to the occupants.

Column 14, Postcrash Fire - Self-explanatory.

Column 15, Remarks - Self-explanatory.

The data presented in Table I is further condensed and presented in bar-graph form in Table II. A review of Table II reveals that:

- The main rotor blade(s) definitely penetrated the cockpit in only 2 of 43 accidents; however, penetration was suspected in several other accidents but could not be definitely established.
- Two of 43 helicopters rolled "end over end".
- Three of 43 helicopters impacted inverted.
- Five of 43 helicopters were subjected to severe "plowing" (longitudinal) forces.
- Eight of 43 helicopters showed definite evidence that the transmission penetrated into the troop area; however, it could not be determined whether or not the transmission had displaced into the troop area in 8 accidents.
- From 23 to 27 occupants were thrown out of the aircraft in 13 of 43 accidents.
- Thirty-nine occupants sustained excessive vertical decelerative forces in 14 of 43 accidents.
- From 24 to 26 occupants were injured by crushing or entrapment in the fuselage in 16 of 43 accidents.

TABLE II. SUMMARY OF KINEMATICS, FIRE, AND INJURY DATA FOR 43 UH-1 ACCIDENTS

Injury Data	Number	Percent
Total Personnel Aboard	265	100
Total Fatalities	39	15
Total Major Injuries	162	61
Total Minor or No Injuries	64	24

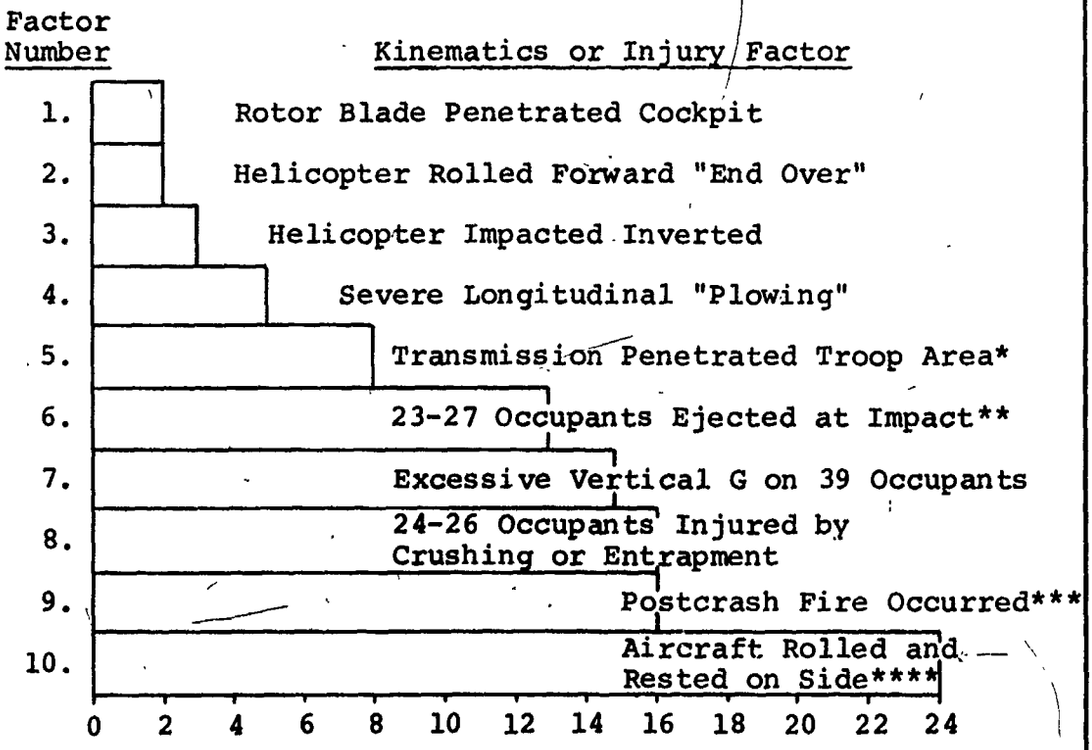

*Transmission was completely severed from helicopter in two additional accidents.
**Failure to use lap belts definitely permitted ejection of seven of the 24 passengers.
***18 fatalities occurred in these postcrash fire accidents.
****2 helicopters struck in a complete lateral impact.

- Postcrash fire occurred in 16 of 43 accidents.
- The aircraft either impacted on its side or rolled over and rested on its side in 24 of 43 accidents.

Further review of Table II shows that Factors 6 through 10 include the most significant causes of impact injuries. Further details on these factors are presented below:

Factor 6 - From 23 to 27 occupants were thrown out of the helicopter during the impact in a total of 13 accidents although 7 of these occupants were definitely ejected due to nonuse of lap belts; in any event, nearly all ejected occupants received injuries of varying degree.

Factor 7 - Excessive vertical decelerative forces accounted for 39 injuries out of 201 injuries (39 fatal plus 162 major injuries)

Factor 8 - Twenty-four occupants received either thermal injuries as a result of entrapment and postcrash fire burns, or impact injuries as a result of inward crushing in a total of 15 accidents.

Factor 9 - Postcrash fire occurred in 16 accidents, resulting in 18 fatalities.

Factor 10 - The helicopter rolled and rested on its side or impacted partially or completely on its side in 24 accidents.

It was not possible to determine the causes of all injuries to personnel since the information was not available on some of the accident forms, especially on condensed Department of the Army Form 232. However, the injuries due to excessive vertical decelerative forces seemed to be an exception since this cause was listed in most cases where vertebral compressive fractures occurred. Although it is possible that slightly more than the 39 of the 201 injured personnel noted in Table I sustained injuries due to vertical decelerative forces, the question is academic. Since this type injury occurred in 35 percent of the accidents studied, it is a serious problem.

Damaged aircraft that sustained primarily vertical forces are shown in Figures 2 through 6. Figures 2 and 3 show the UH-1C helicopter (Case 34) in which 3 out of 4 occupants sustained back injuries. The intact rotor blades in Figure 3 indicate that the blades were nearly stopped prior to impact. The flattened landing skid cross tubes and the upward displacement

Figure 2. Close-up of Fuselage Area. (Accident Case 34)

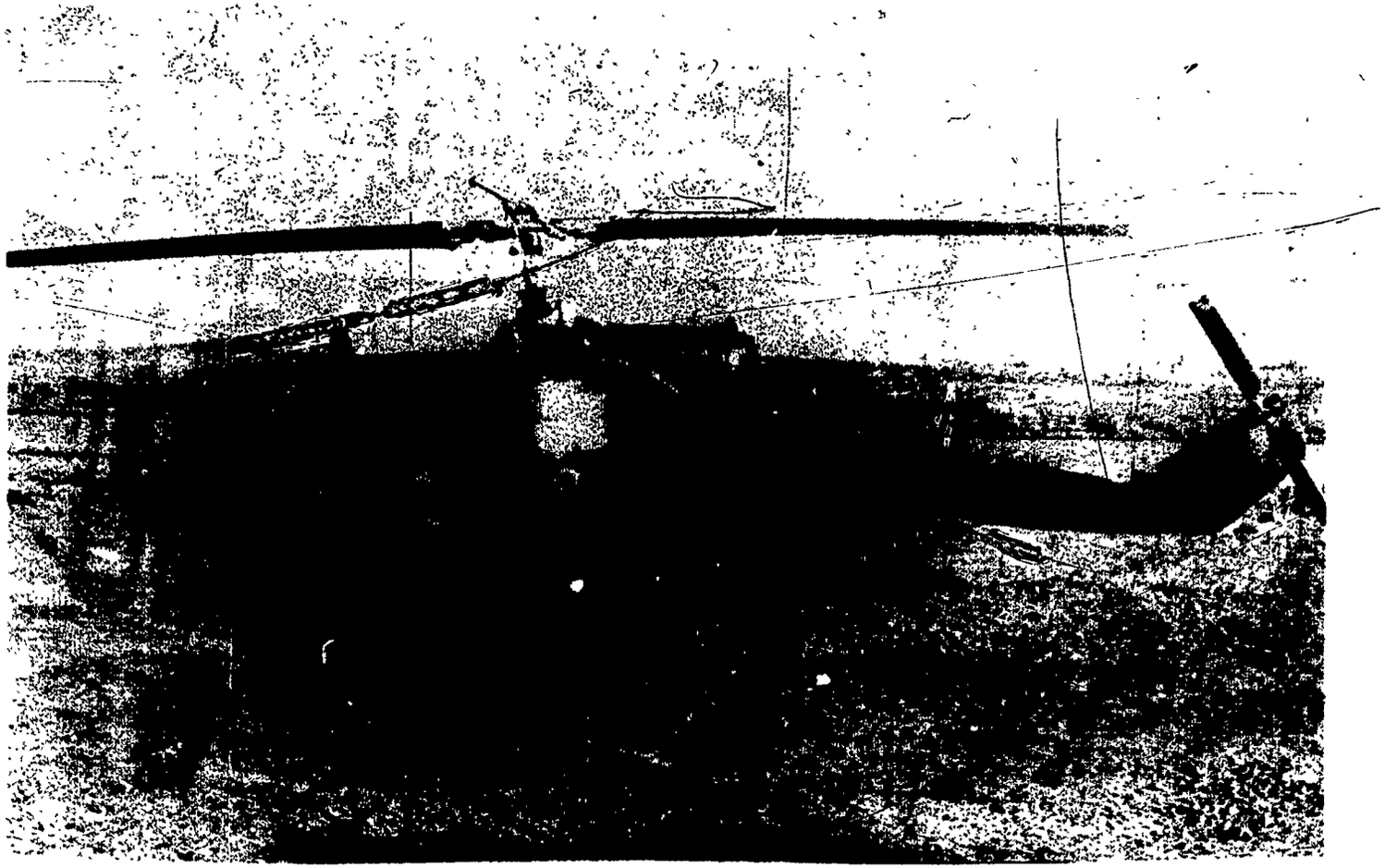

Figure 3. Profile View After Removal From Accident Site. (Note fuselage buckling at forward cross tube.) (Accident Case 34)

Figure 4. Left Profile View of Fuselage. (Accident Case 31)

Figure 5. Right Profile View of Fuselage. (Accident Case 31)

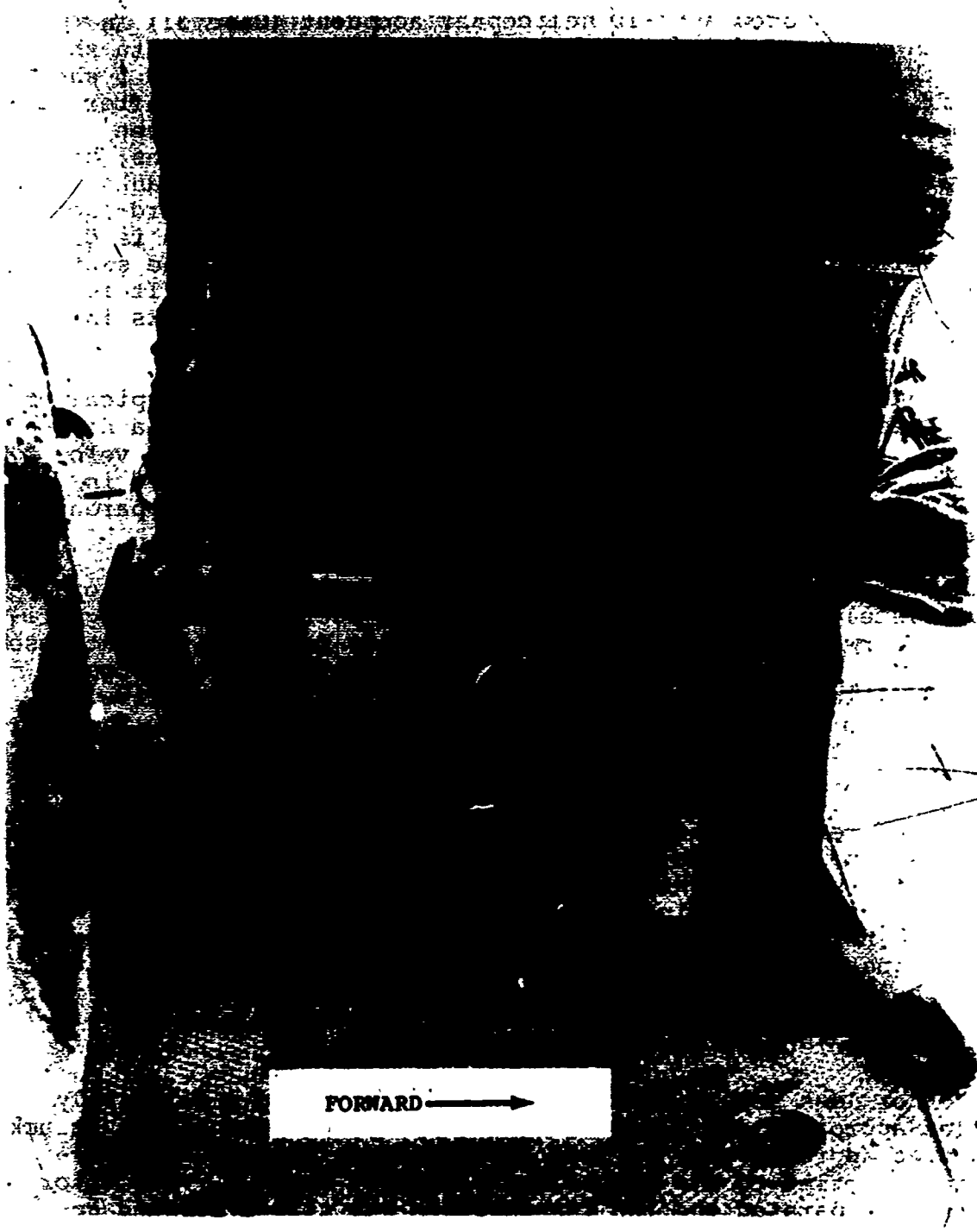

Figure 6. View of Jump Seat Displacement Through Floor. (Accident Case 31)

of the cockpit floor in the area of the forward cross tubes are mute evidence of the upward decelerative force. Figures 4, 5, and 6 show a UH-1D helicopter accident (Case 31) in which 7 out of 8 occupants sustained back injuries (data sheet on this case is presented as Figure 1). Figures 4 and 5 show left and right profile views of the damaged aircraft after removal from the crash site. The rear cross tube has been flattened and displaced upward into the fuel tank areas; however, it could not be determined whether or not the tanks burst. Figure 6 shows the displacement of the sideward-facing "jump" seat into the floor. This type of deformation is desirable in absorbing the vertical energy; however, the seat legs could puncture the fuel tanks below the floor. It is not known if the seat legs did any damage to the fuel tanks in this accident.

The accidents described above (Cases 31 and 34) are typical of crashes in which the helicopter impacts vertically in a nose-high attitude with little, if any, forward or sideward velocity. The transmission was not significantly displaced in either of these accidents because the upward forces apparently acted symmetrically along the mast center.

The transmission and rotor mast were invaribly displaced or completely severed from the fuselage in accidents with significant forward impact velocity (30 knots or more). Accident Case 28 is an example of transmission severance due to high longitudinal impact forces. This helicopter impacted relatively flat into water at a forward speed of 75 to 85 knots. The results of this impact may be seen in Figures 7 and 8 which show left and right profile views of the damaged fuselage, less transmission, and mast. It is probable that this aircraft flipped forward "end-over-end", but the accident report did not so indicate. No fatalities occurred even though the roof and side structure has been nearly torn free. All six occupants were injured in varying degrees. The effect of the water on the nose of this aircraft is readily apparent. Even though this was a severe crash in which it could not be expected that any helicopter fuselage structure would be undamaged, the roof and sidewall should have remained relatively in place to provide a protective shell for the occupants.

Another less severe accident (Case 37) involved a relatively flat approach into a wooded area. The main rotor blades struck a tree approximately 30 feet above ground; however, the aircraft settled to the ground approximately upright. The rotor blades separated and the transmission was tilted forward approximately 45 degrees during the impact. The nose section was pushed upward and rearward, causing multiple injuries to the pilot and copilot. Details of the crash kinematics were

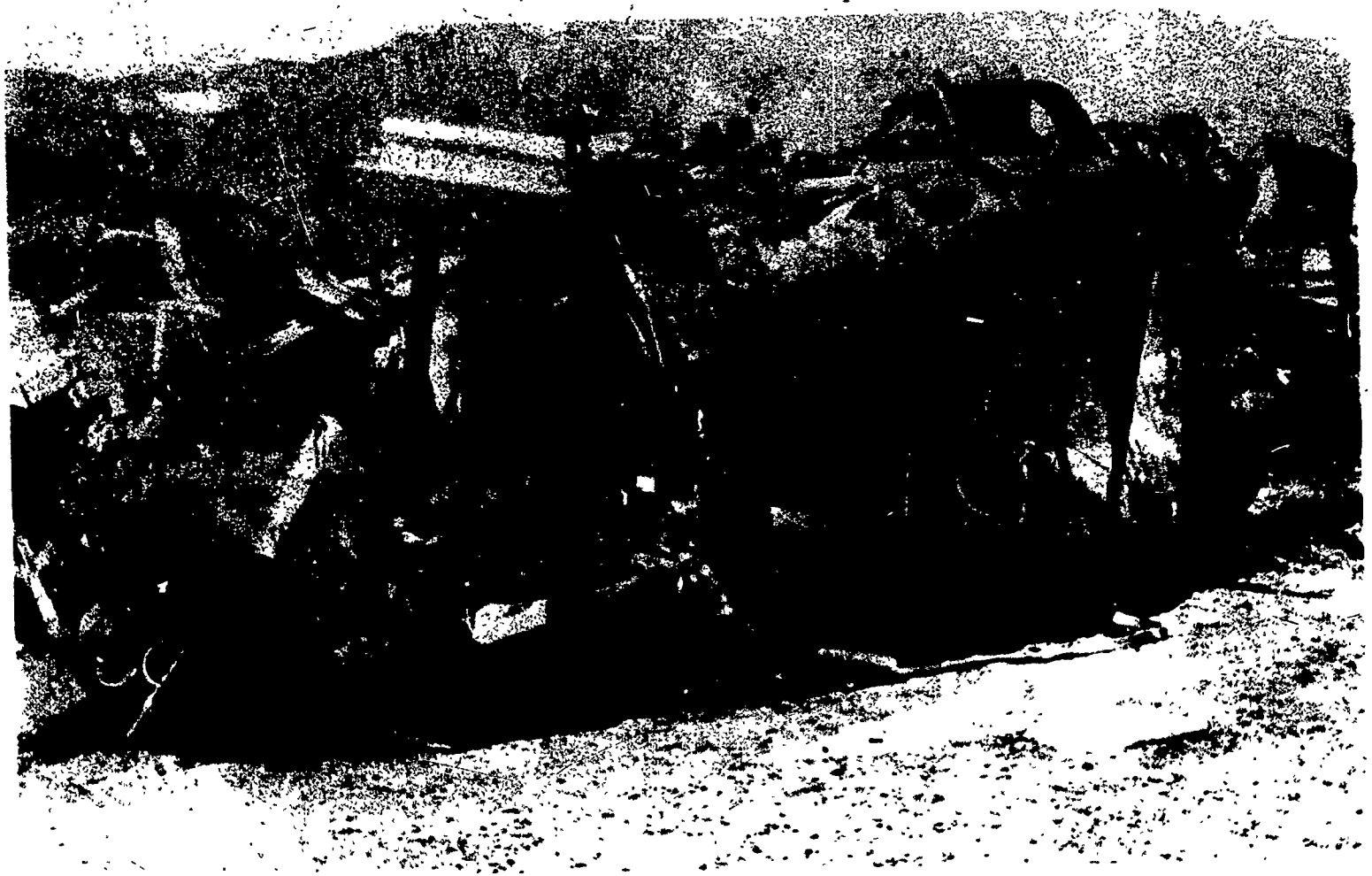

Figure 7. Left Profile View. (Note absence of transmission and damage to nose section.) (Accident Case 28)

Figure 8. Right Profile View Showing Severe Damage to Nose Section. (Accident Case 28)

not available, but it was known that the aircraft moved approximately 150 feet from the tree impact point to the final rest point. An oblique view of the damaged nose area is shown in Figure 9, a photograph made after the aircraft was removed from the crash site. Figure 9 shows that the pilots could have been injured by inward movement of structure.

An example of a purely sideward (lateral) impact may be seen in Figures 10, 11, and 12 (Case 20). Figure 10 shows an overall view of the accident scene with an arrow showing the point of impact with the tree top. Figure 11 shows the front belly of the aircraft; the landing gear cross tube is pushed away from the fuselage on the upper (right) side while it is pushed upward and inward on the left side. The absence of any rearward deflection in the cross tube corroborates other evidence to indicate that the aircraft had minimal forward velocity at impact.

Figure 12 shows the upper right side of the roof as the helicopter rests on the ground. Note that the rotor blades were relatively intact, showing that they were rotating very slowly, if at all, at the time of impact. This view also shows that the fuselage was relatively undeformed on its upper half (right side) and that this section should have been survivable. The two survivors, the pilot and gunner, were seated on this side, but four other occupants seated on the right side of the aircraft did not survive because of inadequate restraint. None of the five occupants seated to the left of center survived. The fuselage crushed inward about 1 foot on the left side; occupants in this area could not have survived. A close look at the cockpit roof shows that it separated from the remaining roof at the forward edge of the roof support bulkhead; the aircraft floor may be seen through this separation. The pilot's seat was missing from this area of the floor.

Results indicate that the most important factor in improving impact protection is improved protection in lateral impacts and "roll-over" accidents, followed closely by protection for the vertical impact. Improved protection in a lateral impact is deemed slightly more important than in a vertical impact because the injuries sustained in severe lateral impacts are generally more severe and incapacitating than those sustained in purely vertical impacts. The use of energy-absorbing seats, designed in accordance with the Crash Survival Design Guide, USAAVLABS Technical Report 70-22, is expected to reduce the number of vertical "G" injuries significantly even though no effective energy-absorbing structure is used below the floor level. However, since these same seats are not expected to absorb any significant energy in sideward impacts, the aircraft fuselage should be designed to attenuate sideward decelerative forces on the occupants.

Figure 9. View of Nose-Section Damage. (Accident Case 37)

Figure 10. Overall View of Accident Scene. (Note intact rotor blade and displacement of cross tubes.) (Accident Case 20)

Figure 11. Close-up of Landing Skid Damage. (Note intact landing light.) (Accident Case 20)

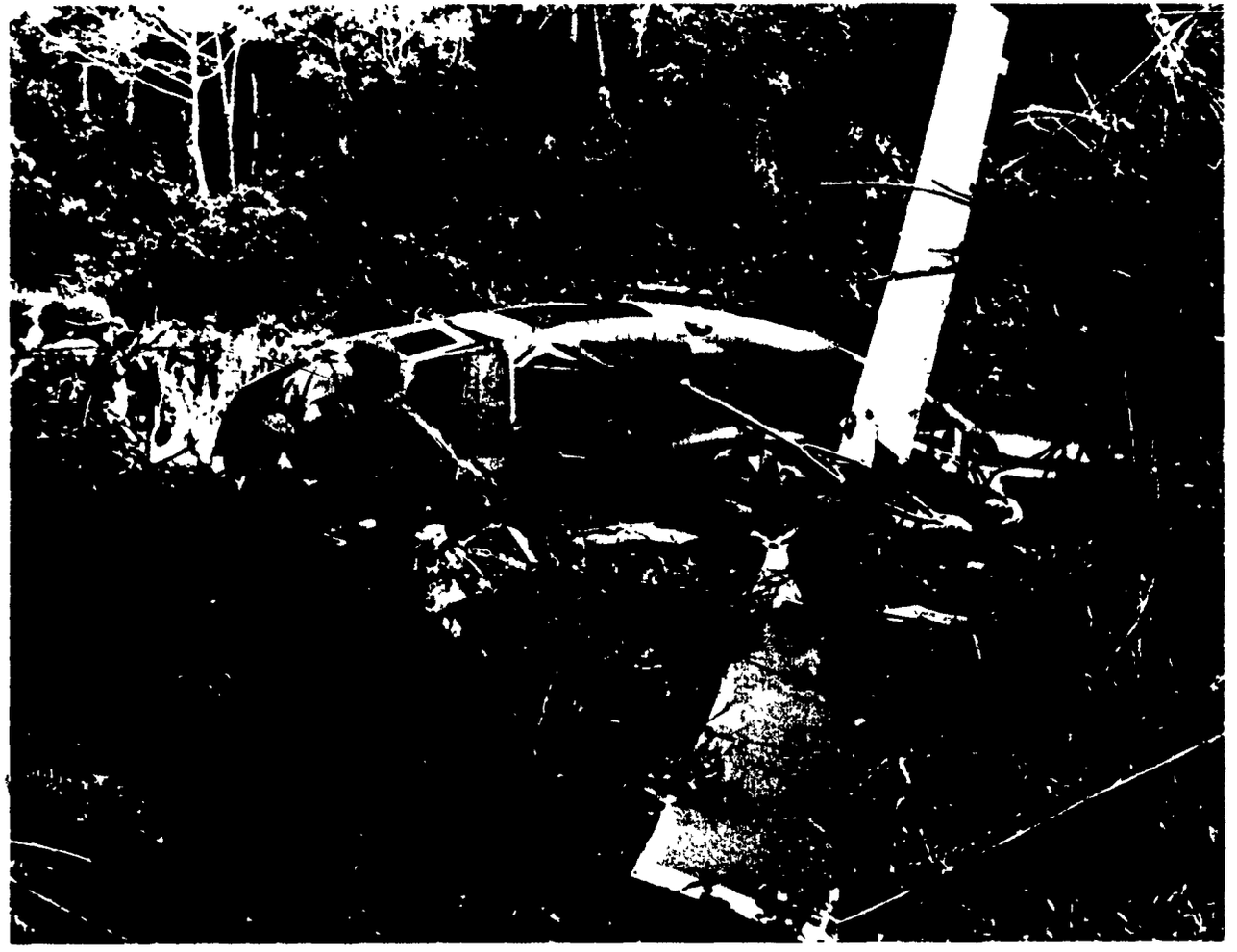

Figure 12. View of Damage to Left Side Showing Intact Rotor Blades. (Accident Case 20)

Based on the results of 43 UH-1 helicopter accidents studied, it was concluded that:

- The sideward (lateral) impact is a significant crash condition, because more than half of the accidents studied resulted in significant lateral forces, and 111 of 201 injuries and fatalities occurred in the roll-over accidents.

- More fatalities were caused by impact force injuries than were caused by postcrash fire thermal injuries in these survivable or partially survivable accidents.

- The fuselage structural design features needing greatest improvement in this type of helicopter are as follows (in order of priority):

  - Structural integrity and energy-absorbing mechanisms to keep personnel in place with a livable volume in sideward (lateral) impacts.

  - Energy-absorbing mechanisms to prevent excessive upward decelerative forces on seated occupants in severe vertical impacts.

  - Fuselage strength and continuity to provide a livable volume in sideward and forward "roll-over" accidents.

  - Transmission retention strength sufficient to prevent penetration of the troop compartment.

After the priority of structural redesign of the UH-1D/H helicopter from an injury prevention viewpoint was determined, the features requiring modification were then compared to determine the overall priority for redesign. Factors considered in this comparison, in addition to injury prevention, were:

- Availability of analytical tools for the determination of design criteria.

- Applicability of the above tools to the redesign of the remaining features.

- Probable extent of structural modification required to reduce the injury potential of each structural weakness.

Based on the results of this comparison, first priority was assigned to investigating methods of providing energy-absorbing mechanisms to reduce upward decelerative forces on seated occupants. This decision was based on the following rationale:

- The analytical tools necessary were available, and, following refinement, could be expanded to the redesign of the remaining features.
- Protection of the occupants from high vertical decelerative loads would substantially reduce injuries.
- One facet of the problem of inadequate transmission retention could be investigated simultaneously with the reduction of vertical decelerations.
- Once design criteria were established, the changes necessary to substantially increase the level of occupant protection would probably not be extensive.

A mathematical model simulating the dynamic response of a helicopter airframe subjected to vertical dynamic loading was developed and adapted to solution by computer. This model was the primary analytical tool used in the investigation of methods of introducing vertical energy-absorbing mechanisms into the UH-1D/H helicopter.

MATHEMATICAL MODEL DESCRIPTION

GENERAL

The mathematical model used in this study represents the airframe structure of a rotary-wing aircraft. It is a nonlinear, lumped mass model having 23 degrees of freedom. To construct the model, the airframe structure is divided into four vertical and three longitudinal sections, as shown in Figure 13. Individual masses are identified by number in Table III. The vertical section divisions are (1) transmission, engine, and rotor section; (2) mass above the floor section; (3) mass below the floor section; and (4) landing gear section. The longitudinal section divisions are (1) nose section, (2) central section, and (3) tail section. The 14 masses are spring connected into the model and are used to represent various sections of the airframe structure. Springs connecting the masses are shown in Figure 14 and identified in Table IV. The vertical section masses permit a parametric study of the distribution of the load-limiting properties throughout the important vertical sections of the airframe structure. The longitudinal masses, shown in Figure 15, permit a study of plastic hinges and shear failures at 4 simulated airframe locations. All masses may not be required to represent a particular section of the airframe structure under study; however, the model is generalized to the degree that single as well as multiengine aircraft may be analyzed.

VERTICAL SECTION DESCRIPTION

The masses representing the 4 vertical sections, when connected into the model, simulate load-deflection characteristics. They are connected into the model with 16 direct- and 7 far-coupled springs. Each spring is combined in parallel with a damper as shown below.

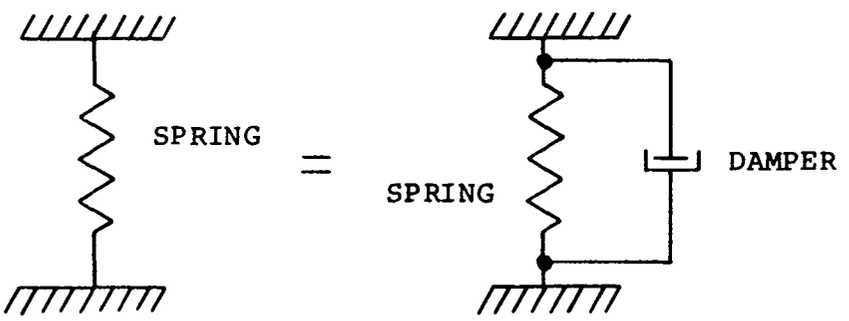

The viscous damping constants are assumed to be proportional to velocity.

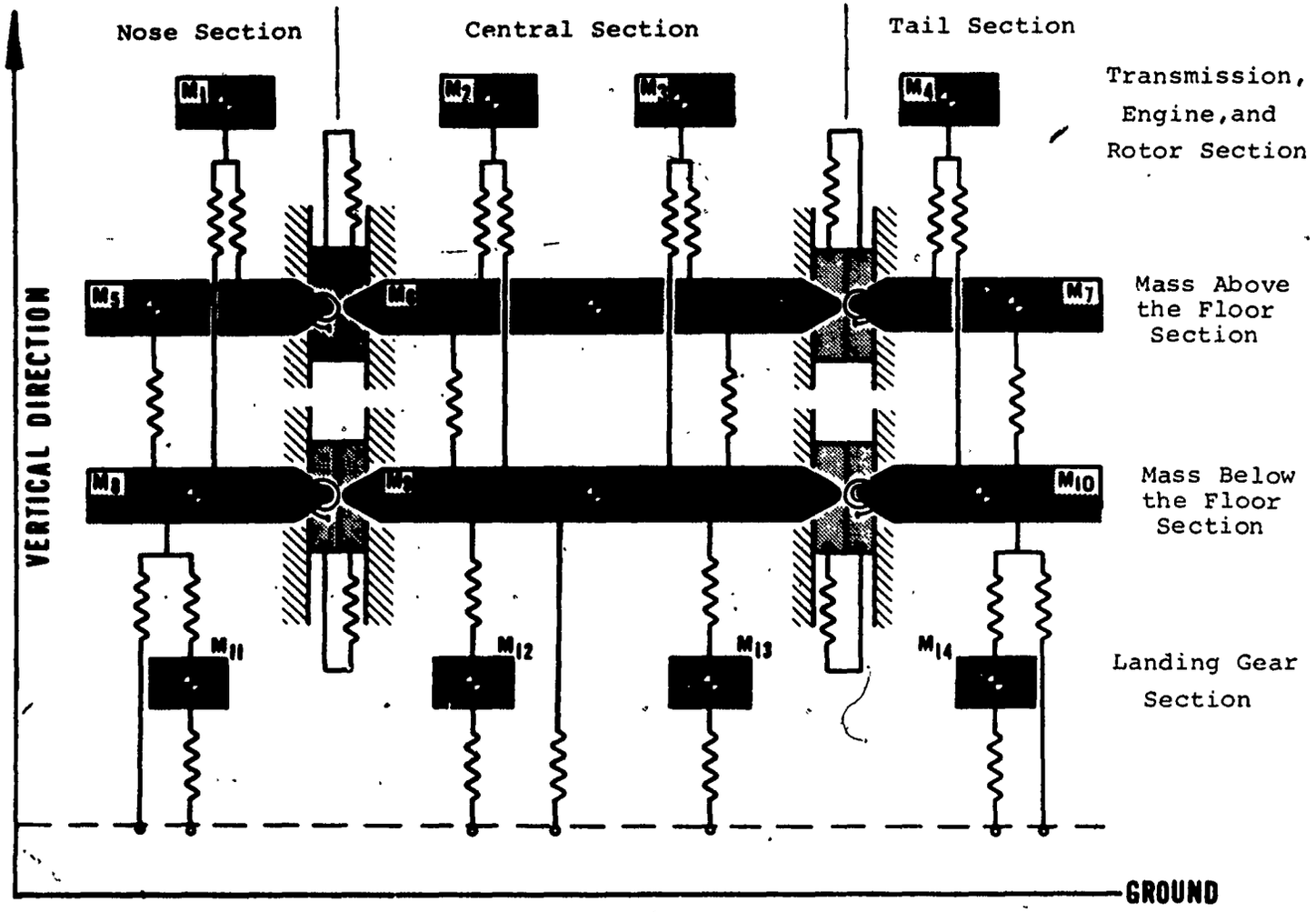

Figure 13. Model Description (Lumped Masses).

TABLE III. MODEL DESCRIPTION (LUMPED MASSES)	
Mass No.	Description
M1 M2 M3 M4	Rotor Assembly, Transmission Assembly, and/or Engine Assemblies
M5 M6 M7	Airframe Structure Above Floor Level
M8 M9 M10	Airframe Structure Below Floor Level and Floor Dead Loads
M11 M12 M13 M14	Landing Support System

Two types of spring damping are considered in the model, internal (hysteresis) damping and external (viscous) damping. Internal damping is introduced into the model through the load-deflection curve shown in Figure 16. By assigning different slope values to the unloading portion of the generalized load-deflection curve, a hysteresis cycle can be generated that will absorb energy. The degree to which the load-deflection curves will reproduce the aircraft structure is dependent upon the quality of data available for the particular aircraft to be studied, and upon the user's ability to interpret available data and comprehend the dynamics of the deforming structure. Weight and load-deflection data may be obtained from the aircraft manufacturer and/or from analysis of accident case histories. Both of these approaches were used to develop the program application which starts on page 55.

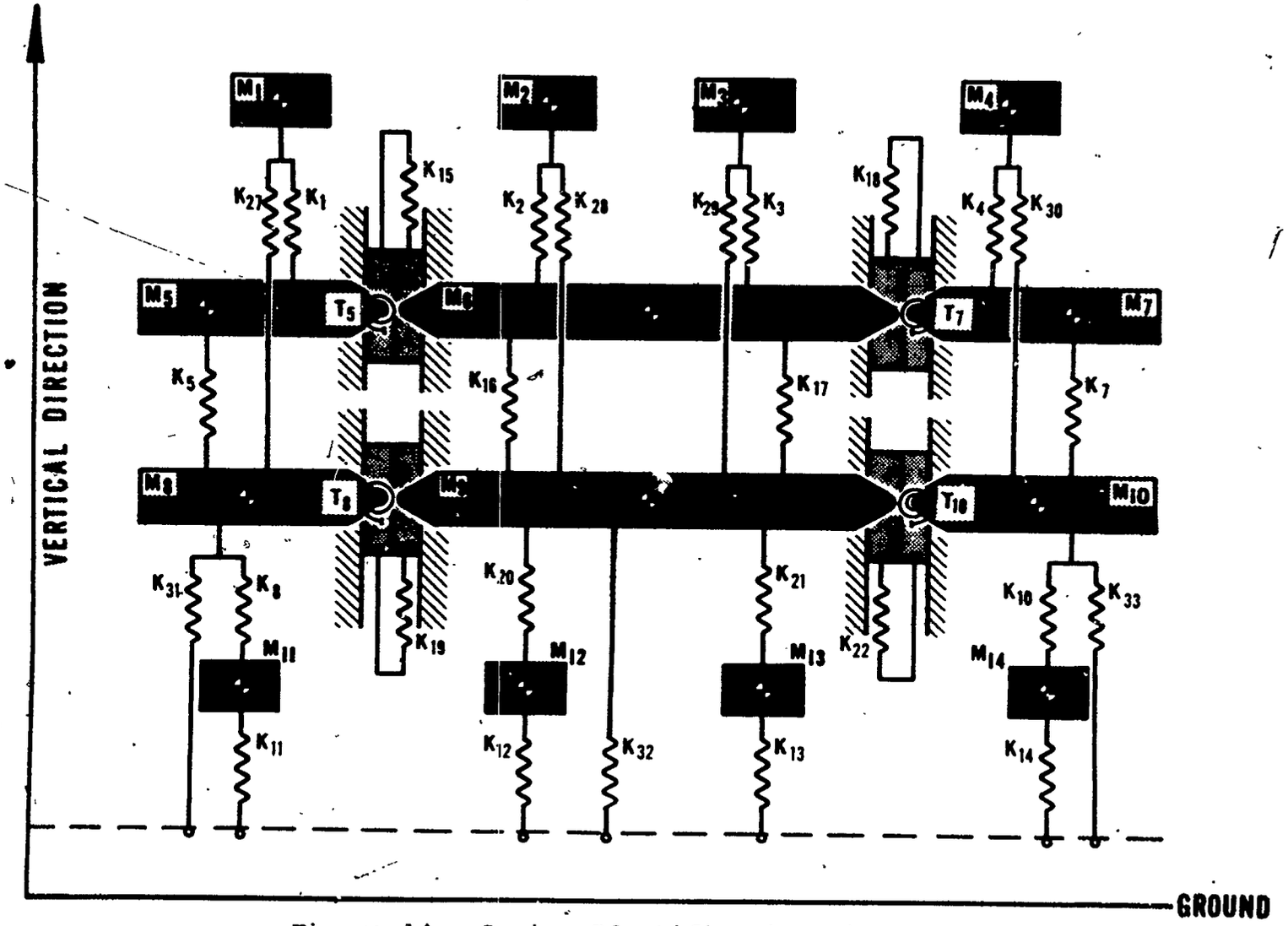

Figure 14. Spring Identification Diagram.

TABLE IV. MODEL SPRING IDENTIFICATION	
Spring No.	Description
K1 K2 K3 K4	Direct-Coupled Load-Deflection Characteristics of Rotor/Transmission and/or Engine Support System to Upper Fuselage
K5 K7 K16 K17	Direct-Coupled Load-Deflection Characteristics of Airframe Structure Above Floor Level
K8 K10 K11 K12 K13 K14 K20 K21	Direct-Coupled Load-Deflection Characteristics of Landing Support System
K15 K18	Direct-Coupled Load-Deflection Characteristics of Airframe Structure Above Floor Level During Shear
K19 K22	Direct-Coupled Load-Deflection Characteristics of Airframe Structure Below Floor Level During Shear
K27 K28 K29 K30	Far-Coupled Load-Deflection Characteristics of Rotor/Transmission and/or Engine Support System to Floor

TABLE IV. Continued	
Spring No.	Description
K31 K32 K33	Far-Coupled Load-Deflection Characteristics of Airframe Structure Below Floor Level
T5 T8	Torsional Load-Deflection Characteristics of Forward Fuselage Section
T7 T10	Torsional Load-Deflection Characteristics of Rear Fuselage Section

External damping is introduced by the use of a constant applied to the rate-of-change of spring deformation. The numerical value of this constant may be determined by an analytical estimate, based on theoretical data, or by performing a series of computer runs using various estimated values for these constants and comparing the results to experimental data.

The springs in the model are classified into two types, depending upon the ability of the structure represented to restrain a tensile rebound, as illustrated in Figure 16. A type-1 spring can restrain tensile rebound, while a type-2 spring cannot.

LONGITUDINAL SECTION DESCRIPTION

The masses simulating the three longitudinal sections of the airframe structure are connected into the model with four torsional springs and four shear springs. Connection details are shown on page 36.

The interface between blocks A and B is frictionless, permitting relative vertical displacements. The resistance against such a vertical displacement is provided by a shear spring. This simulates the possibility of a shear failure occurring in the fuselage, the severity of which is controlled by the shear spring. The two masses are connected to blocks A and B by frictionless pins, thereby permitting relative angles to form between the two masses. Resistance to such rotation is offered

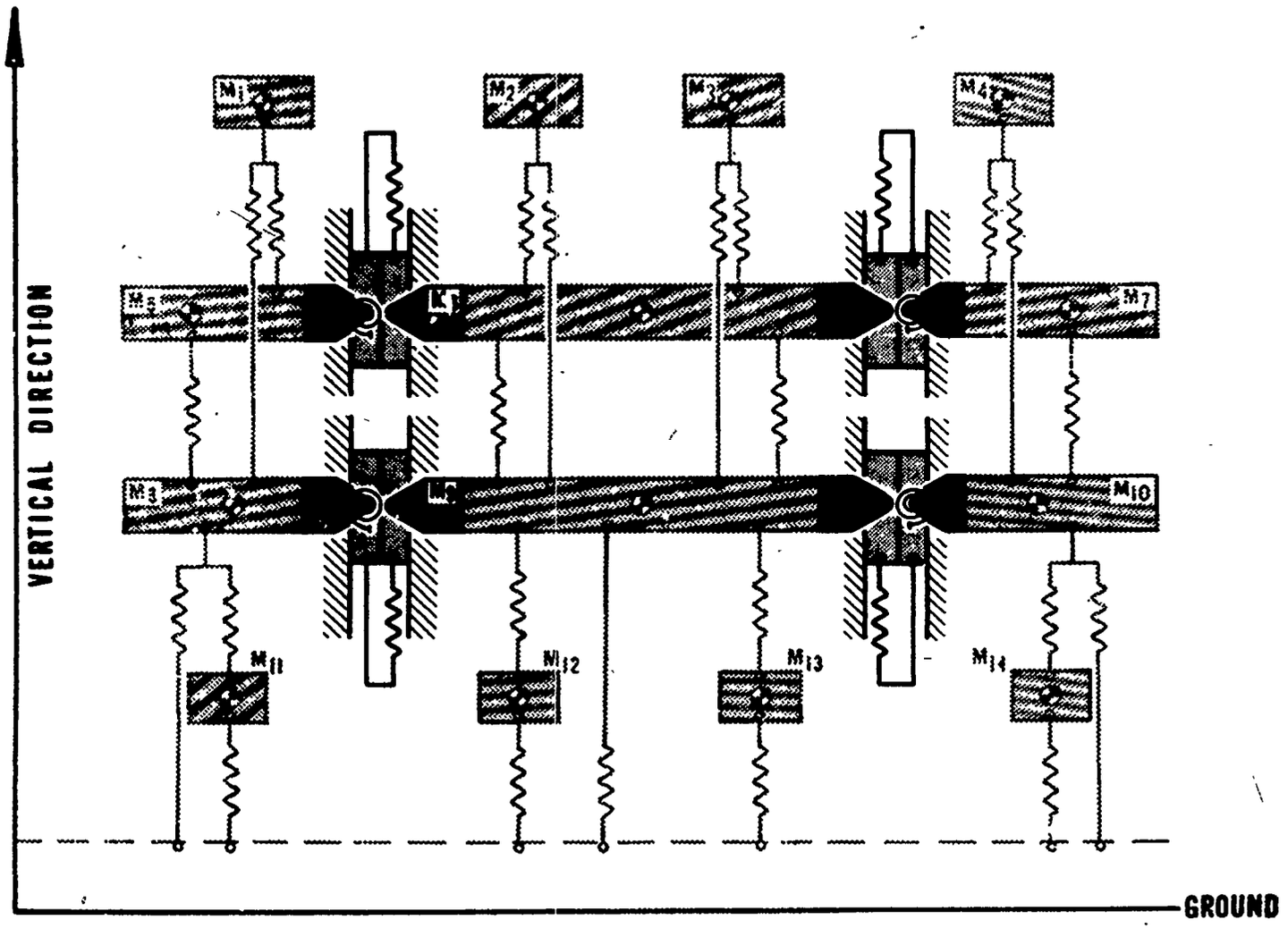

Figure 15. Longitudinal Section Spring Connection Diagram.

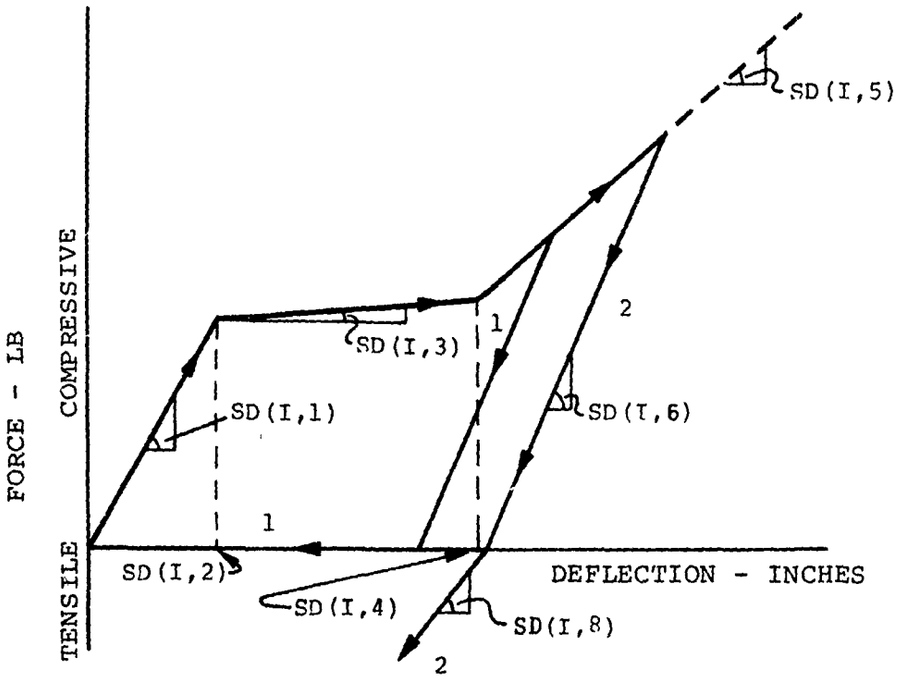

Figure 16. Description of Load-Deflection Curve.

PARAMETER	DESCRIPTION
SD(1,1)	Slope of linear elastic portion of curve.
SD(I,2)	Deflection that causes yielding to occur.
SD(I,3)	Slope of first plastic portion.
SD(I,4)	Deflection at which plastic slope changes.
SD(I,5)	Slope of second plastic portion of curve.
SD(I,6)	Unloading slope.
SD(I,7)	1 {Spring type}, Type "1" follows curve 1 2 {Spring type}, Type "2" follows curve 2
SD(I,8)	Proportionality constant for viscous damping (applies to entire curve).

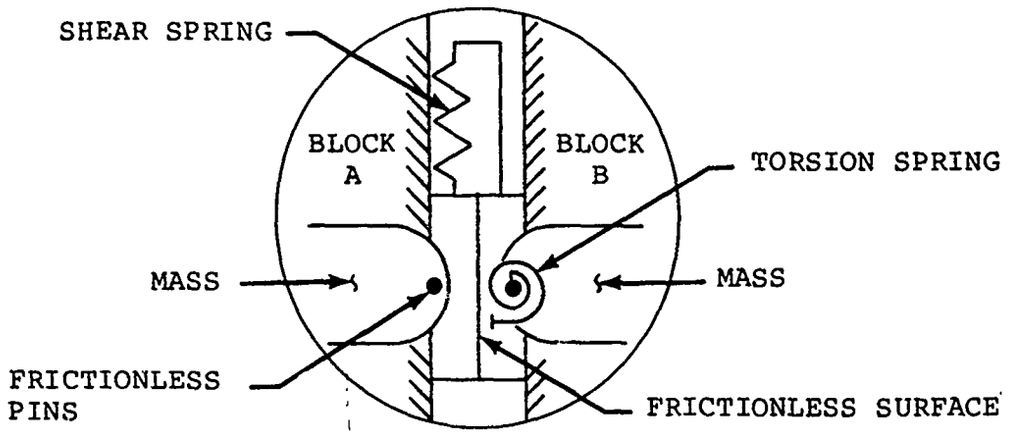

by the torsion spring. This simulates the formation of a plastic hinge in the fuselage. The generalized load-deflection curve used for all springs is shown in Figure 16.

INITIAL CONDITIONS

To initiate a problem solution, 43 initial conditions are required at the time of impact ($t = 0$). The initial velocity and position of each of the 20 generalized coordinates constitute 40 of these conditions that are to be applied to the 20 differential equations. The ground deformation at time of impact provides the remaining three initial conditions. As the problem solution continues, the ground deformations are controlled by the interaction forces between the ground and airframe structure, in the form of fourth-order algebraic equations.

The model responds only to vertical impact; however, the vertical (sink) velocity of each mass may be different, allowing the capability to simulate zero, plus, or minus pitch rates at impact. The airframe structure may be either intact or broken at the time of ground impact.

The transient response of this system within the first 100 milliseconds will serve as the mathematical tool in studying the load-limiting properties.

COMPUTER SIMULATOR MODEL

This section contains the derivation of equations of motion, numerical procedure, computer input notation, and computer simulator output information. Symbols used in the equations are indicated on the List of Symbols. Model coordinates are shown in Figure 17; model dimensions are shown in Figure 18. Reference should be made to Figures 14, 17, and 18 for mass and spring locations mentioned in the following text.

Subsequent to the completion of this study, the computer program underwent minor modification. Input data requirements were reduced, output formats were added or changed where necessary, and reprogramming for use on a second digital computer was completed. The output formats shown in this (Vol. I) report are representative of those obtained with the program prior to modification. The program, as it presently exists after modification, is described in Vol. II (User Manual) of this report. Listings, input coding forms, and additional sample problem output are also included in Vol. II.

DERIVATION OF EQUATIONS OF MOTION

The conventional Newtonian approach is used to obtain the equations of motion. Consider a free-body diagram of Mass (M1),

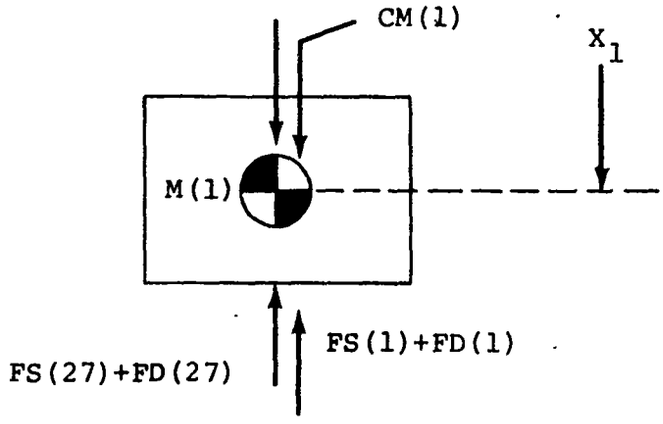

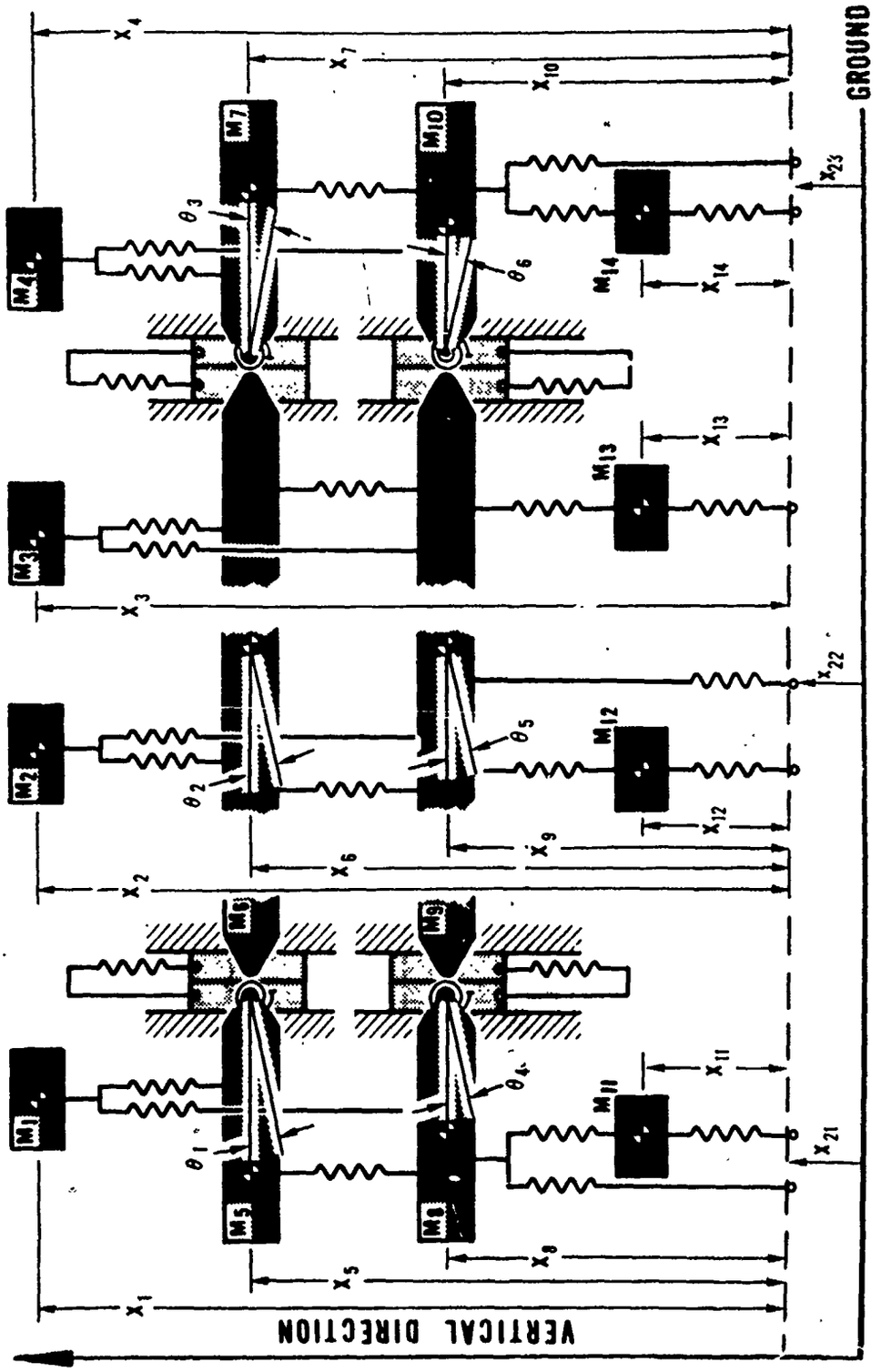

Figure 17. Model Coordinates.

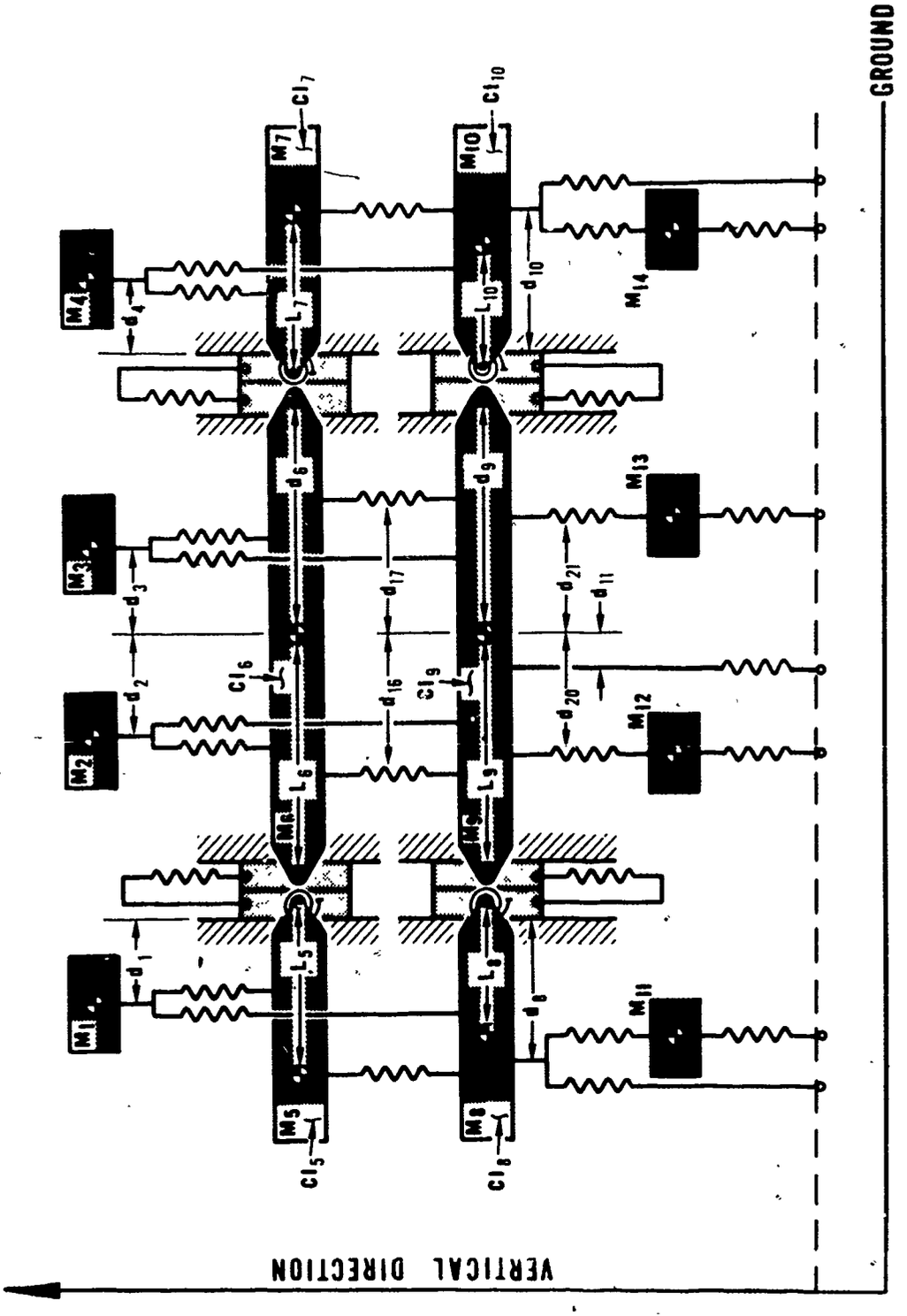

Figure 18. Model Dimensions.

Applying Newton's second law, where displacements, velocities, and accelerations are positive downward,

$$- FS(27) - FD(27) - FS(1) - FD(1) + CM(1) = M(1)\ \ddot{X}_1 \qquad (1)$$

where FS and FD are functions of the relative displacements and velocities experienced by springs (K1) and (K27). Therefore,

$$\begin{aligned} FS(1) &= f_{1s}\ (X_1 - (X_5 + d_1\ \text{SIN}\ \theta_1)) \\ FD(1) &= f_{1d}\ (\dot{X}_1 - (\dot{X}_5 + d_1\ \dot{\theta}_1\ \text{COS}\ \theta_1)) \\ FS(27) &= f_{27s}\ (X_1 - (X_8 + d_1\ \text{SIN}\ \theta_4)) \\ FD(27) &= f_{27d}\ (\dot{X}_1 - (\dot{X}_8 + d_1\ \dot{\theta}_4\ \text{COS}\ \theta_4)) \end{aligned} \qquad (2)$$

The free-body diagrams of masses (M2), (M3), and (M4) are similar to mass (M1). A summary of the equations of motion follows.

For mass (M2),

$$- FS(2) - FD(2) + CM(2) - FS(28) - FD(28) = M(2)\ \ddot{X}_2 \qquad (3)$$

where

$$\begin{aligned} FS(2) &= f_{2s}\ (X_2 - (X_6 + d_2\ \text{SIN}\ \theta_2)) \\ FD(2) &= f_{2d}\ (\dot{X}_2 - (\dot{X}_6 + d_2\ \dot{\theta}_2\ \text{COS}\ \theta_2)) \\ FS(28) &= f_{28s}\ (X_2 - (X_9 + d_2\ \text{SIN}\ \theta_5)) \\ FD(28) &= f_{28d}\ (\dot{X}_2 - (\dot{X}_9 + d_2\ \dot{\theta}_5\ \text{COS}\ \theta_5)) \end{aligned} \qquad (4)$$

For mass (M3),

$$- FS(3) - FD(3) + CM(3) - FS(29) - FD(29) = M(3)\ \ddot{X}_3 \qquad (5)$$

where

$$\begin{aligned} FS(3) &= f_{3s}\ (X_3 - (X_6 - d_3\ \text{SIN}\ \theta_2)) \\ FD(3) &= f_{3d}\ (\dot{X}_3 - (\dot{X}_6 - d_3\ \dot{\theta}_2\ \text{COS}\ \theta_2)) \\ FS(29) &= f_{29s}\ (X_3 - (X_9 - d_3\ \text{SIN}\ \theta_5)) \\ FD(29) &= f_{29d}\ (\dot{X}_3 - (\dot{X}_9 - d_3\ \dot{\theta}_5\ \text{COS}\ \theta_5)) \end{aligned} \qquad (6)$$

For mass (M4),

$$- FS(4) - FD(4) + CM(4) - FS(30) - FD(30) = M(4)\ \ddot{X}_4 \qquad (7)$$

where

$$\begin{aligned} FS(4) &= f_{4s}\ (X_4 - (X_7 + d_4\ SIN\ \theta_3)) \\ FD(4) &= f_{4d}\ (\dot{X}_4 - (\dot{X}_7 + d_4\ \dot{\theta}_3\ COS\ \theta_3)) \\ FS(30) &= f_{30s}\ (X_4 - (X_{10} + d_4\ SIN\ \theta_6)) \\ FD(30) &= f_{30d}\ (\dot{X}_4 - (\dot{X}_{10} + d_4\ \dot{\theta}_6\ COS\ \theta_6)) \end{aligned} \qquad (8)$$

The free-body diagram of mass (M5) is

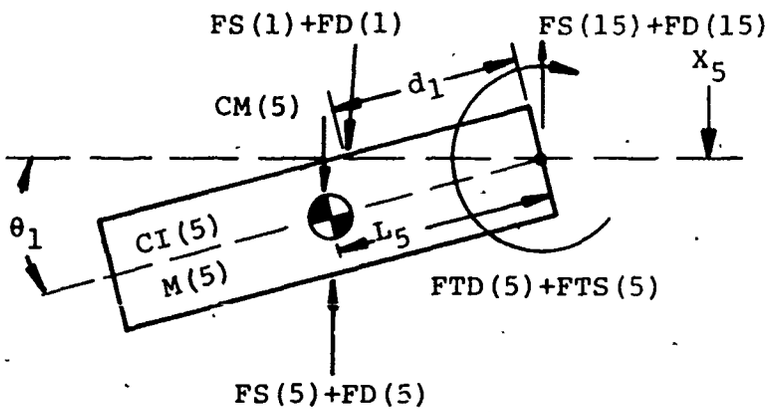

Summation of forces:

$$- FS(5) - FD(5) - FS(15) - FD(15) + FD(1) + FS(1) + CM(5) = M(5)\ (\ddot{X}_5 + L_5\ \ddot{\theta}_1\ COS\ \theta_1 - L_5\ \dot{\theta}^2_1\ SIN\ \theta_1) \qquad (9)$$

where

$$\begin{aligned} FS(5) &= f_{5s}\ ((X_5 + L_5\ SIN\ \theta_1) - (X_8 + L_5\ SIN\ \theta_4)) \\ FD(5) &= f_{5d}\ ((\dot{X}_5 + L_5\ \dot{\theta}_1\ COS\ \theta_1) - (\dot{X}_8 + L_5\ \dot{\theta}_4\ COS\ \theta_4)) \\ FS(15) &= f_{15s}\ (X_5 - (X_6 + L_6\ SIN\ \theta_2)) \\ FD(15) &= f_{15d}\ (\dot{X}_5 - (\dot{X}_6 + L_6\ \dot{\theta}_2\ COS\ \theta_2)) \end{aligned} \qquad (10)$$

Summation of moments about the mass center gives

$$- (FD(1) + FS(1)) (L_5 - d_1) \cos \theta_1 + (FD(15) + FS(15)) L_5 \cos \theta_1 - FTS(5) - FTD(5) = CI(5) \ddot{\theta}_1 \quad (11)$$

where

$$FTS(5) = f_{5ts} (\theta_1)$$

$$FTD(5) = f_{5td} (\dot{\theta}_1) \quad (12)$$

Free body diagram of mass (M6):

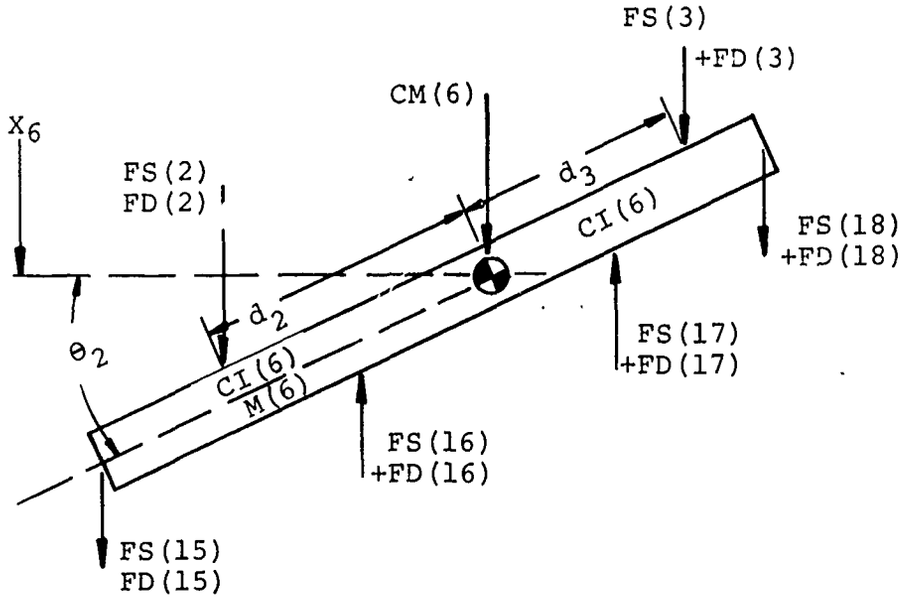

Summation of forces:

$$- FD(16) - FS(16) - FD(17) - FS(17) + FD(2) + FS(2) + FD(3) + FS(3) + FD(18) + FS(18) + FD(15) + FS(15) + CM(6) = M(6) \ddot{X}_6 \quad (13)$$

where

$$FS(16) = f_{16s}\ (\dot{X}_6 - X_9 + (d_{16} + L_9 - L_6)(\text{SIN}\ \theta_2 - \text{SIN}\ \theta_5))$$

$$FD(16) = f_{16d}\ (\dot{X}_6 - \dot{X}_9 + (d_{16} + L_9 - L_6)(\dot{\theta}_2\ \text{COS}\ \theta_2 - \dot{\theta}_5\ \text{COS}\ \theta_5))$$

$$FS(17) = f_{17s}\ (X_6 - X_9 + (d_{17} - L_9 + L_6)(\text{SIN}\ \theta_5 - \text{SIN}\ \theta_2)) \qquad (14)$$

$$FD(17) = f_{17d}\ (\dot{X}_6 - \dot{X}_9 + (d_{17} - L_9 + L_6)(\dot{\theta}_5\ \text{COS}\ \theta_5 - \dot{\theta}_2\ \text{COS}\ \theta_2))$$

$$FS(18) = f_{18s}\ (X_7 - (X_6 - L_6\ \text{SIN}\ \theta_2))$$

$$FD(18) = f_{18d}\ (\dot{X}_7 - (\dot{X}_6 - L_6\ \dot{\theta}_2\ \text{COS}\ \theta_2))$$

Summation of moments about mass center:

$$(FS(17) + FD(17))(d_{17} - L_9 + L_6)\ \text{COS}\ \theta_2 - (FS(16) + FD(16))$$

$$(d_{16} + L_9 - L_6)\ \text{COS}\ \theta_2 - (FS(18) + FD(18))\ d_6\ \text{COS}\ \theta_2$$

$$+ (FS(15) + FD(15))\ L_6\ \text{COS}\ \theta_2 + (FS(2) + FD(2))\ d_2\ \text{COS}\ \theta_2$$

$$- (FS(3) + FD(3))\ d_3\ \text{COS}\ \theta_2 = CI(6)\ \ddot{\theta}_2 \qquad (15)$$

Free-body diagram of mass (M7):

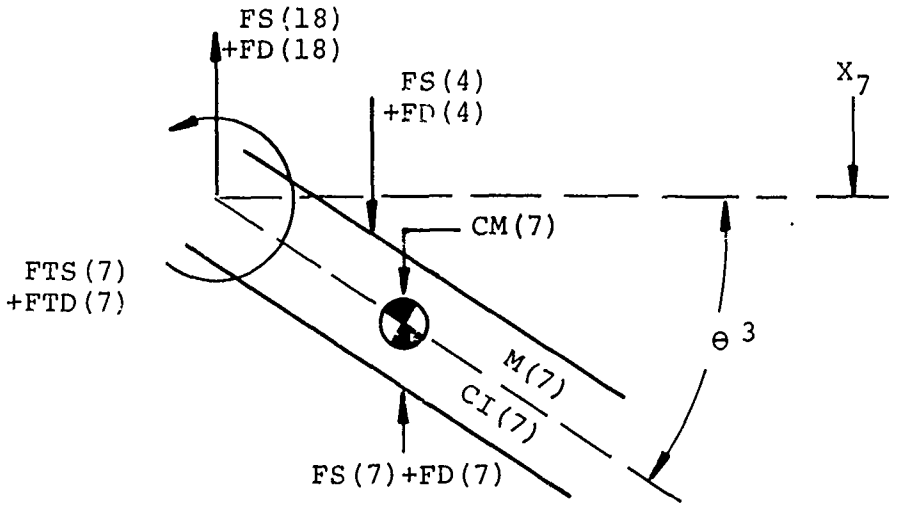

Summation of forces:

$$-FS(7) - FD(7) - FS(18) - FD(18) + FS(4) + FD(4) + CM(7)$$
$$= M(7)(\ddot{X}_7 + L_7 \ddot{\theta}_3 \cos \theta_3 - L_7 \dot{\theta}_3^2 \sin \theta_3) \quad (16$$

where

$$FS(7) = f_{7s}((X_7 + L_7 \sin \theta_3) - (X_{10} + L_7 \sin \theta_6))$$
$$FD(7) = f_{7d}((\dot{X}_7 + L_7 \dot{\theta}_3 \cos \theta_3) - (\dot{X}_{10} + L_7 \dot{\theta}_6 \cos \theta_6)) \quad (17)$$

Summation of moments about mass center:

$$(FS(18) + FD(18)) L_7 \cos \theta_3 - (FS(4) + FD(4))$$
$$(L_7 - d_4) \cos \theta_3 - FTS(7) - FTD(7) = CI(7) \ddot{\theta}_3 \quad (18)$$

where

$$FTS(7) = f_{7ts}(\theta_3)$$
$$FTD(7) = f_{7td}(\dot{\theta}_3) \quad (19)$$

Free-body diagram for mass (M8):

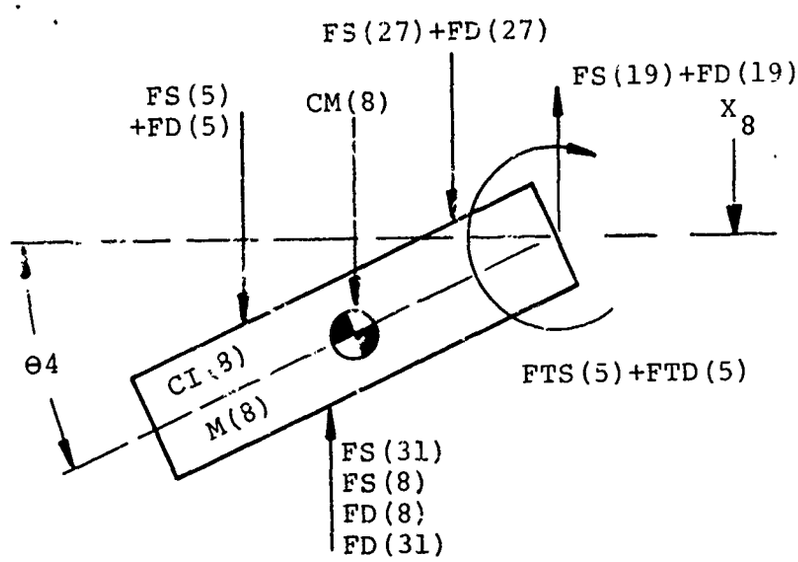

Summation of Forces:

$$- FD(31) - FS(31) - FD(8) - FS(8) + FD(5) + FS(5) + FS(27) + FD(27) - FS(19) - FD(19) + CM(8) = M(8)(\ddot{X}_8 + L_8 \ddot{\theta}_4 \cos \theta_4 - L_3 \dot{\theta}_4^2 \sin \theta_4) \quad (20)$$

where

$$\begin{aligned} FS(8) &= f_{8s}(X_8 - X_{11} + d_8 \sin \theta_4) \\ FD(8) &= f_{8d}(\dot{X}_8 - \dot{X}_{11} + \dot{\theta}_4 d_8 \cos \theta_4) \\ FS(19) &= f_{19s}(X_3 - (X_9 + L_9 \sin \theta_5)) \\ FD(19) &= f_{19d}(\dot{X}_8 - (\dot{X}_9 + L_9 \dot{\theta}_5 \cos \theta_5)) \\ FS(31) &= f_{31s}(X_8 + d_8 \sin \theta_4) \\ FD(31) &= f_{31d}(\dot{X}_8 + d_8 \dot{\theta}_4 \cos \theta_4) \end{aligned} \quad (21)$$

Summation of moments:

$$(FD(5) + FS(5))(L_5 - L_8) \cos \theta_4 + (FD(19) + FS(19)) L_8 \cos \theta_4 - FTS(8) - FTD(8) + (FS(31) + FD(31) + FS(8) + FD(8))(L_8 - d_8) \cos \theta_4 - (FS(27) + FD(27))(L_8 - d_1) \cos \theta_4 = CI(8) \ddot{\theta}_4 \quad (22)$$

where

$$\begin{aligned} FTS(8) &= f_{8ts}(\theta_4) \\ FTD(8) &= f_{8td}(\dot{\theta}_4) \end{aligned} \quad (23)$$

For mass (M9), see free-body diagram for mass (M6).

Summation of forces:

$$- FS(20) - FD(20) - FS(21) - FD(21) + FS(19) + FD(19) - FS(32) - FD(32) + FS(2) + FD(2) + FS(3) + FD(3) + FS(16) + FD(16) + FS(17) + FD(17) + FD(22) + CM(9) + FS(22) = M(9) \ddot{X}_9 \quad (24)$$

where

$$
\begin{aligned}
FS(20) &= f_{20s}\ (X_9 + d_{20}\ \text{SIN}\ \theta_5 - X_{12}) \\
FD(20) &= f_{20d}\ (\dot{X}_9 + d_{20}\ \dot{\theta}_5\ \text{COS}\ \theta_5 - \dot{X}_{12}) \\
FS(21) &= f_{21s}\ (X_9 - d_{21}\ \text{SIN}\ \theta_5 - X_{13}) \\
FD(21) &= f_{21d}\ (\dot{X}_9 - d_{21}\ \dot{\theta}_5\ \text{COS}\ \theta_5 - \dot{X}_{13}) \\
FS(22) &= f_{22s}\ (X_{10} - (X_9 - L_9\ \text{SIN}\ \theta_5)) \\
FD(22) &= f_{22d}\ (\dot{X}_{10} - (\dot{X}_9 - L_9\ \dot{\theta}_5\ \text{COS}\ \theta_5)) \\
FS(32) &= f_{32s}\ (X_9 + d_{11}\ \text{SIN}\ \theta_5) \\
FS(32) &= f_{32d}\ (\dot{X}_9 + d_{11}\ \dot{\theta}_5\ \text{COS}\ \theta_5)
\end{aligned}
\tag{25}
$$

Summation of moments about mass center:

$$
\begin{aligned}
&(FD(19) + FS(19))\ L_9\ \text{COS}\ \theta_5 + (FD(16) + FS(16)) \\
&d_{16}\ \text{COS}\ \theta_5 - (FD(17) + FS(17))\ d_{17}\ \text{COS}\ \theta_5 - (FD(22) \\
&+ FS(22))\ d_9\ \text{COS}\ \theta_5 - (FD(20) + FS(20))\ d_{20}\ \text{COS}\ \theta_5 \\
&+ (FD(21) + FS(21))\ d_{21}\ \text{COS}\ \theta_5 - (FS(32) + FD(32)) \\
&d_{11}\ \text{COS}\ \theta_5 + ((L_9 - L_6) + d_2)(FS(2) + FD(2))\ \text{COS}\ \theta_5 \\
&- (d_3 - (L_9 - L_6))(FS(3) + FD(3))\ \text{COS}\ \theta_5 = CI(9)\ \ddot{\theta}_5
\end{aligned}
\tag{26}
$$

Free-body diagram for mass (M.0):

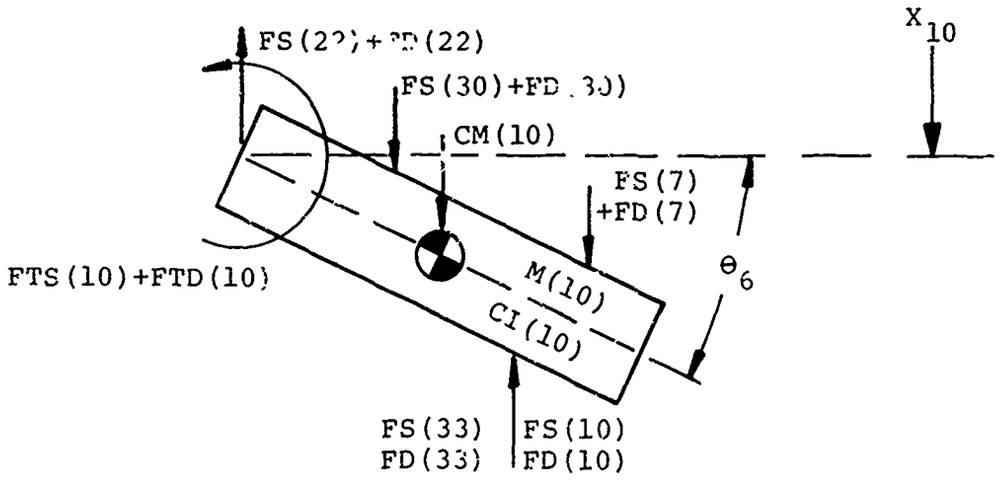

Summation of forces:

$$- FS(33) - FD(33) - FS(10) - FD(10) - FD(22) - FS(22)$$
$$+ FS(7) + FD(7) + FS(30) + FD(30) + CM(10)$$
$$= M(10)(\ddot{X}_{10} + L_{10}\ddot{\theta}_6 \cos\theta_6 - L_{10}\dot{\theta}_6^2 \sin\theta_6) \quad (27)$$

where

$$FS(10) = f_{10s}(X_{10} + d_{10}\sin\theta_6 - X_{14})$$
$$FD(10) = f_{10d}(\dot{X}_{10} + d_{10}\dot{\theta}_6\cos\theta_6 - \dot{X}_{14}) \quad (28)$$
$$FS(33) = f_{33s}(X_{10} + d_{10}\sin\theta_6)$$
$$FD(33) = f_{33d}(\dot{X}_{10} + d_{10}\dot{\theta}_6\cos\theta_6)$$

Summation of moments about mass center:

$$(FD(22) + FS(22))L_{10}\cos\theta_6 + (FD(7) + FS(7))(L_7 - L_{10})$$
$$\cos\theta_6 - FTS(10) - FTD(10) + FD(10) + FS(32)$$
$$+ FD(32))(L_{10} - d_{10})\cos\theta_6 - (FS(30) + FD(30))(L_{10} - d_4)$$
$$\cos\theta_6 = CI(10)\ddot{\theta}_6 \quad (29)$$

where

$$FTS(10) = f_{10ts}(\theta_6)$$
$$FTD(10) = f_{10ts}(\dot{\theta}_6) \quad (30)$$

Free-body diagram for mass (M11):

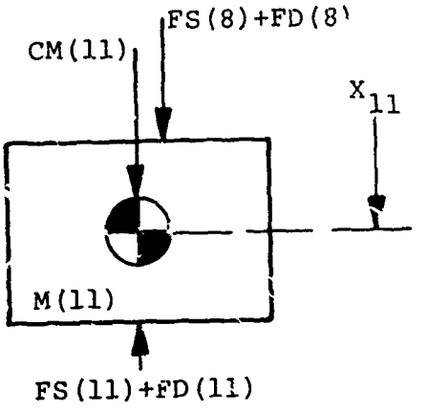

Summation of forces:

$$- FS(11) - FD(11) + FS(8)' + FD(8) + CM(11) = M(11)\ \ddot{X}_{11} \tag{31}$$

where

$$\begin{aligned} FS(11) &= f_{11s}\ (X_{11}) \\ FD(11) &= f_{11d}\ (\dot{X}_{11}) \end{aligned} \tag{32}$$

For mass (M12), refer to free-body diagram for mass (M11).

Summation of forces:

$$- FS(12) - FD(12) + FS(20) + FD(20) + CM(12) = M(12)\ \ddot{X}_{12} \tag{33}$$

where

$$\begin{aligned} FS(12) &= f_{12s}\ (X_{12}) \\ FD(12) &= f_{12d}\ (\dot{X}_{12}) \end{aligned} \tag{34}$$

For mass (M13), refer to free-body diagram for mass (M11).

Summation of forces:

$$- FS(13) - FD(13) + FS(21) + FD(21) + CM(13) = M(13)\ \ddot{X}_{13} \tag{35}$$

where

$$\begin{aligned} FS(13) &= f_{13s}\ (X_{13}) \\ FD(13) &= f_{13d}\ (\dot{X}_{13}) \end{aligned} \tag{36}$$

For mass (M14), refer to free-body diagram for mass (M11).

Summation of forces:

$$- FS(14) - FD(14) + FS(10) + FD(10) + CM(14) = M(14)\ \ddot{X}_{14} \tag{37}$$

where

$$\begin{aligned} FS(14) &= f_{14s}\ (X_{14}) \\ FD(14) &= f_{14d}\ (\dot{X}_{14}) \end{aligned} \tag{38}$$

The interaction between the fuselage and ground is mathematically represented by three fourth-order algebraic equations. The deflections of coordinates X_{21}, X_{22}, X_{23} are computed as functions of the forces in springs K_{31}, K_{32}, and K_{33}.

$$X_{21} = G_1 \ (FS(31))$$
$$X_{22} = G_2 \ (FS(32)) \qquad (39)$$
$$X_{23} = G_3 \ (FS(33))$$

where

$$Gj = GD(j,1)\ FS(j + 30) + GD(j,2)\ FS(j + 30)^2 + GD(j,3)\ FS(j + 30)^3 + GD(j,4)\ FS(j + 30)^4$$

$$\text{for } j = 1, 2, 3 \qquad (40)$$

NUMERICAL PROCEDURE

Equations (1) through (39) represent the equations of motion of the 23-degree-of-freedom model shown in Figure 13. They define a set of 20 simultaneous nonlinear, second-order, ordinary differential equations.

Restating equations (1) and (2):

$$\ddot{X}_1 \ M(1) = - FS(1) - FD(1) - FS(27) - FD(27) + CM(1) \qquad (41)$$

$$\begin{aligned} FS(1) &= f_{1s} \ (X_1 - (X_5 + d_1 \ SIN \ \theta_1)) \\ FD(1) &= f_{1d} \ (\dot{X}_1 - (\dot{X}_5 + d_1 \ \dot{\theta}_1 \ COS \ \theta_1)) \\ FS(27) &= f_{27s} \ (X_1 - (X_8 + d_1 \ SIN \ \theta_4)) \\ FD(27) &= f_{27d} \ (\dot{X}_1 - (\dot{X}_8 + d_1 \ \dot{\theta}_4 \ COS \ \theta_4)) \end{aligned} \qquad (42)$$

Equation (1) may therefore be expressed functionally as:

$$\ddot{X}_1 = F \ (X_1, X_5, X_8, \theta_1, \theta_4, \dot{X}_1, \dot{X}_5, \dot{X}_8, \dot{\theta}_1, \dot{\theta}_4) \qquad (43)$$

Let $\theta_1, \theta_2, \ldots \theta_6$ be represented by $X_{15}, X_{16}, \ldots X_{20}$

Then, equation (43) may be written as:

$$\ddot{X}_1 = F \ (X_1, X_5, X_8, X_{15}, X_{18}, \dot{X}_1, \dot{X}_5, \dot{X}_8, \dot{X}_{15}, \dot{X}_{18})$$

or, generalizing:

$$\ddot{X}_i = F \ (X_1, \ldots X_{20}, \dot{X}_1, \ldots \dot{X}_{20}) \qquad (44)$$

All of the equations of motion except four (9), (16), (20), and (27) are represented by the general form (44).

These four equations are written as,

$$\ddot{X}_1 = F\ (X_1, \ldots X_{20}, \dot{X}_1, \ldots \dot{X}_{20}, \ddot{X}_j) \tag{45}$$

Notice that in these four cases, $\ddot{X}_i$ (i = 5, 7, 8, 10) are functions of $\ddot{X}_j$ (j = 15, 17, 18, 20) respectively. Therefore, $\ddot{X}_{15}$, $\ddot{X}_{17}$, $\ddot{X}_{18}$, $\ddot{X}_{20}$ in the form of (44) are substituted into, $\ddot{X}_5$, $\ddot{X}_7$, $\ddot{X}_8$, $\ddot{X}_{10}$ to reduce all 20 equations to the common form as given in (44). This substitution is accomplished numerically rather than algebraically due to the complex form of the nonlinear characteristics of the springs.

The resulting motion of the mathematical model is summarized by the following initial value problem:

$$\ddot{X}_i = F_i\ (X_j, \dot{X}_j) \qquad j = 1, 2, \ldots 20;\ i = 1, 2, \ldots 20 \tag{46}$$

with initial conditions

$$X_i(o) = XI(i)$$
$$\dot{X}_i(o) = XDI(i) \qquad i = 1, 2, \ldots 20 \tag{47}$$

Now, let:

$$Z_i = \dot{X}_i \tag{48a}$$

Then:

$$\dot{Z}_i = \ddot{X}_i \tag{48b}$$

Substitution of (48b) in (46) yields

$$\dot{Z}_i = F_i\ (X_j, \dot{X}_j) \qquad j = 1, 2, \ldots 20 \qquad i = 1, 2, \ldots 20 \tag{49}$$

with initial conditions:

$$X_i(o) = XI(i)$$
$$Z_i(o) = XDI(i) \tag{50}$$

The second-order set of 20 equations (46) and associated initial conditions (47) are transformed into a set of 40 first-order equations (48a, 49) and initial conditions (50).

The fourth-order Runge-Kutta method is employed to numerically solve the above set of equations. The outline of the method is briefly described for completeness.

The position of the jth coordinate, X_j, at a time corresponding to $(N + 1)$ time increments is given by:

$$X_j (N + 1) = X_j (N) + 1/6 (k_1 + 2k_2 + 2k_3 + k_4)$$

$$J = 1, \ldots 40 \quad (51)$$

where

$$\begin{aligned} k_1 &= (\Delta T) F_j (X_j (N)) \\ k_2 &= (\Delta T) F_j (X_j (N) + 1/2 k_1) \\ k_3 &= (\Delta T) F_j (X_j (N) + 1/2 k_2) \\ k_4 &= (\Delta T) F_j (X_j (N) + k_3) \end{aligned} \quad (52)$$

$$J = 1, \ldots 40$$

and where: ΔT = time increment of the numerical calculation

F_j = functional relationships of equations (48a) and (49)

Summarizing,

X = displacement

$Z = \dot{X}$ = velocity

$\dot{Z} = \ddot{X}$ = acceleration

COMPUTER INPUT NOTATION

Input to the computer simulator is entered through the main program and subroutine "READ". All input is matched with one of the following formats: 7A1, 16I5, and 8E10.0. Acronymic and abbreviated titles are assigned to the input and internal parameters and are listed in the List of Symbols. If the acronym for a floating-point variable is one of the fixed-point letters, the acronym or abbreviation is, generally, preceded by the letter C.

COMPUTER SIMULATOR OUTPUT

The output from the computer simulator consists of (1) a tabulation of the input data concerning initial velocity, weight, initial position, angular rotation, and moment of inertia for the 14 masses which make up the model, (2) a tabulation of the input data concerning the spring constants for the 33 springs which connect the masses, and (3) combination tabulations and plots of the computed data for any of the 129 parameters shown in Table V. Items (1) and (2) above will be printed out for every run, without input instructions. The parameters to be plotted in Item (3) must be specifically requested by code number through input. Only those parameters so requested will be plotted as output.

A further discussion of the output format, along with specific examples, will be found in the following section.

TABLE V. DESCRIPTION OF PLOTTING CODE USED FOR COMPUTER OUTPUT

Definition: KP(I,J) = CODE
I = Plot Number
J = Number of Curve on plot I; J = 1, 2, 3

CODE	OUTPUT PARAMETER	
0	Curve Omitted	
1	Vertical Deflection of Coordinate	1
2		2
3		3
4		4
5		5
6		6
7		7
8		8
9		9
10		10
11		11
12		12
13		13
14		14
15	Angle of Mass Number	5
16		6
17		7
18		8
19		9
20		10

TABLE V. Continued

CODE	OUTPUT PARAMETER	
21	Vertical Velocity of Coordinate	1
22		2
23		3
24		4
25		5
26		6
27		7
28		8
29		9
30		10
31		11
32		12
33		13
34		14
35	Angular Velocity of Mass Number	5
36		6
37		7
38		8
39		9
40		10
41	Acceleration of Coordinate Number	1
42		2
43		3
44		4
45		5
46		6
47		7
48		8
49		9
50		10
51		11
52		12
53		13
54		14
55	Angular Acceleration of Mass Number	5
56		6
57		7
58		8
59		9
60		10

TABLE V. Continued

CODE	OUTPUT PARAMETER	
61	Elongation of Spring Number	1
62		2
63		3
64		4
65		5
67		7
68		8
70		10
71		11
72		12
73		13
74		14
75		15
76		16
77		17
78		18
79		19
80		20
81		21
82		22
83	Angular Rotation of Torsional Spring	5
84		7
85		8
86		10
87	Elongation of Far-Coupled Spring Number	27
88		28
89		29
90		30
91		31
92		32
93		33
94	Force in Spring Number	1
95		2
96		3
97		4
98		5
100		7
101		8
103		10
104		11
105		12

TABLE V. Continued

CODE	OUTPUT PARAMETER	
106	Force in Spring Number	13
107		14
108		15
109		16
110		17
111		18
112		19
113		20
114		21
115		22
116	Movement in Torsional Spring Number	5
117		7
118		8
119		10
120	Force in Far-Coupled Spring Number	27
121		28
122		29
123		30
124		31
125		32
126		33
127	Vertical Displacement of Coordinate	21
128		22
129		23

APPLICATION OF COMPUTER SIMULATOR

Input

The computer simulator just discussed was used to investigate the effects of vertical impacts on a UH-1D/H helicopter. This aircraft, shown in Figure 19, is in widespread use by the Army, Air Force, and Marine Corps as a tactical transport. It is a thirteen-place, all-metal helicopter with a single, two-bladed main rotor and a single tail rotor. These studies were run with a twofold purpose: to verify the assumed spring constants used as input, and to obtain base line data for the parametric study to follow.

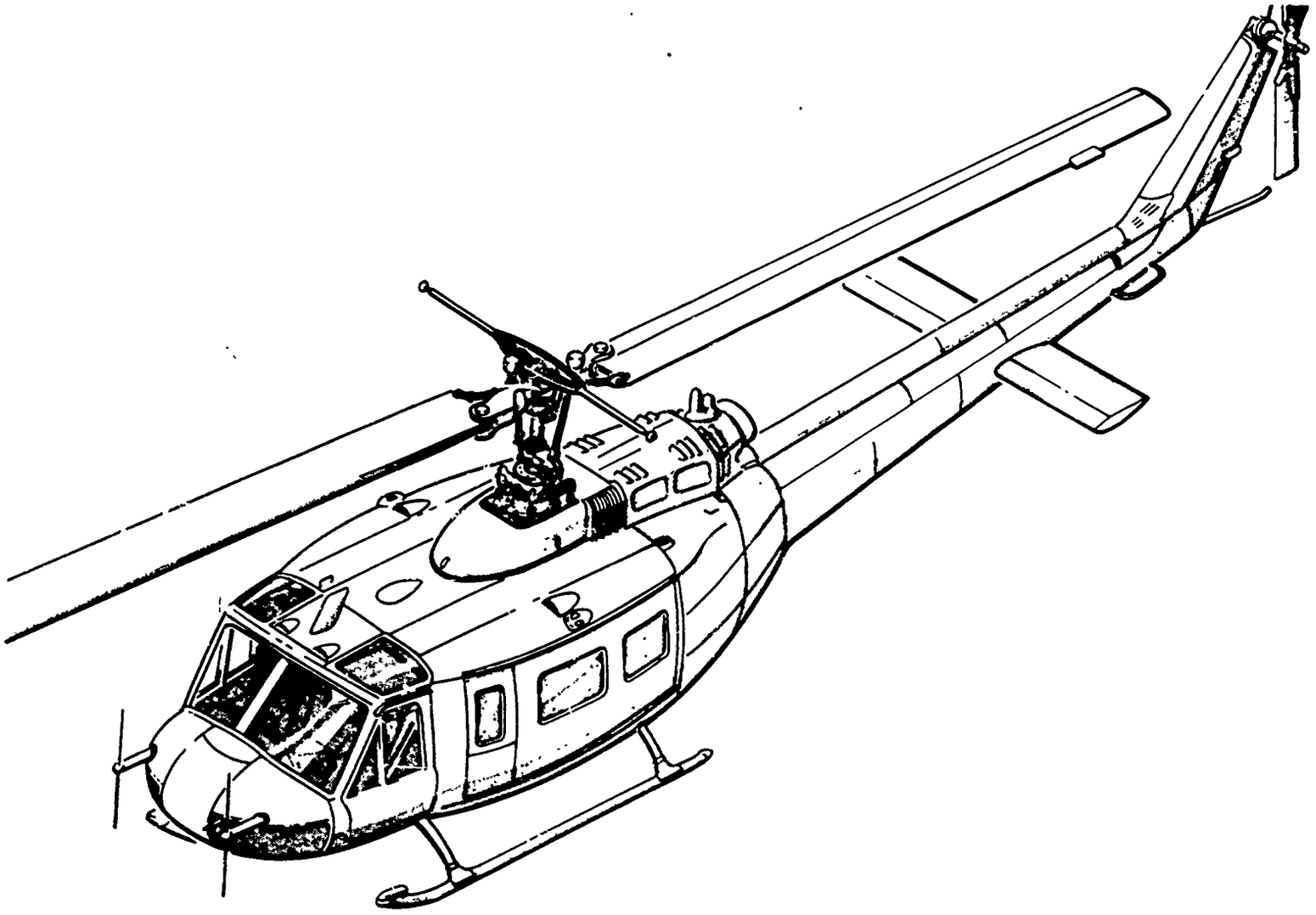

Figure 19. Helicopter Model UH-1D/H.

Two major categories of input data were required; namely, weight data to apply to the lumped mass simulation, and spring constant data to apply to the various springs connecting the masses.

Information supplied by the helicopter manufacturer was used to distribute the weight in the lumped mass model. This weight distribution is shown in Table VI for the empty aircraft and for the aircraft configured as a troop carrier.

TABLE VI. UH-1D/H WEIGHT DISTRIBUTION

MASS NO.	A/C EMPTY (lb)	TROOP CARRIER (lb)	TOTAL (lb)
M1	0	-	0
M2	980	-	980
M3	1047	25	1072
M4	60	-	60
M5	250	-	250
M6	847	1300	2147
M7	230	-	230
M8	1306	1645	2951
M9	270	1100	1370
M10	0	-	0
M11	60	-	60
M12	0	-	0
M13	60	-	60
M14	0	-	0
TOTALS	5110	4070	9180

The helicopter airframe structure was mathematically represented by the system of lumped masses (Figure 20) superimposed on a general side view of the fuselage. Comparison with Figure 13 will illustrate the application of the generalized model to the UH-1D/H helicopter.

Of the 14 masses available in the model, only 10 were used to represent this aircraft. Mass (M1) was not used, since in this aircraft the engine, gearbox, and rotor are located in close proximity. Mass (M2) was used to represent the main rotor assembly, while the engine and gearbox were simulated by

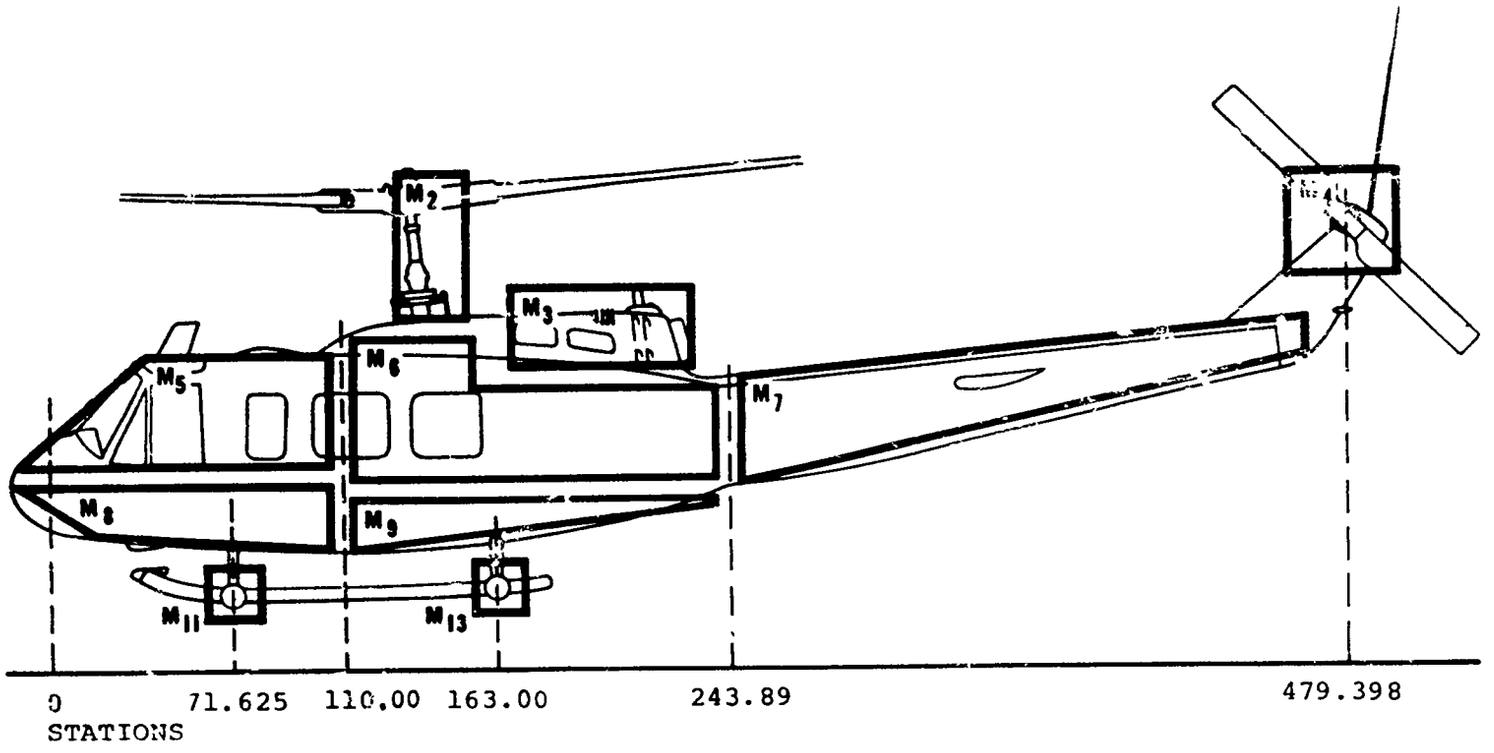

Figure 20. Lump Mass Representation of the UH-1D/H.

mass (M3). Mass (M4) depicts the tail rotor and 90-degree gearbox. The upper portion of the cockpit section was simulated by mass (M5), while mass (M6) represents the upper portion of the passenger compartment and the aft fuel cells. Mass (M7) simulates the tail-boom structure. The floor loads and the structure below the floor including the forward fuel cells were represented by masses (M8) and (M9), which were located to either side of a possible break point in the fuselage. Mass (M10) was not used, although the possibility of employing it in combination with mass (M7) to simulate crushing of the tail boom was considered. However, since the tail-boom weight is small, and since in severe crashes, peak floor accelerations will occur before tail-boom crushing, the effect of this mass would be negligible. Masses (M11) and (M13) were chosen to represent the landing skids. Those masses not used were assigned a weight of 1 pound.

Analysis of accident case histories involving the UH-1D/H aircraft revealed that two possible locations existed for the formation of a plastic hinge, one just forward of the main rotor and another at the juncture of the tail boom and fuselage. The lumped mass model was therefore arranged so that these hinges were simulated between the masses at stations 110.00 and 243.89, as shown in Figure 20.

The load-deflection characteristics of the UH-1D/H airframe structure were simulated by the combinations of springs shown in Figure 21. Comparison with Figure 14 shows the application of the generalized model to this specific case.

Spring constant data for the system were estimated by analysis of accident case histories obtained from the helicopter manufacturer, from the U. S. Army Board for Aviation Accident Research (USABAAR), and by inspection of wrecked airframe structures at the U. S. Army Aeronautical Depot Maintenance Center (ARADMAC).

The main rotor and transmission in the UH-1D/H are supported by a sturdy box structure that ties directly to the floor. To simulate this structure, spring (K2) was omitted from the system and far-coupled spring (K28) was used to support mass (M2) at the floor, so the rotor and transmission loads would bypass the upper fuselage structure. The load-deflection characteristics of the transmission and rotor support system (Figure 22) allow approximately 1/2 inch of elastic deflection at a load of 8,000 pounds before failure of the transmission supports.

The engine mass (M3) is supported by the upper fuselage section mass (M6) through spring (K3), whose load-deflection

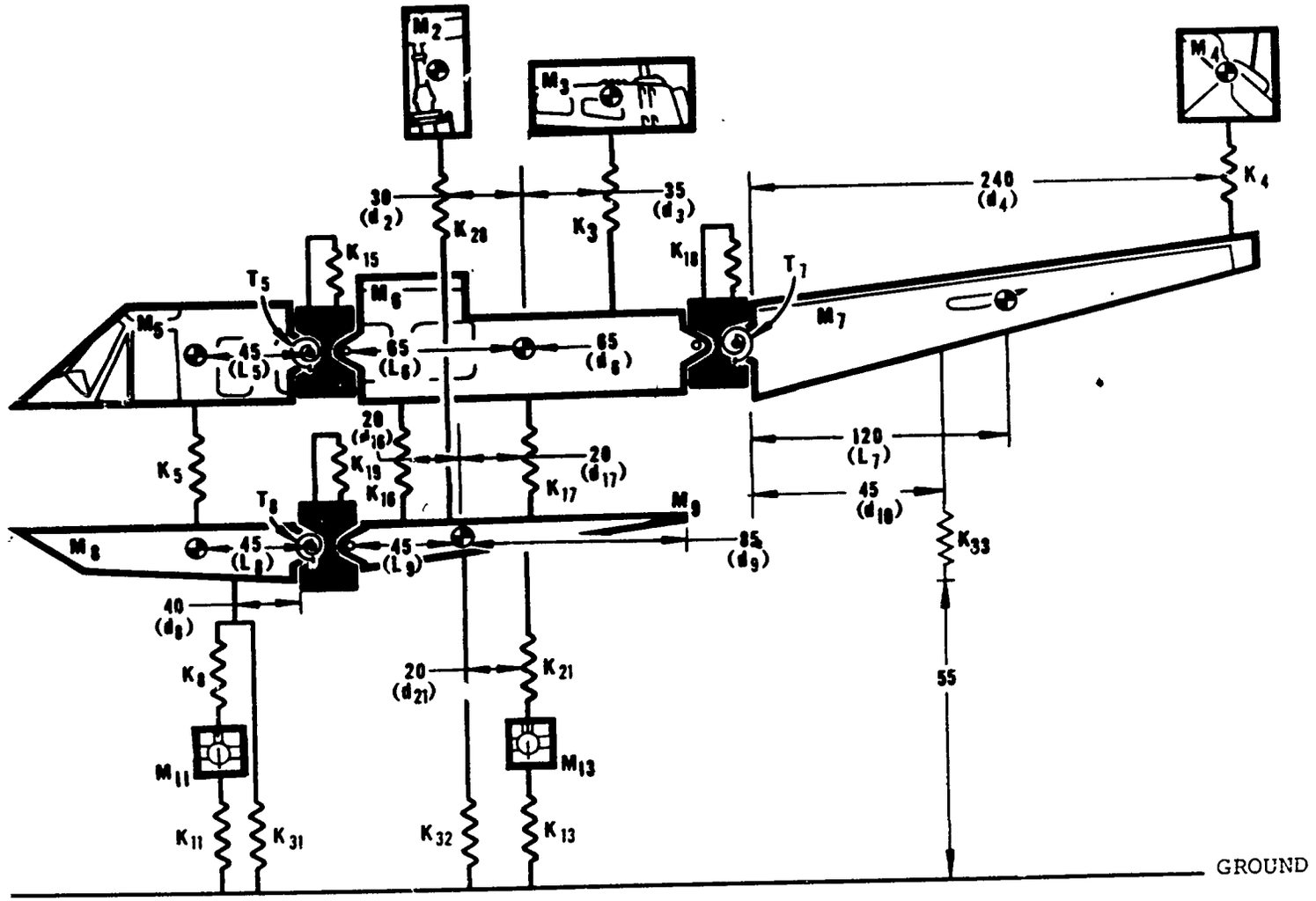

Figure 21. Load-Deflection Characteristics of UH-1D/H.

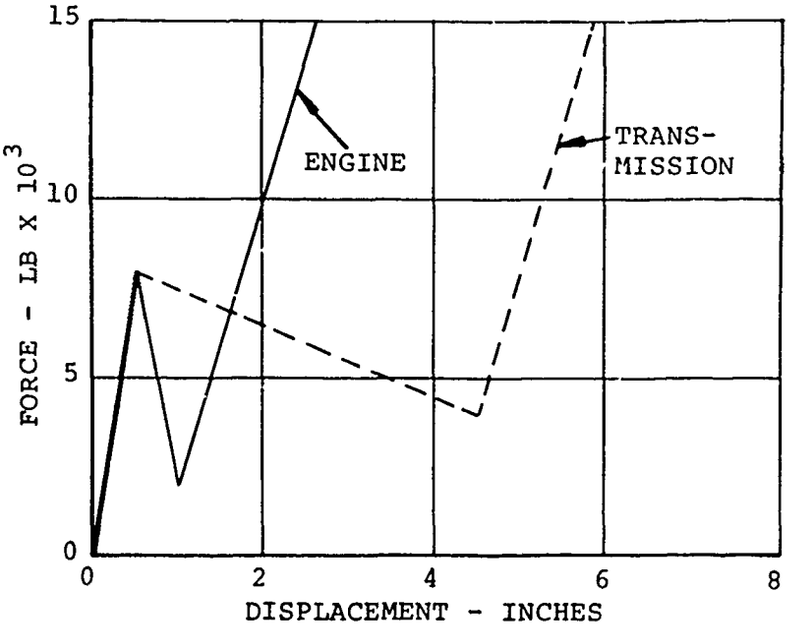

Figure 22. Load-Deflection Curve (Engine and Transmission) for UH-1D/H.

characteristics are similar to those of spring (K28), as shown in Figure 22. The sudden decrease in the load-carrying ability of springs (K3) and (K28) represents local buckling of structural members.

The displacement of the tail-boom mass (M7) is controlled by 3 springs; torsional spring (T7), far-coupled spring (K33), and shear spring (K18). The load-deflection characteristics of spring (T7), shown in Figure 23, permit a 2-degree rotation before a plastic hinge forms. This plastic hinge can then rotate up to 15 degrees before failure occurs and the tail boom becomes incapable of resisting further rotation. This unlimited rotation is controlled by spring (K33), whose characteristics simulate the tail boom striking the ground after a predetermined displacement of the center of gravity of mass (M7). Shear spring (K18) is essentially rigid, so that no shear deformation occurs at the hinge point.

Rotation of the forward portion of fuselage masses (M5) and (M8) about the potential plastic hinge at station 110 (Figure 20) is controlled by torsional springs (T5) and (T8). The load-deflection characteristics of these springs are shown in

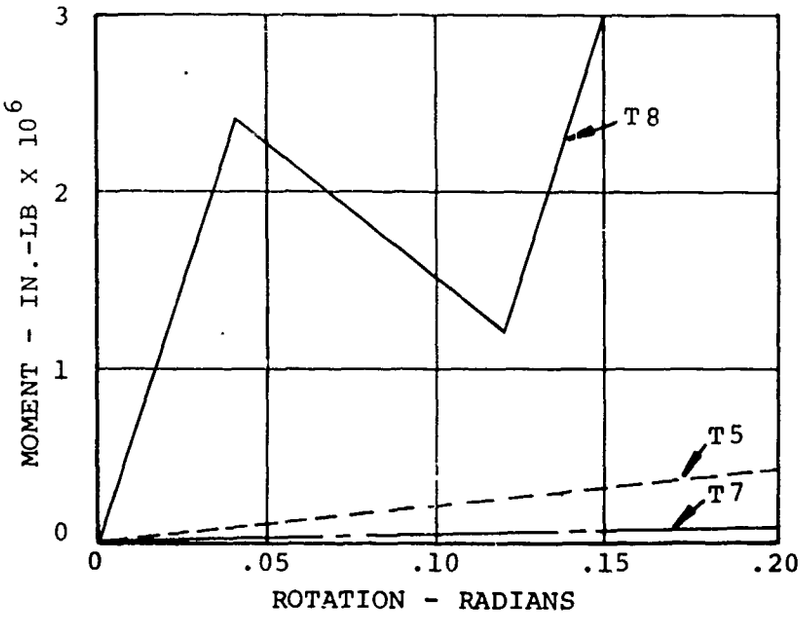

Figure 23. Load-Deflection Curves for Torsional Springs.

Figure 23. Shear springs (K15) and (K19) control shear deformation at the hinge point. As with spring (K18), these shear springs allow no shear deformation.

The load-deflection characteristics of the landing skids are represented by 2 sets of springs, 1 for the forward portion of the skids and 1 for the rear portion. Each set consists of 3 springs, 1 far-coupled and 2 direct-coupled, with springs (K8), (K11), and (K31) representing the front portion of the skids and springs (K13), (K21), and (K32) representing the rear portion. Each of these sets allows simulation of elastic deformation, plastic deformation, skid failure, and ground contact of the fuselage. The load-deflection characteristics of these springs are presented in Figure 24.

Consider the set formed by springs (K8), (K11), and (K31). Spring (K11) allows elastic deformation up to 2 inches with an applied load of 18,000 pounds, at which point the spring becomes essentially rigid. Spring (K8) also allows elastic deformation of approximately 2 inches with an applied load of 18,000 pounds. This spring combination allows a deflection of 4 inches at a total peak load of about 36,000 pounds, or about 2 G on the 9,000-pound aircraft for each gear. Both skids then allow plastic deformation at the 18,000-pound load for an

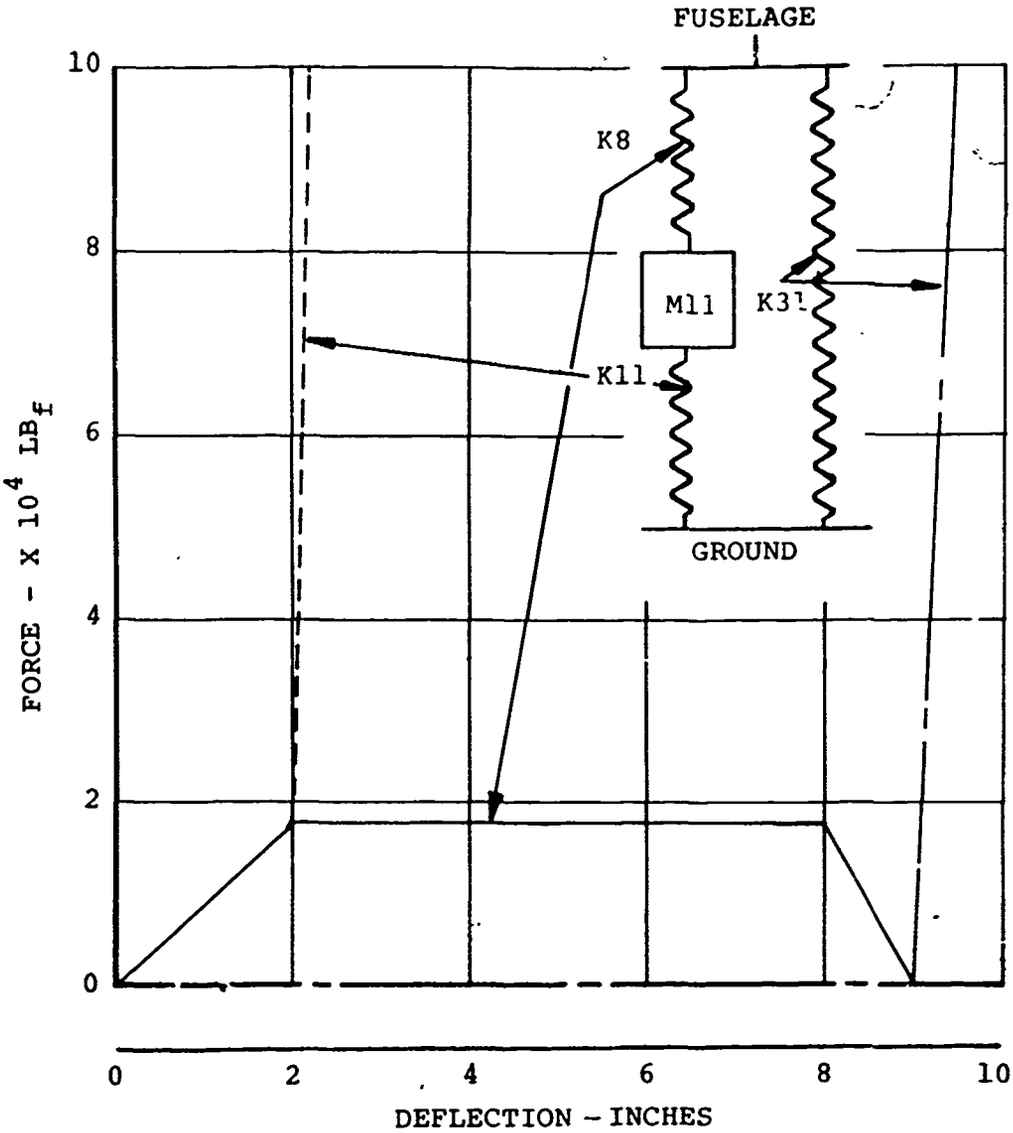

Figure 24. Load-Deflection Characteristics (Forward Landing Skid) for UH-1D/H.

additional 7 inches, at which point the skids fail, the fuselage contacts the ground, and the influence of spring (K31) is felt. This spring represents the interaction of the fuselage and the impact surface, and therefore, carries no load until the total deflection exceeds 9 inches.

A detailed listing of the input used to simulate the UH-1D/H helicopter is shown in Figures 25 and 26. The initial conditions for this example are a vertical impact velocity of 10 ft/sec, with all masses having zero angular velocity.

Output

The output from the simulator takes three forms: a tabulation of input data, a tabulation of output parameters at selected time increments, and combination tabulation-plots of the output parameters called for through the input. Therefore, Figures 25 and 26 are printouts of the input data.

The tabulation-plots furnish the user with tabulated digital printout of each requested parameter, along with a graphical representation of each parameter. The first column of each tabulation gives the time in seconds, while each succeeding column gives the value of the parameter requested in the plot title. Examples of plotted output for several parameters, for the 10 ft/sec impact velocity case, are shown in Figures 27 through 29. Figure 27 shows the acceleration-time histories of the transmission mass (M2), the engine mass (M3), and the tail rotor mass (M4). The accelerations of the forward floor mass (M8) and the rear floor mass (M9) are shown in Figure 28. Figure 29 presents the displacement of the transmission with respect to the floor, and the displacement of the forward and rear floor with respect to the ground. These latter deflections are 7.4 and 9.1 inches, respectively. Therefore, the 9-inch available stroke for the landing skids was slightly exceeded, so that the fuselage barely touched the ground. As a comparison, portions of the plotted output for an initial impact velocity of 30 ft/sec are shown in Figures 30 through 32. The acceleration levels for the engine, transmission, and floor, presented in Figures 30 and 31, should be compared with Figures 27 and 28. The relative displacements, shown in Figure 32, should be compared with Figure 29. The floor displacements in Figure 32 are 11.6 and 11.4 inches. This indicates that the 9-inch available landing skid stroke has been exceeded and that 2.6 and 2.4 inches of deformation occurred in the forward and rear fuselage belly, respectively.

The computed acceleration-time histories of the floor were found to agree, both in magnitude and shape, with experimental data from a vertical drop test of a modified UH-1D/H helicopter.

AIRFRAME CRASHWORTHINESS STUDY, MODEL NO. 1

THE FOLLOWING PLOTS HAVE BEEN REQUESTED

PLOT NO.	PLOTTING PARAMETERS		
1	42	43	44
2	62	63	0
3	45	46	47
4	48	49	0
5		91	92
6	116	117	118
7	121	124	125

NO RELATIVE DEFORMATIONS ARE RESTRICTED

	LUMPED MASS NUMBER 1	2	3	4	5	6	7
WEIGHT OF MASS (LB)-	1.00	980.00	1072.00	60.00	250.00	2147.00	230.00
HALF LENGTH (IN) -	-	-	-	-	45.00	65.00	120.00
MOMENT OF INERTIA -	-	-	-	-	437.00	7833.00	2856.00
VERT POSITION (IN) -	0.0	120.00	80.00	140.00	70.00	70.00	75.00
INITIAL ANGLE (RAD)-	-	-	-	-	0.0	0.0	0.17800
VERT VELOCITY (T=0)-	120.00	120.00	120.00	120.00	120.00	120.00	120.00
ANG VELOCITY (T=0) -	-	-	-	-	0.0	0.0	0.0

	8	9	10	11	12	13	14
WEIGHT OF MASS (LB)-	2951.00	1370.00	1.00	60.00	60.00	1.00	1.00
HALF LENGTH (IN) -	45.00	45.00	0.0	-	-	-	-
MOMENT OF INERTIA -	5160.00	5727.00	1.00	-	-	-	-
VERT POSITION (IN) -	30.00	30.00	0.0	20.00	0.0	20.00	0.0
INITIAL ANGLE (RAD)-	0.0	0.0	0.0	-	-	-	-
VERT VELOCITY (T=0)-	120.00	120.00	120.00	120.00	120.00	120.00	120.00
ANG VELOCITY (T=0) -	0.0	0.0	0.0	-	-	-	-

THE GROUND IS CONSIDERED RIGID

Figure 25. Output Tabulation of Input Data.

CHARACTERISTICS OF NONLINEAR SPRINGS

* SD(I,1)= SLOPE OF ELASTIC PORTION — SD(I,5)= SLOPE OF SECOND PLASTIC PORTION
* SD(I,2)= DEFLECTION FOR YIELDING — SD(I,6)= UNLOADING SLOPE
* SD(I,3)= SLOPE OF FIRST PLASTIC PORTION — SD(I,7)= TYPE 1 , 2 IF TENSION POSSIBLE
* SD(I,4)= DEFLECTION TO CHANGE PLASTIC SLOPE — SD(I,8)= VISCOUS DAMPING CONSTANT

	1	2	3	4	5	6	7	8	9	10	11
SD(I,1) LB/IN -	0.0	0.0	16000.00	6000.00	6000.00	0.0	0.0	9000.00	0.0	0.0	9000.00
SD(I,2) IN -	0.0	0.0	0.50	0.50	0.50	0.0	0.0	2.00	0.0	0.0	2.00
SD(I,3) LB/IN -	0.0	0.0	-12000.00	0.0	2250.00	0.0	0.0	0.0	0.0	0.0	1000000.00
SD(I,4) IN -	0.0	0.0	1.00	100.00	4.50	0.0	0.0	8.00	0.0	0.0	100.00
SD(I,5) LB/IN -	0.0	0.0	16000.00	0.0	-4000.00	0.0	0.0	-18000.00	0.0	0.0	0.0
SD(I,6) LB/IN -	0.0	0.0	20000.00	6000.00	8000.00	0.0	0.0	12000.00	0.0	0.0	1000000.00
SD(I,7) -	0.0	0.0	1.00	1.00	1.00	0.0	0.0	2.00	0.0	0.0	2.00
SD(I,8) -	0.0	0.0	50.00	50.00	50.00	0.0	0.0	0.0	0.0	0.0	0.0
HOR. DIST. IN -	0.0	30.00	35.00	240.00	35.00	65.00	45.00	45.00	85.00	45.00	0.0

	12	13	14	15	16	17	18	19	20	21	22
SD(I,1) LB/IN -	0.0	9000.00	0.0	500000.00	75000.00	75000.00	250000.00	1000000.00	0.0	9000.00	0.0
SD(I,2) IN -	0.0	2.00	0.0	100.00	1.00	1.00	100.00	100.00	0.0	2.00	0.0
SD(I,3) LB/IN -	0.0	1000000.00	0.0	0.0	-45000.00	-45000.00	0.0	0.0	0.0	0.0	0.0
SD(I,4) IN -	0.0	100.00	0.0	0.0	2.00	2.00	0.0	0.0	0.0	4.00	0.0
SD(I,5) LB/IN -	0.0	0.0	0.0	0.0	100000.00	100000.00	0.0	0.0	0.0	-18000.00	0.0
SD(I,6) LB/IN -	0.0	1000000.00	0.0	500000.00	400000.00	400000.00	250000.00	1000000.00	0.0	12000.00	0.0
SD(I,7) -	0.0	2.00	0.0	1.00	1.00	1.00	1.00	1.00	0.0	2.00	0.0
SD(I,8) -	0.0	0.0	0.0	0.0	50.00	50.00	0.0	0.0	0.0	0.0	0.0
HOR. DIST. IN -	0.0	0.0	0.0	0.0	20.00	20.00	0.0	0.0	0.0	20.00	0.0

TORSIONAL SPRING DATA

	5	7	8	10
SD(I,1)IN-LB/R -	2000000.000	1200000.000	60000000.000	0.0
SD(I,2) RAD -	2.000	0.035	0.040	0.0
SD(I,3)IN-LB/R -	0.0	1.000	-15000000.000	0.0
SD(I,4) RAD -	0.0	0.265	0.120	0.0
SD(I,5)IN-LB/R -	0.0	-2000000.000	60000000.000	0.0
SD(I,6)IN-LB/R -	2000000.000	1200000.000	60000000.000	0.0
SPRING TYPE -	1.000	1.000	2.000	0.0
SD(I,8) -	0.0	50.000	0.0	0.0

FAR COUPLED SPRINGS

	27	28	29	30	31	32	33
SD(I,1) LB/IN -	0.0	16000.000	0.0	0.0	0.0	0.0	0.0
SD(I,2) IN -	0.0	0.500	0.0	0.0	9.000	9.000	55.000
SD(I,3)IN-LB/R -	0.0	-1000.000	0.0	0.0	200000.000	200000.000	1000.000
SD(I,4) RAD -	0.0	4.500	0.0	0.0	9.500	9.500	100.000
SD(I,5) LB/IN -	0.0	8000.000	0.0	0.0	80000.000	80000.000	0.0
SD(I,6) LB/IN -	0.0	20000.000	0.0	0.0	250000.000	250000.000	1000.000
SPRING TYPE -	0.0	1.000	0.0	0.0	2.000	2.000	1.000
SD(I,8) -	0.0	50.000	0.0	0.0	0.0	0.0	0.0
HOR. DIST. IN. -	0.0	30.000	35.000	240.000	45.000	35.000	45.000

Figure 26. Output Tabulation of Input Data.

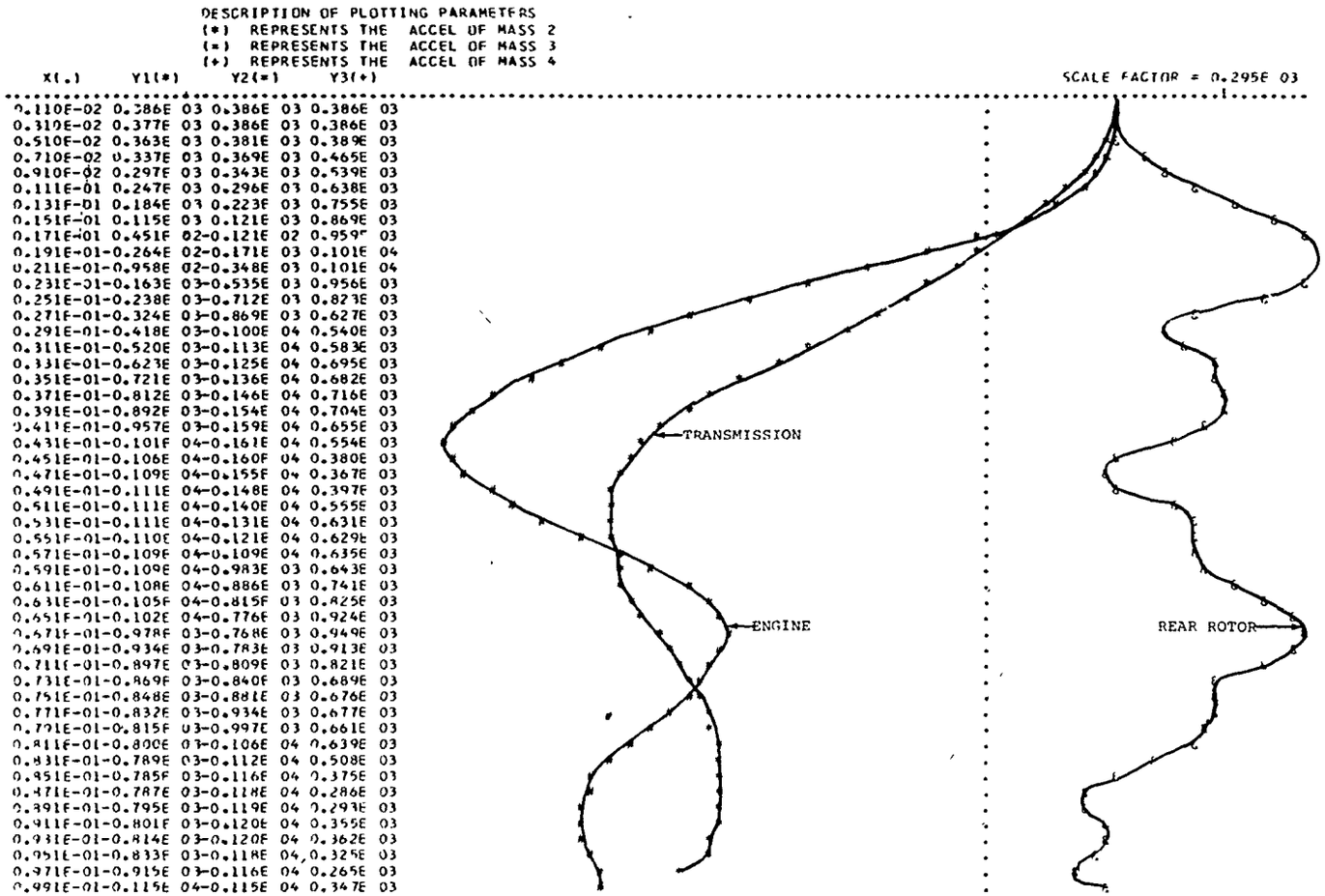

Figure 27. Computer Output (Transmission, Engine, Rotor at 10 ft/sec Vertical Impact) Vertical Accelerations for UH-1D/H.

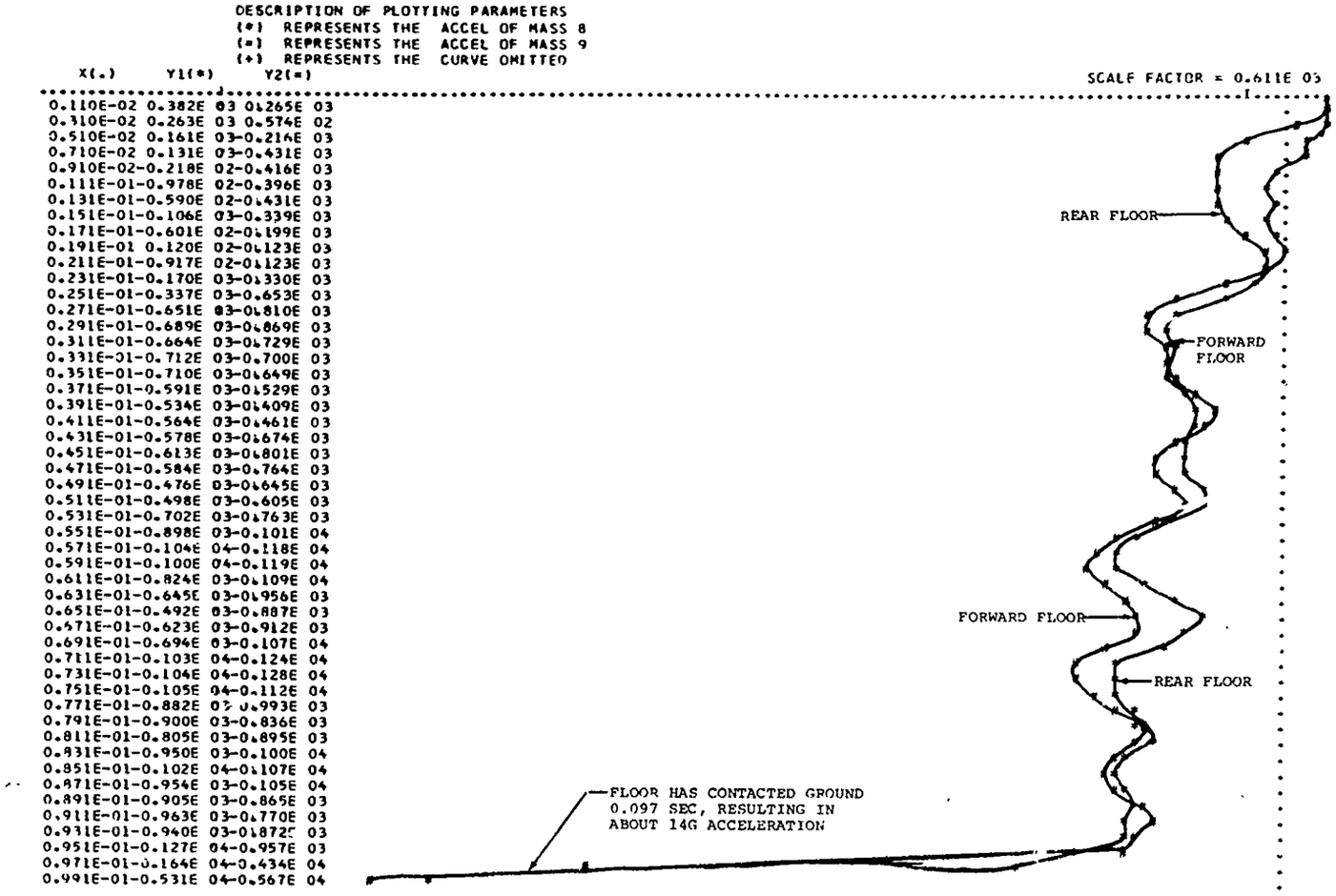

Figure 28. Computer Output (Forward Floor Hinges, Rear Floor at 10 ft/sec Vertical Impact) Vertical Accelerations for UH-1D/H.

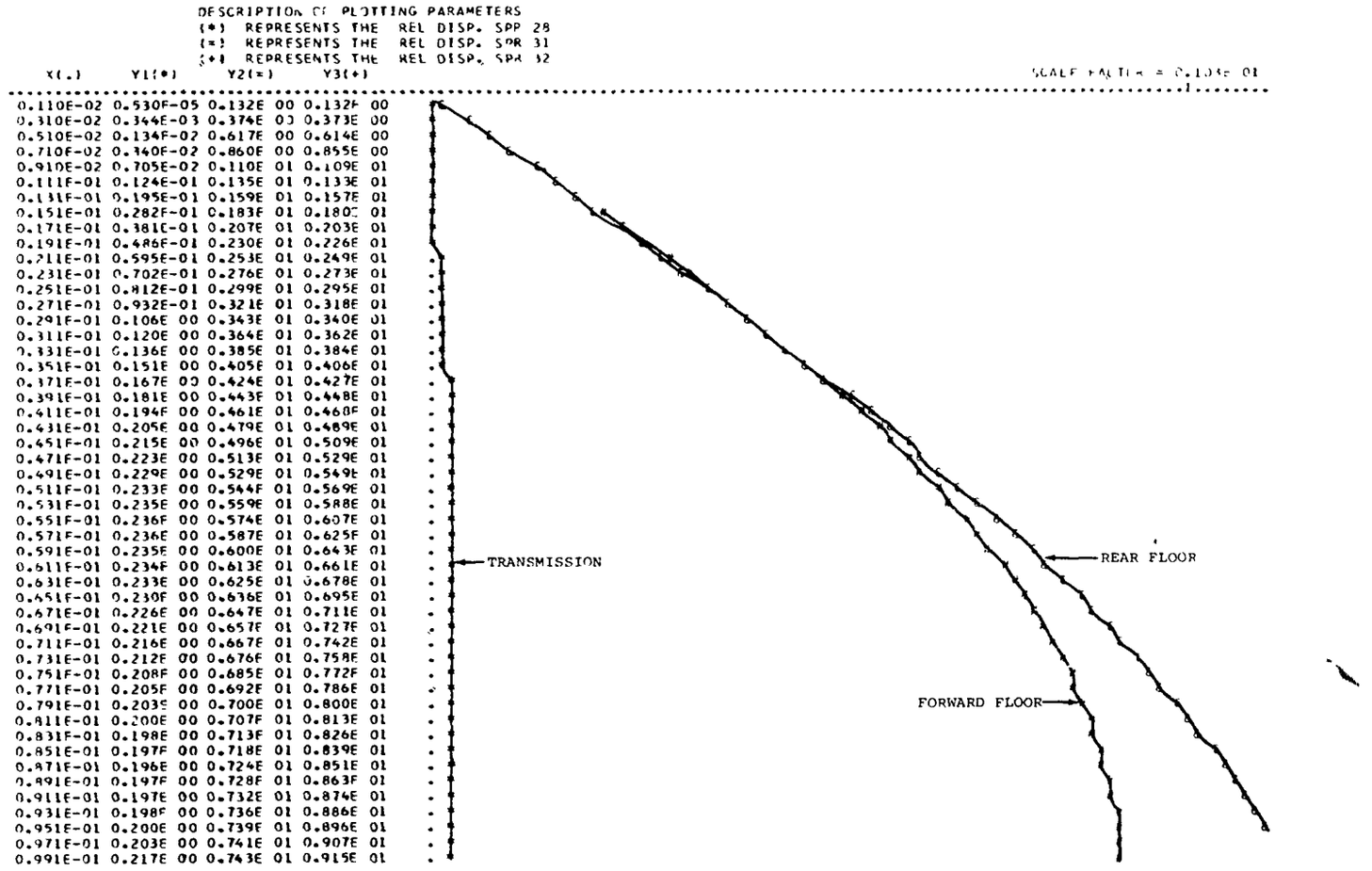

Figure 29. Computer Output (Forward Floor, Rear Floor, Transmission at 10 ft/sec Vertical Impact) Relative Displacements for UH-1D/H.

DESCRIPTION OF PLOTTING PARAMETERS
(*) REPRESENTS THE ACCEL OF MASS 2
(=) REPRESENTS THE ACCEL OF MASS 3
(+) REPRESENTS THE ACCEL OF MASS 4

X(.)	Y1(*)	Y2(=)	Y3(+)
0.110E-02	0.386E 03	0.386E 03	0.386E 03
0.310E-02	0.360E 03	0.386E 03	0.386E 03
0.510E-02	0.318E 03	0.372E 03	0.475E 03
0.710E-02	0.240E 03	0.336E 03	0.602E 03
0.910E-02	0.122E 03	0.258E 03	0.829E 03
0.111E-01	-0.279E 02	0.119E 03	0.114E 04
0.131E-01	-0.195E 03	-0.984E 02	0.149E 04
0.151E-01	-0.338E 03	-0.399E 01	0.180E 04
0.171E-01	-0.454E 03	-0.771E 01	0.196E 04
0.191E-01	-0.550E 03	-0.119E 02	0.193E 04
0.211E-01	-0.635E 03	-0.158E 02	0.152E 04
0.231E-01	-0.749E 03	-0.185E 02	0.419E 03
0.251E-01	-0.870E 03	-0.201E 02	-0.334E 03
0.271E-01	-0.130E 04	-0.209E 02	-0.271E 03
0.291E-01	-0.278E 04	-0.233E 02	0.723E 03
0.311E-01	-0.468E 04	-0.286E 02	0.368E 04
0.331E-01	-0.584E 04	-0.837E 04	0.573E 04
0.351E-01	-0.652E 04	-0.352E 04	0.102E 05
0.371E-01	-0.704E 04	-0.363E 04	0.133E 05
0.391E-01	-0.798E 04	-0.651E 04	0.118E 05
0.411E-01	-0.860E 04	-0.959E 04	0.854E 04
0.431E-01	-0.872E 04	-0.127E 05	0.620E 04
0.451E-01	-0.866E 04	-0.159E 05	0.577E 04
0.471E-01	-0.888E 04	-0.192E 05	0.515E 04
0.491E-01	-0.949E 04	-0.220E 05	0.349E 04
0.511E-01	-0.102E 05	-0.241E 05	-0.308E 04
0.531E-01	-0.109E 05	-0.249E 05	-0.683E 04
0.551E-01	-0.120E 05	-0.240E 05	-0.152E 05
0.571E-01	-0.138E 05	-0.213E 05	-0.190E 05
0.591E-01	-0.152E 05	-0.172E 05	-0.175E 05
0.611E-01	-0.161E 05	-0.126E 05	-0.126E 05
0.631E-01	-0.164E 05	-0.829E 04	-0.334E 04
0.651E-01	-0.158E 05	-0.441E 04	0.108E 04
0.671E-01	-0.151E 05	-0.956E 03	0.491E 04
0.691E-01	-0.144E 05	0.220E 04	0.591E 04
0.711E-01	-0.134E 05	0.486E 04	0.468E 04
0.731E-01	-0.128E 05	0.694E 04	0.364E 04
0.751E-01	-0.119E 05	0.869E 04	0.197E 04
0.771E-01	-0.108E 05	0.992E 04	0.528E 04
0.791E-01	-0.102E 05	0.105E 05	0.528E 04
0.811E-01	-0.908E 04	0.105E 05	0.737E 04
0.831E-01	-0.780E 04	0.980E 04	0.853E 04
0.851E-01	-0.6 5E 04	0.845E 04	0.817E 04
0.871E-01	-0.5 3E 04	0.667E 04	0.899E 04
0.891E-01	-0.4 3E 04	0.481E 04	0.424E 04
0.911E-01	-0.313E 04	0.312E 04	0.105E 04
0.931E-01	-0.158E 04	0.149E 04	-0.111E 04
0.951E-01	-0.134E 03	-0.143E 03	-0.103E 04
0.971E-01	0.175E 04	-0.207E 04	0.374E 03
0.991E-01	0.416E 04	-0.447E 04	0.174E 04

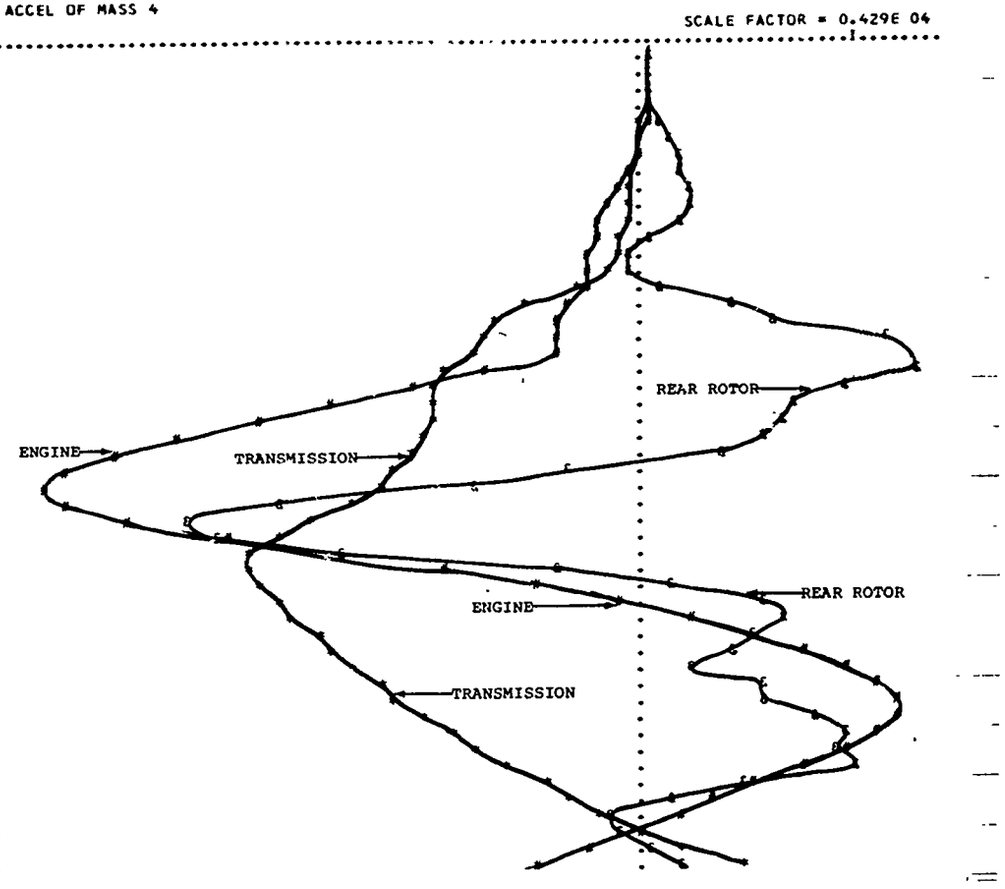

Figure 30. Computer Output (Transmission, Engine, Rear Rotor at 30 ft/sec Vertical Impact) Vertical Accelerations for UH-1D/H.

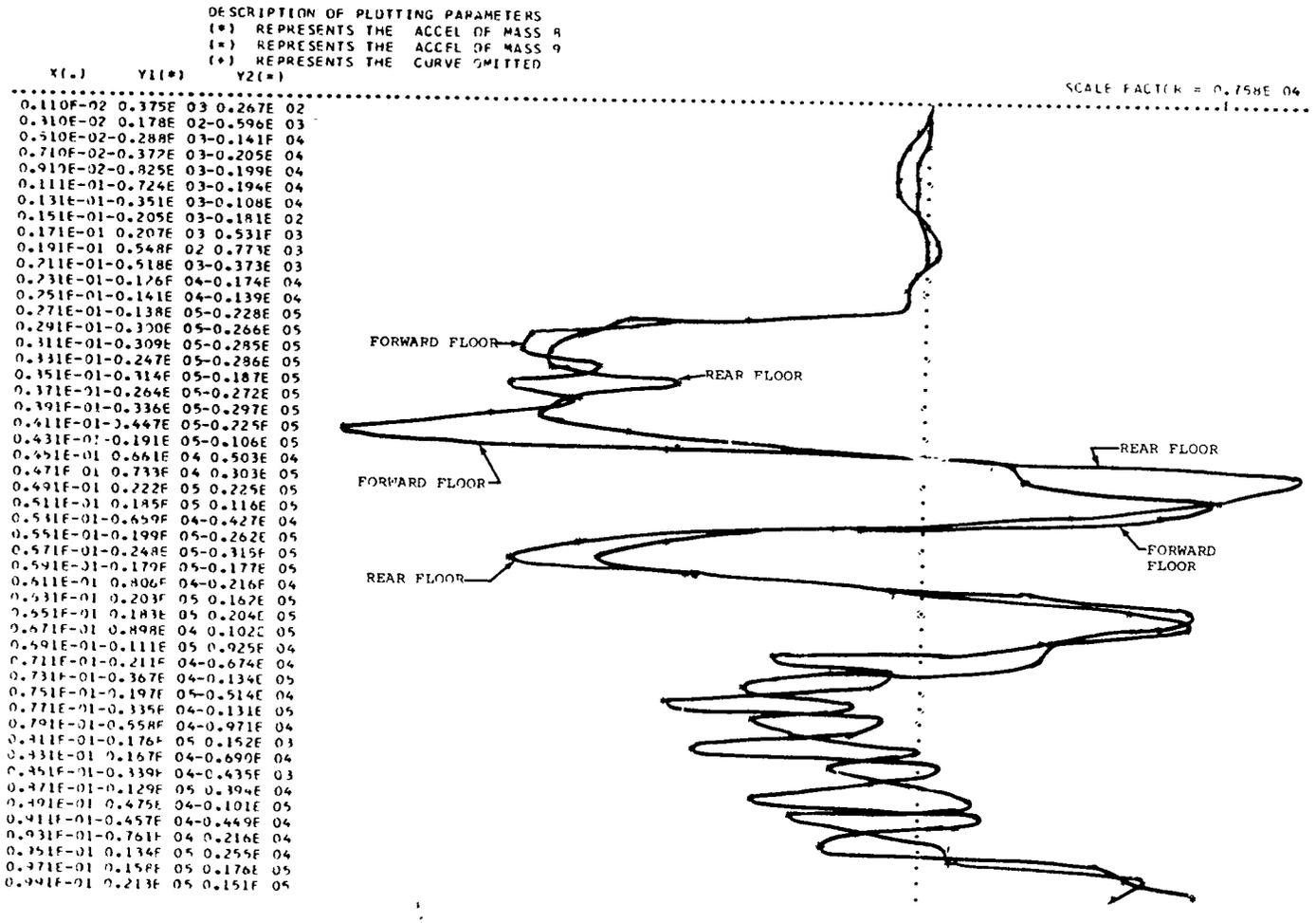

Figure 31. Computer Output (Forward Floor Hinges, Rear Floor at 30 ft/sec Vertical Impact) Vertical Accelerations for UH-1D/H.

DESCRIPTION OF PLOTTING PARAMETERS
(*) REPRESENTS THE REL DISP. SPR 28
(=) REPRESENTS THE REL DISP. SPR 31
(+) REPRESENTS THE REL DISP. SPR 32

SCALE FACTOR = 0.130E 01

X(.)	Y1(*)	Y2(=)	Y3(+)
0.110E-02	0.169E-04	0.396E 00	0.396E 00
0.310E-02	0.103E-02	0.112E 01	0.112E 01
0.510E-02	0.401E-02	0.184E 01	0.183E 01
0.710E-02	0.101E-01	0.256E 01	0.254E 01
0.910E-02	0.210E-01	0.328E 01	0.325E 01
0.111E-01	0.369E-01	0.400E 01	0.394E 01
0.131E-01	0.575E-01	0.470E 01	0.463E 01
0.151E-01	0.800E-01	0.540E 01	0.532E 01
0.171E-01	0.101E 00	0.610E 01	0.600E 01
0.191E-01	0.121E 00	0.679E 01	0.669E 01
0.211E-01	0.137E 00	0.748E 01	0.737E 01
0.231E-01	0.153E 00	0.816E 01	0.806E 01
0.251E-01	0.171E 00	0.883E 01	0.874E 01
0.271E-01	0.195E 00	0.949E 01	0.941E 01
0.291E-01	0.288E 00	0.101E 02	0.100E 02
0.311E-01	0.464E 00	0.106E 02	0.105E 02
0.331E-01	0.731E 00	0.110E 02	0.109E 02
0.351E-01	0.110E 01	0.113E 02	0.111E 02
0.371E-01	0.153E 01	0.115E 02	0.113E 02
0.391E-01	0.207E 01	0.116E 02	0.114E 02
0.411E-01	0.271E 01	0.115E 02	0.113E 02
0.431E-01	0.341E 01	0.113E 02	0.112E 02
0.451E-01	0.415E 01	0.111E 02	0.111E 02
0.471E-01	0.486E 01	0.107E 02	0.109E 02
0.491E-01	0.546E 01	0.104E 02	0.109E 02
0.511E-01	0.595E 01	0.101E 02	0.109E 02
0.531E-01	0.637E 01	0.982E 01	0.110E 02
0.551E-01	0.675E 01	0.955E 01	0.111E 02
0.571E-01	0.715E 01	0.925E 01	0.111E 02
0.591E-01	0.759E 01	0.894E 01	0.109E 02
0.611E-01	0.801E 01	0.862E 01	0.107E 02
0.631E-01	0.836E 01	0.831E 01	0.105E 02
0.651E-01	0.860E 01	0.801E 01	0.104E 02
0.671E-01	0.872E 01	0.774E 01	0.103E 02
0.691E-01	0.874E 01	0.747E 01	0.103E 02
0.711E-01	0.869E 01	0.720E 01	0.102E 02
0.731E-01	0.861E 01	0.692E 01	0.102E 02
0.751E-01	0.853E 01	0.664E 01	0.101E 02
0.771E-01	0.842E 01	0.633E 01	0.100E 02
0.791E-01	0.831E 01	0.603E 01	0.989E 01
0.811E-01	0.821E 01	0.572E 01	0.971E 01
0.831E-01	0.807E 01	0.539E 01	0.952E 01
0.851E-01	0.793E 01	0.507E 01	0.930E 01
0.871E-01	0.779E 01	0.474E 01	0.909E 01
0.891E-01	0.762E 01	0.440E 01	0.888E 01
0.911E-01	0.747E 01	0.407E 01	0.864E 01
0.931E-01	0.731E 01	0.374E 01	0.838E 01
0.951E-01	0.714E 01	0.341E 01	0.812E 01
0.971E-01	0.694E 01	0.308E 01	0.788E 01
0.991E-01	0.669E 01	0.278E 01	0.771E 01

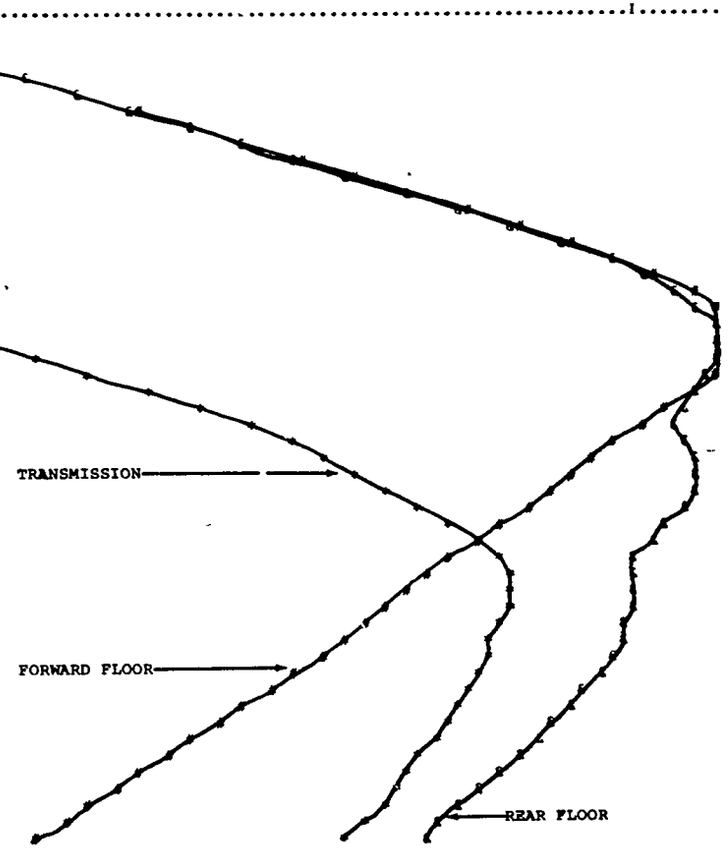

Figure 32. Computer Output (Forward Floor, Rear Floor, Transmission at 30 ft/sec Vertical Impact) Relative Displacements for UH-1D/H.

Table VII presents a comparison summary of other important output parameters for 10 ft/sec and 30 ft/sec vertical impacts for the standard UH-1D/H.

TABLE VII. COMPARISON OF OUTPUT FOR STANDARD UH-1D/H FOR 10- AND 30-FT/SEC IMPACT

Description	10-ft/sec Vertical Impact (*)	30-ft/sec Vertical Impact (*)
Maximum Acceleration of Engine	-1613.9	-24898.1
Maximum Acceleration of Transmission	-1114.6	-16390.9
Maximum Acceleration of Rear Rotor	1007.2	-18971.1
Maximum Acceleration of Floor	-5667.8	-44695.9
Maximum Rebound Acceleration of Engine	-	10544.0
Maximum Rebound Acceleration of Transmission	-	-
Maximum Rebound Acceleration of Rear Rotor	-	8994.0
Maximum Rebound Acceleration of Floor	-	30348.7
Maximum Angular Acceleration of Boom	13.20	-389.6
Maximum Angular Acceleration of Forward Floor	63.5	436.3
Maximum Angular Acceleration of Rear Floor	68.3	-361.9
Maximum Relative Deformation of Gear (Forward)	7.4	9.0
Maximum Relative Deformation of Gear (Rear)	9.0	9.0
Maximum Relative Deformation of Forward Floor	None	2.60

TABLE VII. Continued		
Description	10-ft/sec Vertical Impact (*)	30-ft/sec Vertical Impact (*)
Maximum Relative Deformation of Rear Floor	0.1	2.40
Maximum Relative Deformation of Engine	0.34	4.94
Maximum Relative Deformation of Transmission	0.25	8.74
Maximum Relative Deformation of Rear Rotor	.011	0.23
Maximum Angular Deformation of Boom	0.03	0.12
Maximum Angular Deformation of Forward Fuselage	-.057	-.026
Qualitative Results		
Did Boom Break?	No	Yes
Did Landing Gear Break?	No	Yes
Did Fuselage Contact Ground?	Yes	Yes
Did Boom Contact Ground?	No	No
Did Transmission Break Loose?	No	Yes

*Units of acceleration are in/sec^2 and rad/sec^2
Units of deformation are inch and radian

PARAMETRIC STUDY

GENERAL

The computer simulator model of the UH-1D/H is used to perform a parametric study of the distribution of load-limiting capability throughout the helicopter's airframe structure. The basic configuration of the generalized model permits investigation of the load-limiting capability in 4 sections of the helicopter's airframe structure: the landing gear, the belly of the aircraft fuselage, the upper portion of the fuselage, and the rotor and engine. The load-limiting properties of the upper portion of the fuselage are deemphasized in this study due to the structural design of the UH-1D/H transmission and rotor mounts and the rearward location of the engine with respect to the passenger compartments. The results from approximately 110 computer runs are used to summarize a parametric study concerning the load-limiting capabilities of the remaining 3 sections of the airframe structure. This study is centered around the present or standard UH-1D/H airframe and is an attempt to indicate areas in which an improved crashworthiness design may be developed. Extensive experimental data for a UH-1D/H subjected to vertical impact loadings are not available. Although the quantitative results of the study are felt to be valid, the study is most effective if viewed on a qualitative basis.

FACTORS INFLUENCING LOAD-LIMITING PARAMETRIC STUDY, UH-1D/H HELICOPTER

The primary factors influencing the load-limiting parametric study around the standard UH-1D/H helicopter are concerned with the 3 areas of possible load-limiting improvements; namely, the landing gear system, the crushable belly of the fuselage, and the transmission and rotor support system. In each of these 3 areas, the basic parameters are the strength of the system, the level of load limiting, and the available load-limiting stroke. Each of these design parameters is varied for the possible load-limiting areas of the helicopter. In each case, the 2 remaining areas of investigation are held constant at a value representative of the standard UH-1D/H helicopter. In this manner, crashworthiness improvements in the UH-1D/H helicopter may be illustrated through the improvement of each of the 3 areas of investigation.

LANDING GEAR SYSTEM

Consider a variation of landing gear parameters and their effect on the remaining portion of the standard helicopter. Three load-limiting strength landing gears have been chosen

along with 3 available load-limiting strokes. The standard or present UH-1D/H helicopter is represented in the model as possessing a 4G load-limiting strength gear system with an available stroke of 9 inches. The characteristics of these 4 possible load-deflection curves for the landing gear are shown in Figure 33, along with the total gear stroke required to avoid fuselage contact with the ground. This figure indicates that the fuselage of the standard UH-1D/H helicopter would contact the ground due to a vertical impact velocity of approximately 10 ft/sec. As the load-limiting strength of the gear increases, and as the available stroke of the gear increases, fuselage contact with the ground occurs at a higher impact velocity. This parametric study considered a 16G gear with a 15-inch stroke as the practical upper bound. In this case, fuselage contact with the ground occurs at approximately 29 ft/sec. The resulting effect upon floor acceleration for the standard UH-1D/H helicopter for vertical impact velocities of 10 and 20 ft/sec is shown in Figure 34. Consider the resulting floor acceleration in G's for the 10-ft/sec impact case. Figure 33 indicates that the necessary gear stroke required to avoid fuselage contact with the ground is approximately 9.0 inches for the 4G strength gear. Therefore, the results shown in Figure 34 for the 10-ft/sec case for available stroke levels of 9, 12, and 15 inches converge to a single curve showing increasing floor acceleration with increasing G strength of the gear. Notice, however, that at an impact velocity of 20 ft/sec, as the strength of the gear decreases, the available 9-inch stroke and the 12-inch stroke of the gear are used in load limiting as the fuselage contacts the ground. When this contact occurs, high floor accelerations are experienced. The resulting floor and transmission accelerations due to this variation of landing gear parameters are shown in Figures 34 and 35 for the vertical impacts of 10 and 20 ft/sec. These curves illustrate that significant crashworthiness improvements of the present UH-1D/H helicopter can be obtained through an improvement of the landing gear system. Considering the 20-ft/sec impact case, an increase of G strength of the gear from 4 to 8 and an increase of available stroke from approximately 9 inches to 15 inches produces a significant decrease in transmission and floor accelerations. Transmission acceleration is reduced from 18G to approximately 8G. Floor acceleration is reduced from approximately 65G to 12G.

Studies similar to the ones just described were performed using an impact velocity of 30 ft/sec. The resulting floor and transmission accelerations are shown in Figure 36.

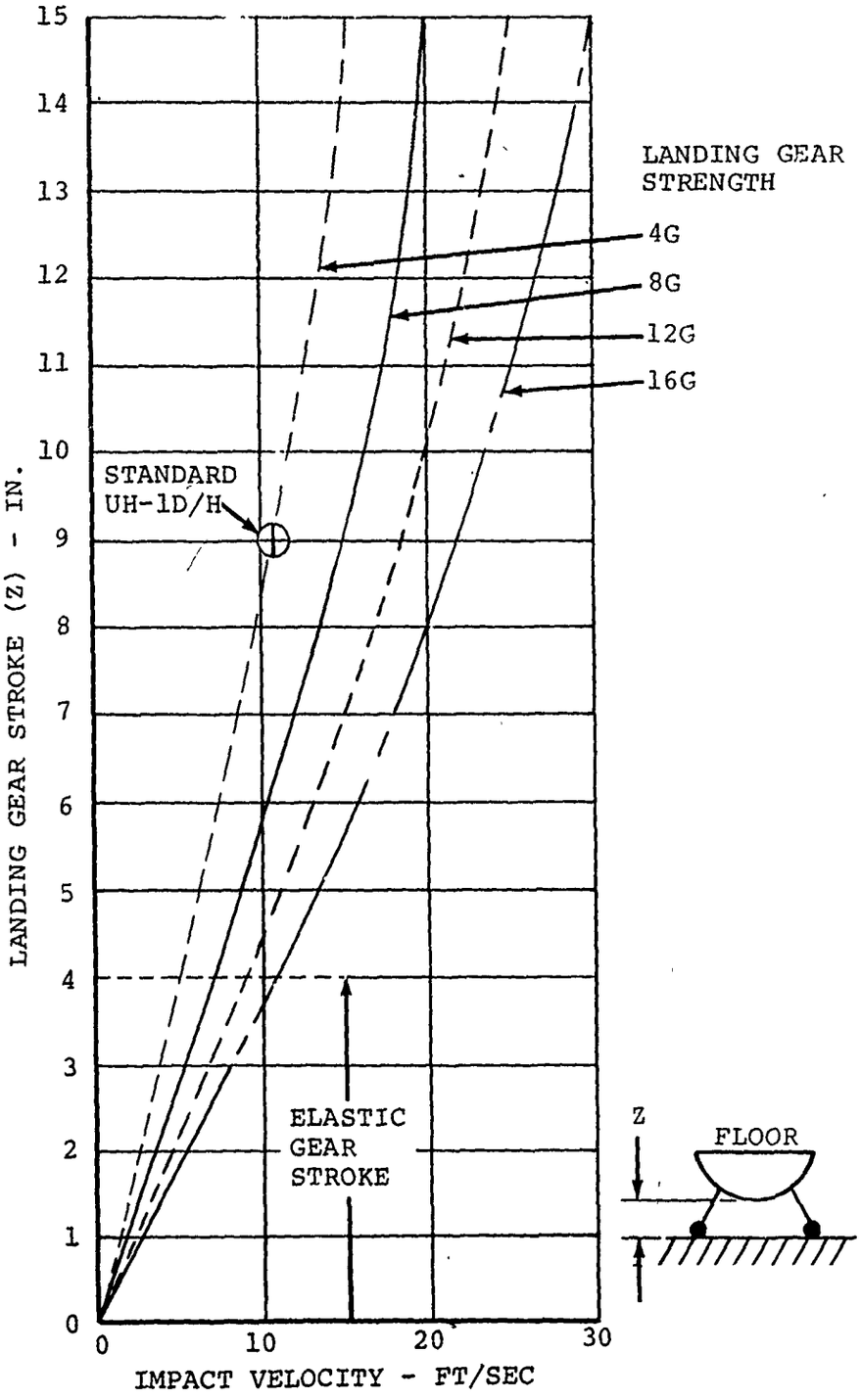

Figure 33. Landing Gear Stroke Required to Avoid Fuselage Contact With Ground.

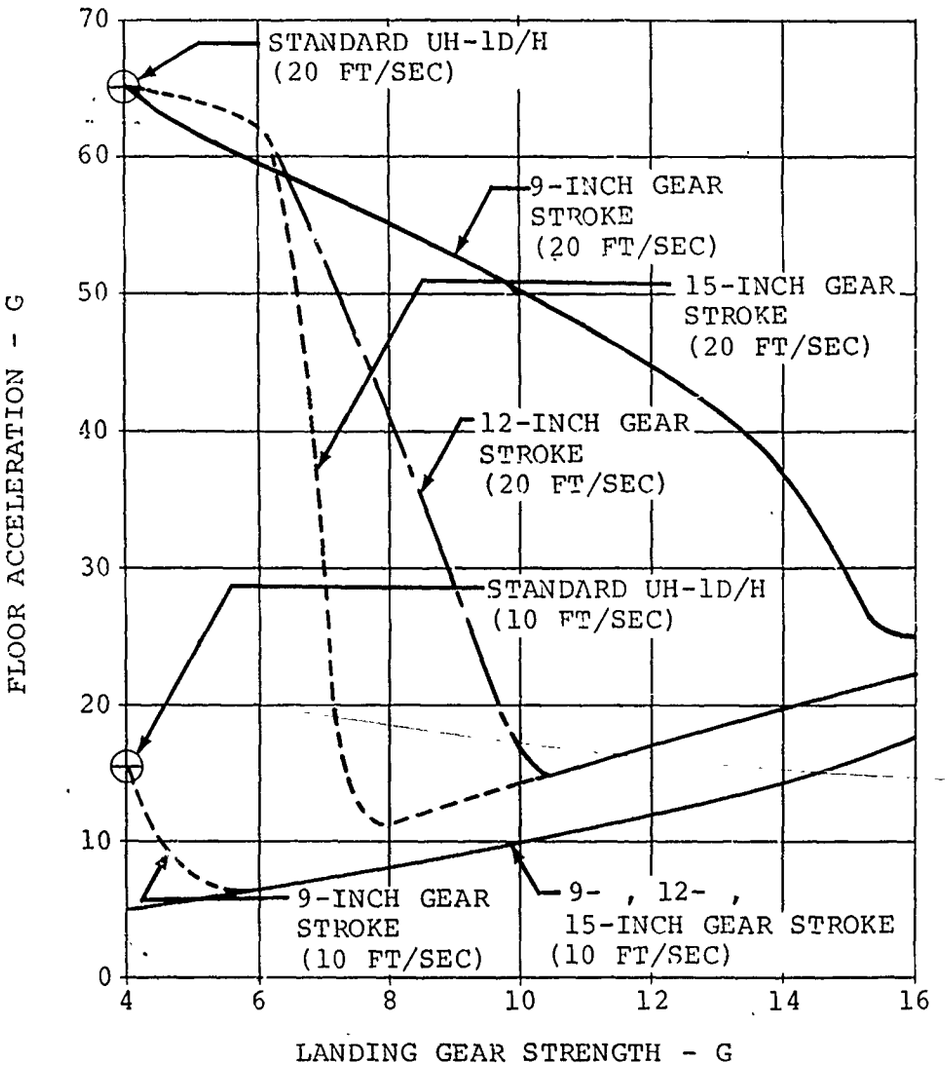

Figure 34. Floor Acceleration as a Function of Landing Gear G Level, Available Gear Stroke, and Vertical Impact Velocity for UH-1D/H.

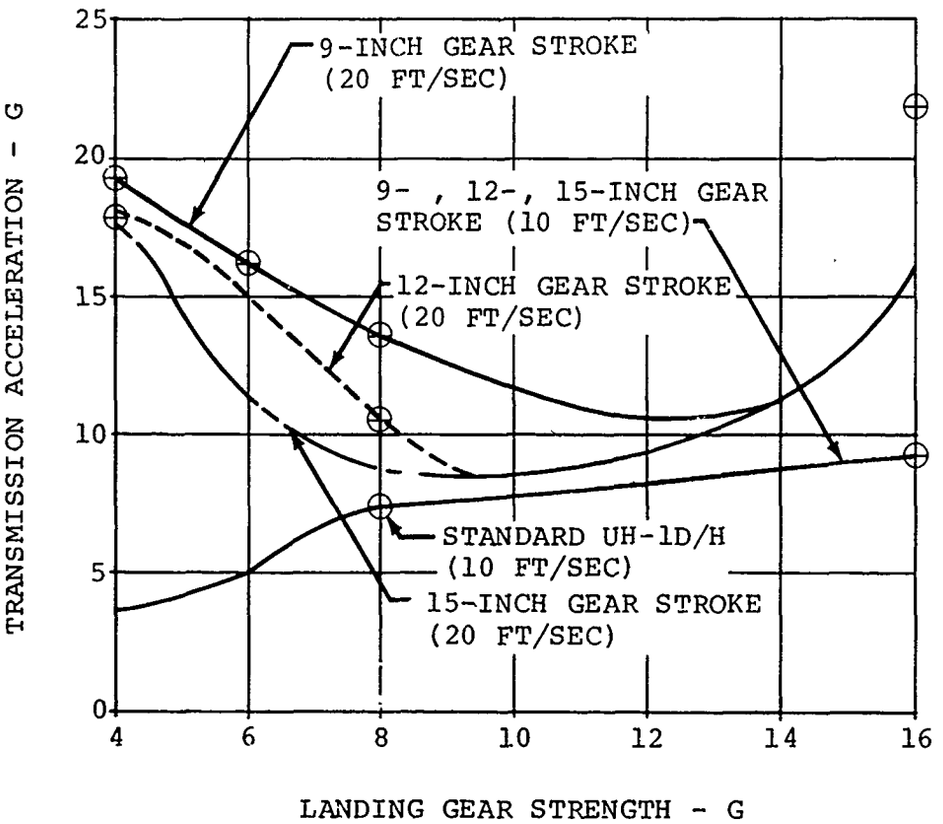

Figure 35. Transmission Acceleration as a Function of Landing Gear G Level, Available Gear Stroke, and Vertical Impact Velocity for UH-1D/H.

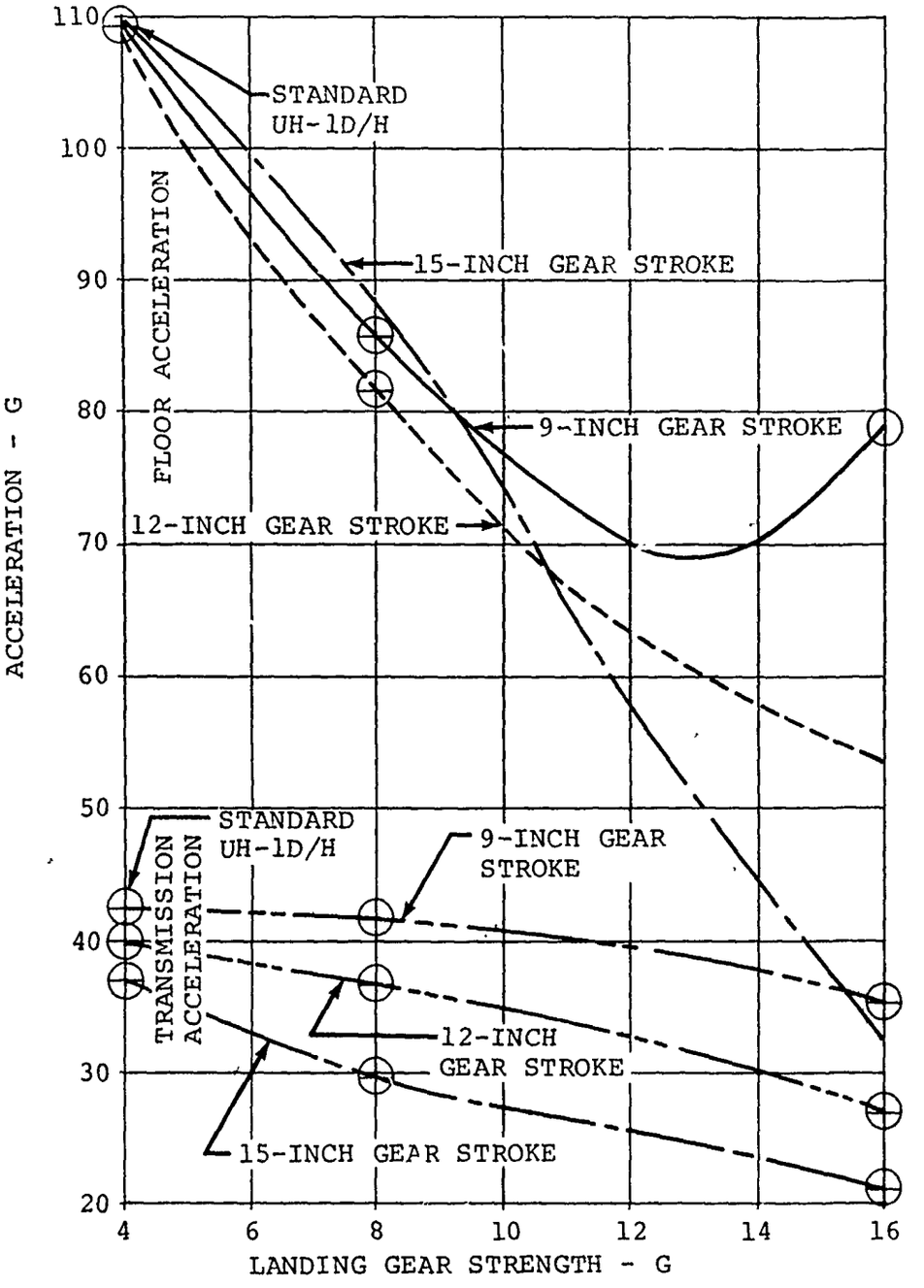

Figure 36. Floor and Transmission Acceleration (30-ft/sec Impact Velocity) as a Function of Landing Gear G Level and Available Gear Stroke for UH-1D/H.

CRUSHABLE FUSELAGE BELLY

A series of studies of the design parameters for the crushable belly of the fuselage was performed for a vertical impact velocity range of 30 to 50 ft/sec. The strength of the fuselage belly, the level of load limiting, and the available crush distance are varied in a manner similar to those in the landing gear study. The strength of the fuselage belly is expressed in G's and is based upon the maximum gross weight of the aircraft. A range of elastic G strengths from 11 to 22 was investigated, each with a linear plastic slope of 0, 10, and 20G-per-inch. A variation of these load-deflection characteristics is shown in Figure 37, along with the resulting fuselage deformation during a vertical impact range of 30 to 50 ft/sec. The standard UH-1D/H fuselage belly with an elastic G strength of 22 and a 20G-per-inch plastic slope is considered a lower bound for this parametric study. As the strength of the floor is decreased and the load-limiting available stroke increased, floor accelerations will decrease. An 11G floor and a zero G plastic slope were chosen as an upper bound since this floor strokes 35 inches at 50-ft/sec vertical impact. The resulting floor, transmission, and engine accelerations are presented in Figures 38, 39, and 40 for these fuselage belly parameters.

TRANSMISSION AND ROTOR SUPPORT SYSTEM

A third parametric study of the transmission and rotor support system involves 3 linear elastic, perfectly plastic load-deflection curves as shown in Figure 41, along with the rotor and transmission stroke required for various rotor G strength and impact velocities.

RESULTS

The results of the parametric studies show that a significant reduction in floor acceleration for the 10- to 30-ft/sec impact velocity range may be obtained for the UH-1D/H by an improvement in the landing gear system. An increase in gear strength from 4G to 8G with a corresponding increase in available load-limiting stroke from 9 inches to 15 inches reduces the floor acceleration from 65G to approximately 12G for the 20-ft/sec impact condition. The standard UH-1D/H transmission acceleration is reduced by 10G, while engine acceleration is not noticeably affected. The standard UH-1D/H fuselage will contact the ground with an initial impact velocity of approximately 10 ft/sec. The improved landing gear increases this velocity to 20 ft/sec. At 30-ft/sec vertical velocity, the floor acceleration of the standard UH-1D/H is reduced 20 percent while the transmission acceleration is reduced 30 percent.

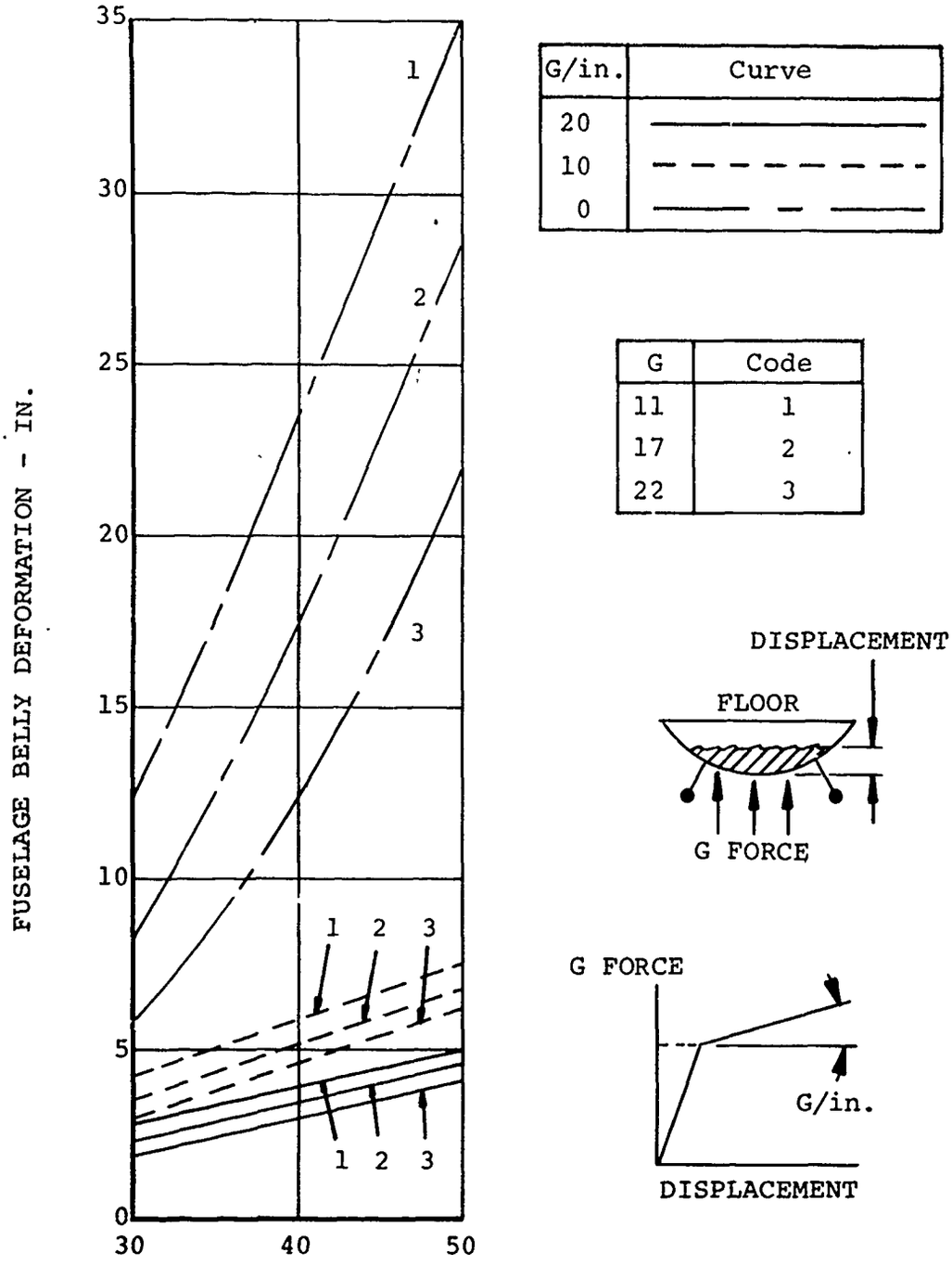

Figure 37. Fuselage Belly Deformation Required for Various Belly Strengths and Impact Velocities for UH-1D/H.

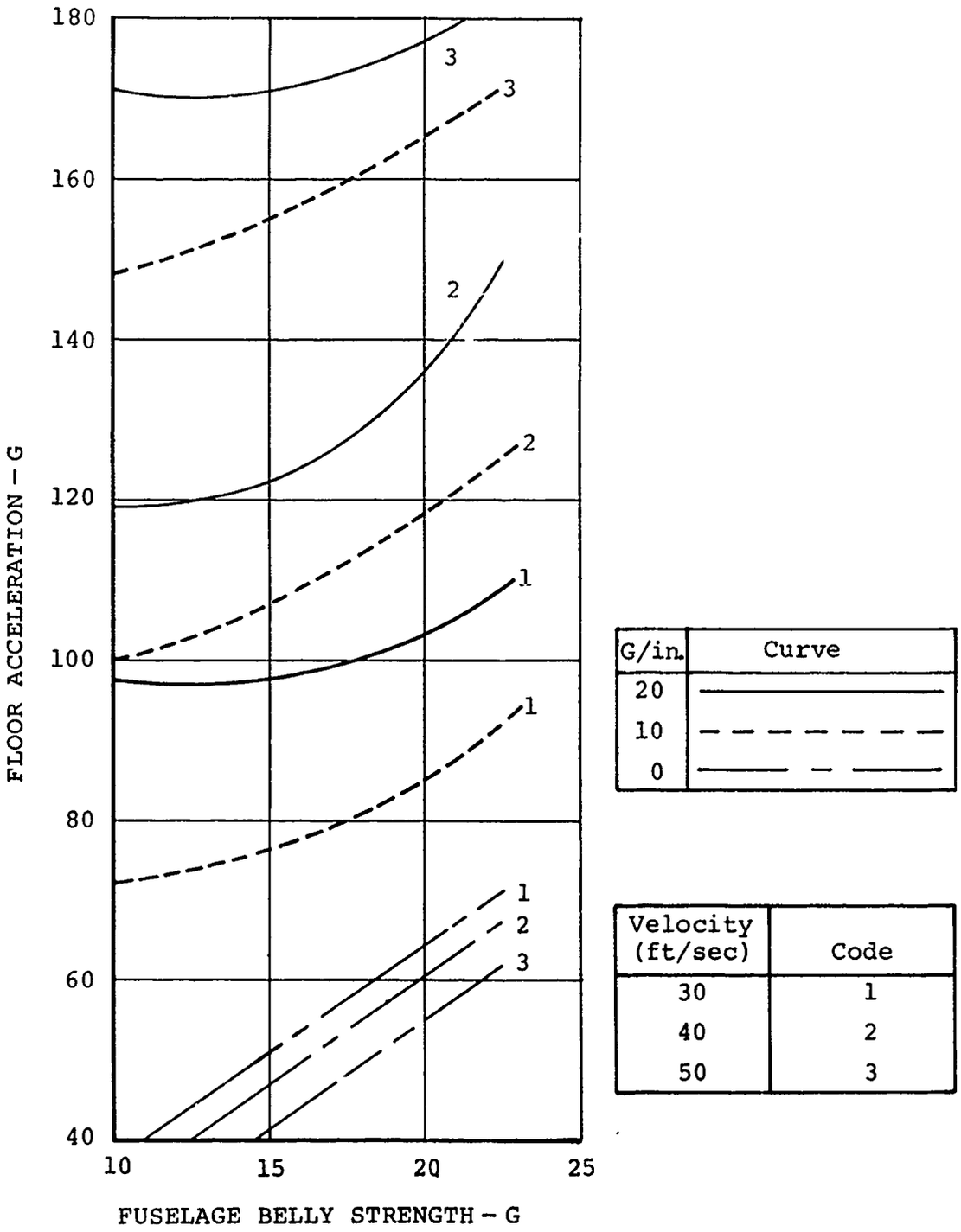

Figure 38. Floor Acceleration for Various Fuselage Belly Strengths and Vertical Impact Velocities for UH-1D/H.

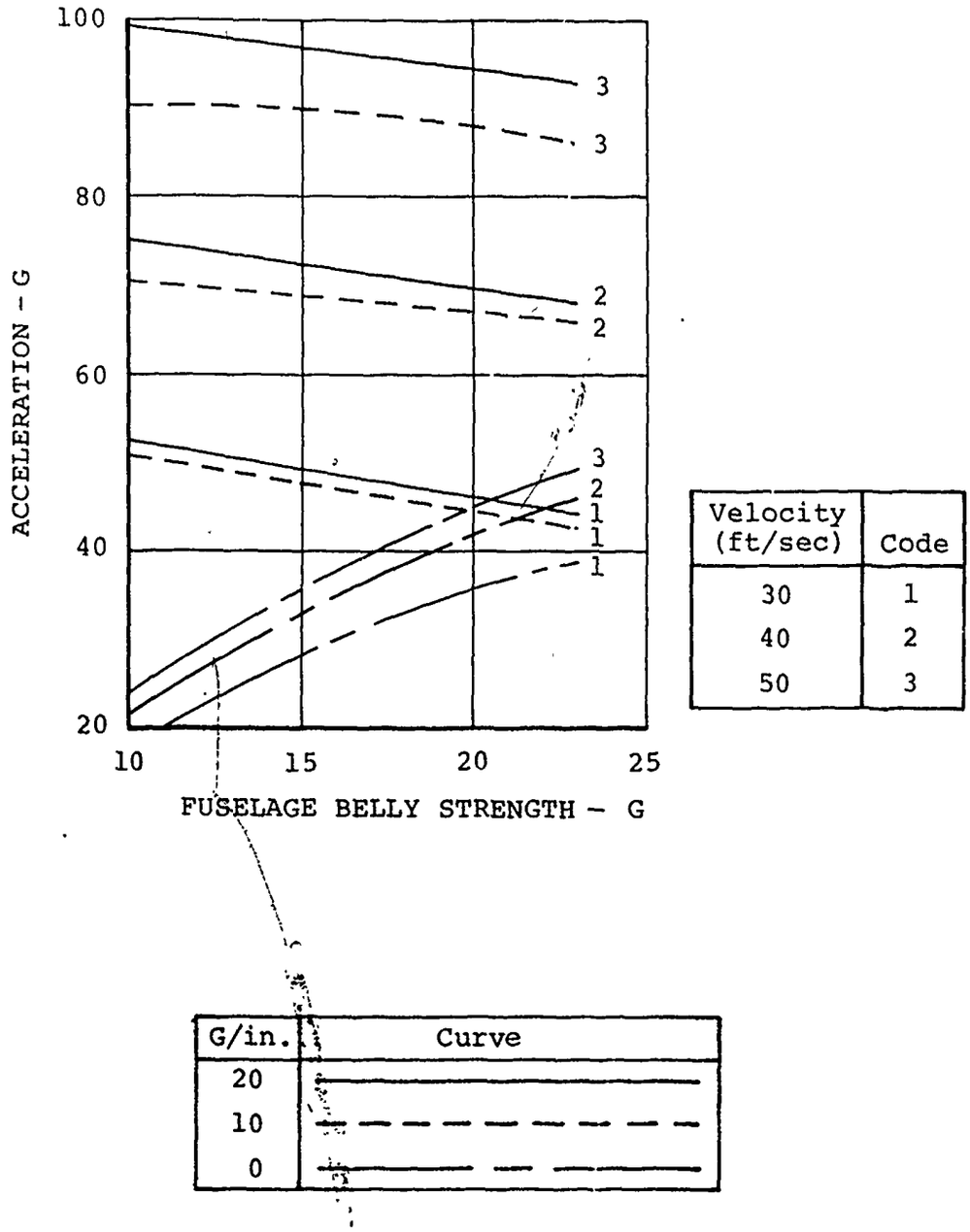

Figure 39. Transmission Accelerations for Various Fuselage Belly Strengths and Vertical Impact Velocities for UH-1D/H.

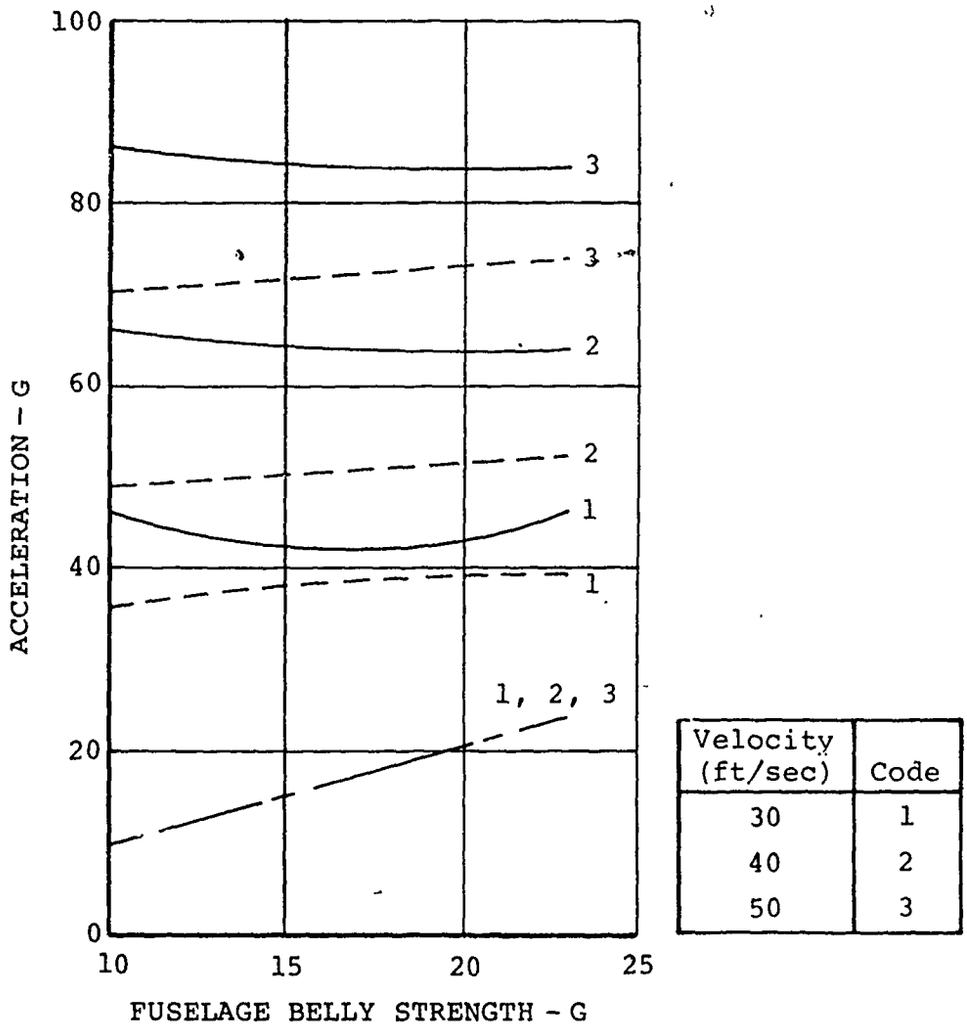

Velocity (ft/sec)	Code
30	1
40	2
50	3

G/in.	Curve
20	———
10	— — — —
0	——— · ———

Figure 40. Engine Acceleration for Various Fuselage Belly Strengths and Vertical Impact Velocities for UH-1D/H.

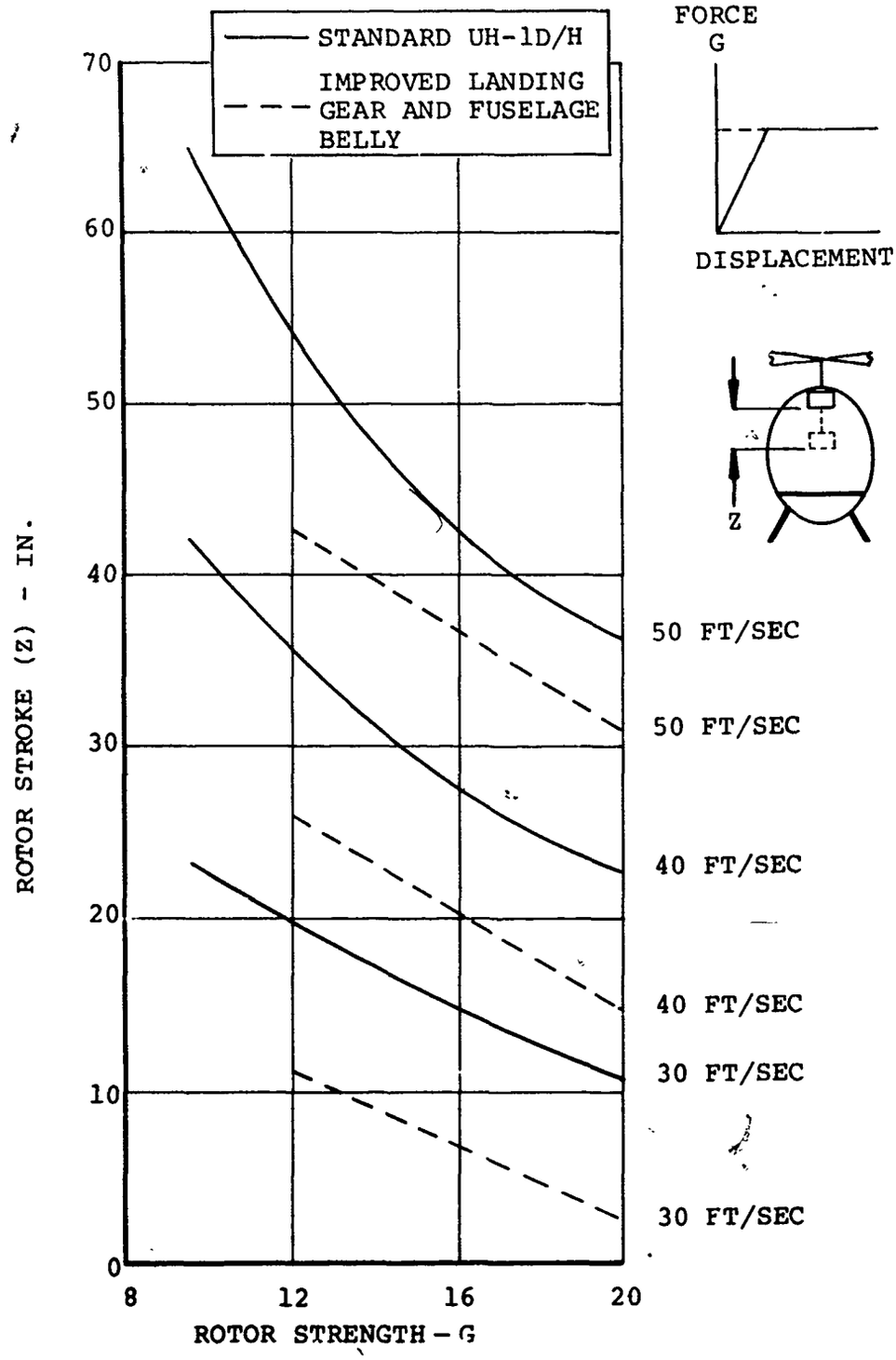

Figure 41. Rotor Stroke Required for Various Rotor G Strengths and Vertical Impact Velocities.

Floor accelerations may also be reduced by improving the crushable belly of the fuselage (see Figure 37). Perhaps an acceptable upper bound for crushable material beneath the floor is 15 inches. This amount of available load limiting with a plastic load-deflection curve having zero slope is used at an impact velocity of 40 ft/sec; the required floor strength would be approximately 19G based upon the maximum weight of the helicopter.

Referring to Figure 38, the improved floor (belly strength of 19G and plastic slope of zero G/inch) reduces the floor acceleration due to a 30 ft/sec impact velocity to 62G from a value of 110G (belly strength 22G and plastic slope of 20G/inch). The analogous values for an impact velocity of 40 ft/sec are 58G and 148G, respectively. For these load-deflection properties, the 50-ft/sec data in Figure 38 would not be valid since the available 15 inches of crushable distance (belly) has been used at 40-ft/sec impact velocity as indicated in the preceding paragraph and in Figure 37. Floor accelerations would be further improved by incorporating a better gear with a better crushable belly to attenuate floor accelerations (see Figure 38). The floor acceleration which would be obtained due to the use of a more optimum landing gear system; namely, 8G with a 15-inch available stroke, along with an improved fuselage is lowered from the standard value of 110G to 40G (from Figure 36, the decrease effected by the landing gear change is approximately 22G which is then subtracted from the previously discussed load of 62G).

Adjustments in the load-deflection characteristics of the rotor and transmission assembly do not affect floor acceleration. Also, due to the structural design of the UH-1D/H, adjustments in transmission and rotor parameters do not affect upper fuselage deflection. A range of load-limited transmission is presented here as a further example of possible improvement. Figure 41 illustrates the stroke required for various transmission load-limiting G levels for both the standard UH-1D/H landing gear and fuselage. These studies indicate that a 20G load-limited transmission in the present UH-1D/H helicopter would restrict the transmission vertical displacement to a maximum allowable value of 10 inches for a vertical impact velocity of 30 ft/sec. The improved landing gear and floor would permit a vertical impact velocity of approximately 38 ft/sec before the 10-inch displacement is exceeded. The vertical transmission displacement for the improved helicopter at 30 ft/sec is only 2 inches. A 20G transmission combined with an improved landing gear system and a more crushable fuselage belly produces a significant improvement in the ability to retain the transmission. A summary of the floor acceleration at 30 ft/sec is given in Figure 42 for individual improvement

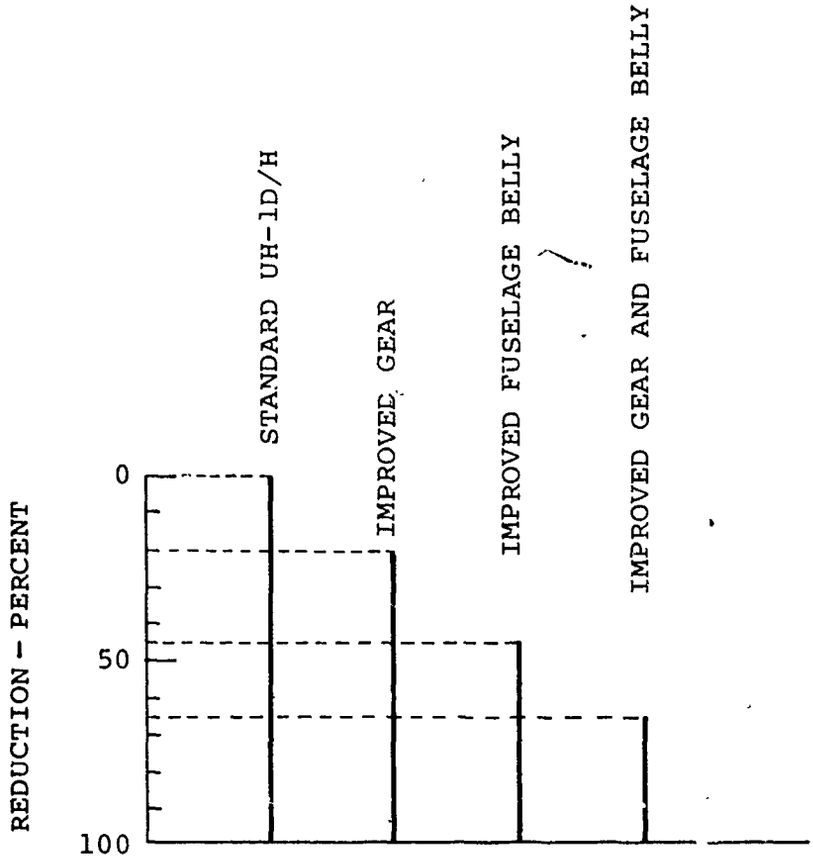

Figure 42. Floor Acceleration Comparisons (30-ft/sec Vertical Impact) for UH-1D/H.

in both fuselage belly and gear system, and for a combined improvement of both the gear system and the fuselage. A summary of transmission retention is given in Figure 43.

The application of all findings to the standard UH-1D/H helicopter is limited, although the improvements in both the landing gear system and the transmission and rotor support system could apply on a retrofit basis. It may be unrealistic to redesign this particular helicopter to provide 15 inches of crushable material beneath floor level. The findings provide more concrete evidence that the structural redesign of the fuselage belly can provide a significant improvement in crashworthiness for future helicopters.

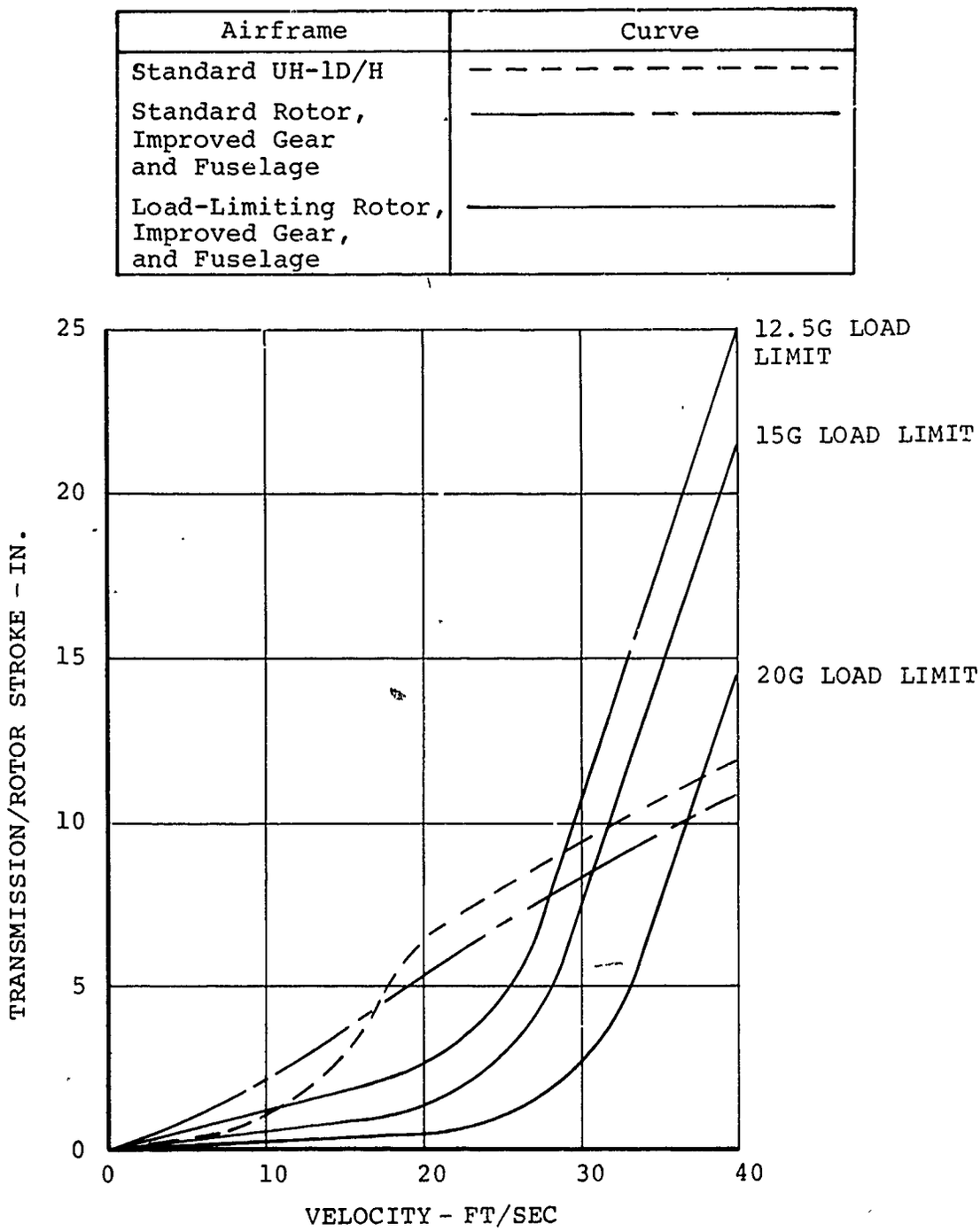

Figure 43. Required Transmission Stroke as a Function of Impact Velocity and Transmission Load-Limiting Level.

EXPERIMENTAL PROGRAM

The results of the parametric study performed with the mathematical model indicated that considerable relative improvement in crashworthiness of the UH-1D/H helicopter could be achieved through relatively minor structural modifications. However, the base-line data used in these studies were established on numerous assumptions and estimates concerning the structural response of this aircraft. To ascertain the true potential for crashworthiness improvement, these assumptions and estimates and the entire modeling concept require validation.

To this end, a full-scale vertical drop test of a UH-1D/H airframe was conducted with instrumentation aboard to measure accelerations and deflections at key points. Since a full-scale crash test is expensive, instrumentation related to other projects was installed in the test vehicle. These included:

- Ancillary equipment retention experiments
- Investigation of fuel system damage in vertical impact
- Evaluation of acceleration-sensitive switching devices
- Crew-seat occupant response to vertical acceleration

The aircraft was to be ballasted to a gross weight of 9,000 pounds and allowed to impact vertically on a concrete drop pad at an impact velocity of 30 feet per second. These test conditions were selected to duplicate criteria used in the modeling analysis. A schematic of the test setup is shown in Figure 44.

TEST VEHICLE DESCRIPTION

General

The test vehicle was basically a UH-1D tactical transport helicopter. The UH-1D is a thirteen-place, all-metal helicopter having a single, two-bladed main rotor and a single tail rotor. The aircraft is powered by one T53 gas turbine. Distinguishable features of the UH-1 series helicopter include the two-bladed main rotor, low silhouette, wide cabin, and skid-type landing gear (Figure 45).

Fuselage and Tail Boom

The primary structure in the forward section of the UH-1D helicopter consists of two longitudinal beams connected by transverse bulkheads. The beams provide the supporting structure

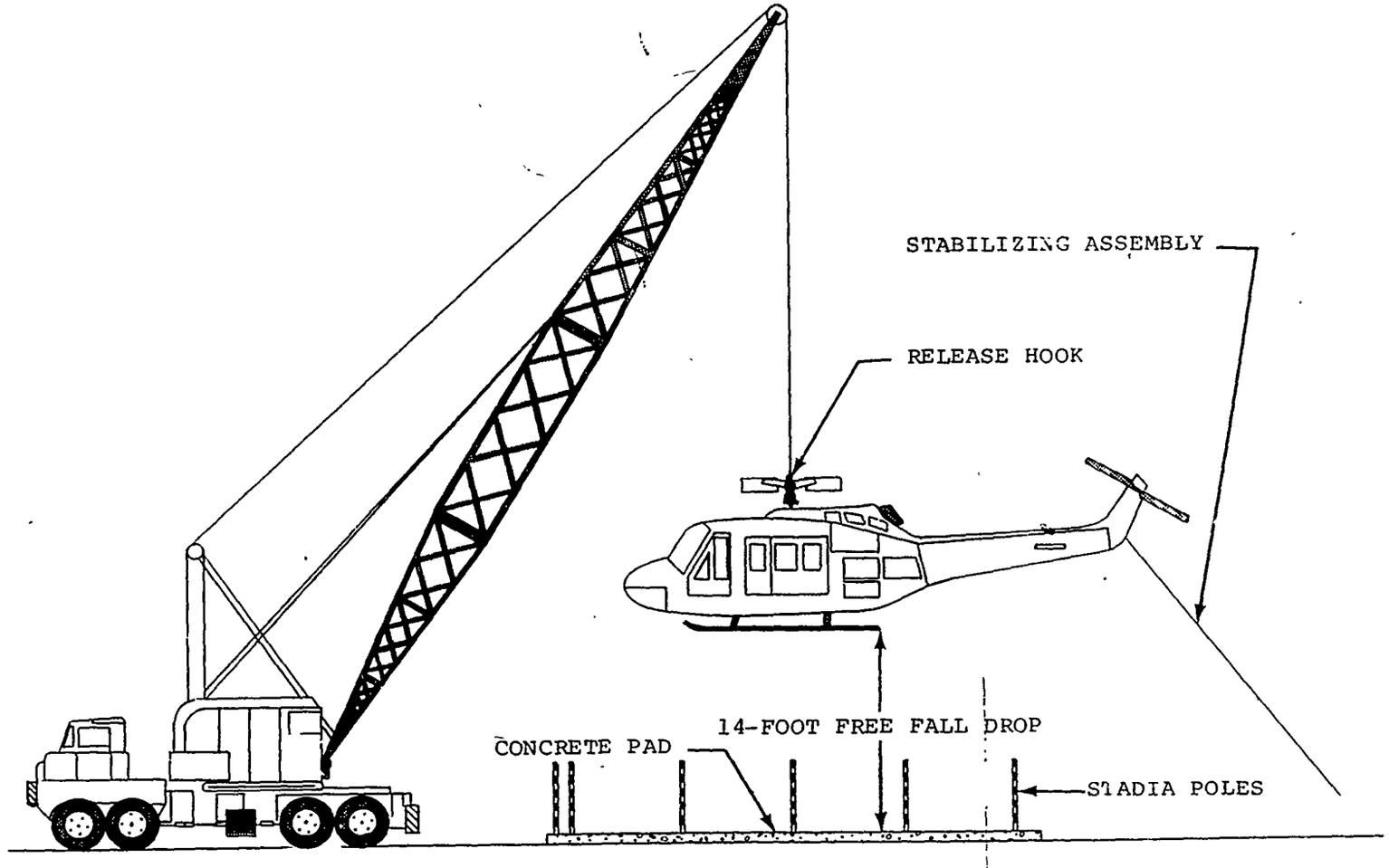

Figure 44. Test Setup Schematic.

Figure 45. UH-1D Helicopter.

for the cabin sections, landing gear, fuel tanks, transmission, engine, and tail boom. A skid-type landing gear is used and attaches to the fuselage at four points. Avionics equipment and electronic equipment are located in left rear compartments and the nose compartment. The battery is located in the nose compartment or in an aft fuselage compartment. The tail boom is an all-metal semimonocoque structure attached to the forward section with bolts to allow easy removal or replacement. The rear of the tail boom supports the tail rotor, vertical fin, and synchronized elevator. A tail skid is provided on the lower aft end of the tail boom to protect the tail rotor.

Access to the crew compartment is gained through two swing-out doors that are hinged at the forward side. A large sliding door operating on rollers and tracks gives access to the cargo-passenger area on each side of the cabin. A hinged panel door is located just forward of the sliding cargo door to provide a wider cargo opening for cargo loading.

Power Plant

The engine used on the UH-1D helicopter is a Lycoming T53-L-11 gas-turbine power plant. The engine is suspended at three

points by supports made of steel tubing that are attached to fittings on the service deck. The engine and accessories are easily accessible through removable hinged cowlings. The engine assembly is equipped with quick-disconnect couplings in the oil and fuel system to facilitate replacement of individual assemblies or the complete engine.

Fuel System

The UH-1D fuel system consists of five interconnected cells that act as a single tank with a total capacity of 224 gallons. Three cells are located across the fuselage below the engine deck aft of the cabin area, with the filler cap for the entire system on the right-hand cell. Two forward cells, located under the cabin floor, are gravity fed from the aft cells. Each of the forward cells is provided with a boost pump. The forward under-floor cells are divided into compartments by a lateral baffle fitted with a flapper valve that permits fuel to flow from front to rear. The boost pumps are mounted on sump assemblies near the aft end of each under-floor cell. Two quantity gage sending units are located in the right cell and are interconnected with another in the center aft cell. The left cell has a low level float switch.

Oil System

The engine oil reservoir consists of a supply tank mounted on the right side of the engine compartment. Oil is supplied to the engine-driven oil pump through a quick-disconnect hose. Scavenge oil is circulated through external lines to a thermal bypass valve and oil cooler in the fuselage compartment below the service deck and then returned to the supply tank.

Transmission and Rotor System

The transmission is located directly ahead of the engine and is suspended by pylon isolating mounts on structural supports. These structural supports deliver the rotor loads into a sturdy box-like structure that is tied directly into the aircraft floor. The unit is coupled to the engine through a short drive shaft. A tubular steel shaft supports and drives a two-bladed main rotor of all metal construction with a honeycomb core.

Landing Gear

The landing gear is made up of formed aluminum alloy tubes, consisting of two skids attached on the ends of two arched cross tubes that are secured to the fuselage structure by four padded caps. The cross tubes are fitted with bearing straps at mounting points.

Crew and Passenger Seats

The UH-1D is equipped with adjustable, non-reclining crew seats, mounted on tracks fixed to the cabin floor. Armored seats may also be installed in the UH-1D. The seat armor, constructed from a composite ceramic-metal material, is designed to protect the pilot and copilot against small-arms ball and armor-piercing ammunition. The shoulder harness is attached to an inertia reel on the helicopter floor with a standard seat and to the back of the armored seat.

The UH-1D may be equipped for seating eleven passengers in the cargo compartment by using folding cloth seats. Individual lap-type seat belts are provided for all troop seats. Litters may also be installed in place of some of the cargo compartment seats.

PREPARATION OF TEST VEHICLE

General

The UH-1D used as a test vehicle was modified and equipped to satisfy the test requirement as described in the following paragraphs. Figure 46 shows the test vehicle prior to the test drop, Army Test Number 34 (T-34).

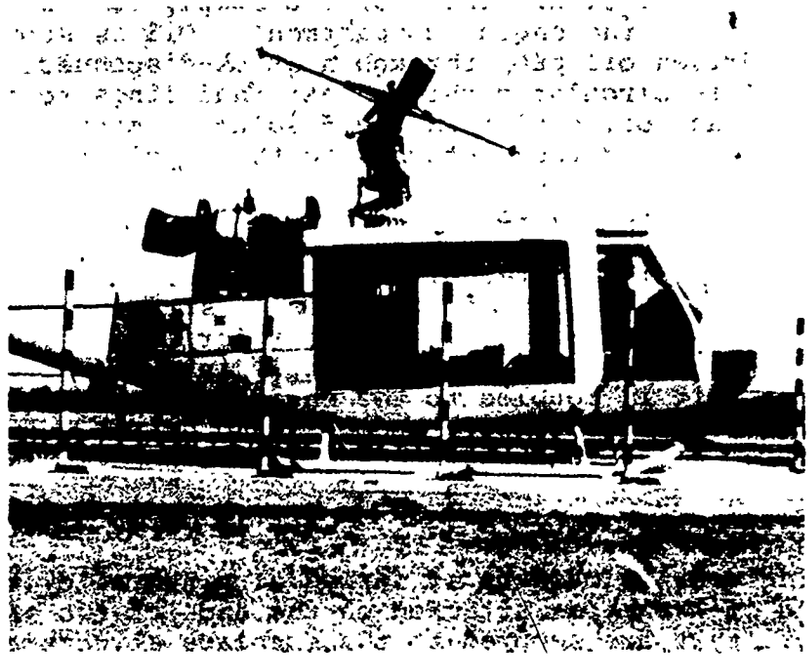

Figure 46. Modified UH-1D Test Vehicle.

Fuselage and Tail Boom

The UH-1D used as the drop vehicle had previously sustained damage to the right rear fuselage structure. This damaged section was removed and replaced with an undamaged portion from another UH-1D. The helicopter structure was returned to as near an original configuration and strength as possible. A tail boom for a UH-1D was not available; therefore, a UH-1A tail boom was adapted to the UH-1D fuselage. Ballast was added to duplicate the mass of a UH-1D tail boom and tail rotor assembly.

All avionics and electronic equipment had been previously removed from the aircraft. The battery was positioned in the aft fuselage compartment.

The crew doors and cargo doors contribute very little to the structural strength of the fuselage for this particular crash condition, since they are sliding doors and do not form an integral part of the fuselage structure. The door runners and fastener would absorb a certain amount of the vertical energy, but its contribution to increased crashworthiness (in a purely vertical impact) is considered minor. Therefore, the sliding doors were omitted from this test in order to obtain better photographic coverage of the helicopter interior.

Power Plant

Since the engine mounts were badly damaged, new engine mounts were fabricated using the original attachment fittings and the same type of steel tubing. The T53-L-1 gas-turbine power plant that was used in Army Test Number T-31 was installed on these mounts. Ballast was added to the engine to simulate the weight of the UH-1D/H power plant.

New hoses and quick-disconnect valves were incorporated in flammable fluid lines between the engine and oil tank, service deck, and fuel filter.

Three small stadia poles marked off in 1-inch segments were prepared and installed on the service deck to the right of the engine. These poles provided a dimensional reference to enable study of engine deflection in the high-speed movies. The engine compartment and stadia pole installation are shown in Figure 47.

Fuel System

The fuel system in the test vehicle was the standard UH-1D fuel system described previosuly. The fuel cells, as received in

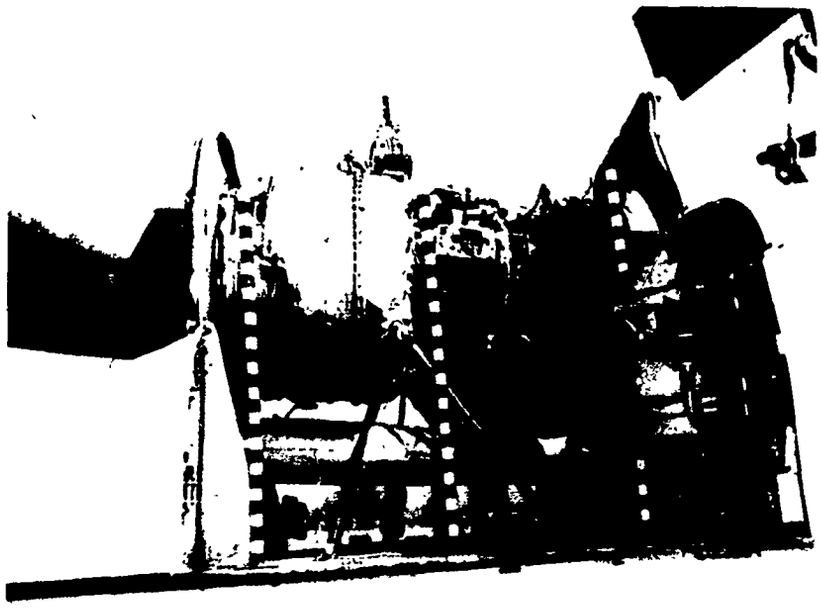

Figure 47. Stadia Pole Installation in Engine Compartment.

the UH-1D fuselage, were undamaged except for a slight leak in the lower right edge of the center tank. This leak was repaired and successfully leak tested. All interconnecting hoses in the tank system were replaced with new hoses. The fuel system was filled with colored water and again checked to insure that no leaks were present.

Oil System

The standard UH-1D oil system was used. The system was filled to the proper level with Grade 1010 jet engine oil prior to the test. The entire oil system was checked prior to the test to insure chat no leaks existed.

Transmission and Rotor Assembly

The UH-1D transmission and rotor mast were not available for installation in the test vehicle. It was therefore necessary to substitute the UH-1A transmission and rotor mast that had been used in the T-31 crash test. The broken support case was replaced and lead ballast was added to bring the transmission assembly up to the proper transmission and rotor assembly weight for the UH-1D.

The main rotor blades from the previous T-31 crash test were also used. The damaged outer portions of these blades were removed. Equivalent ballast weights were securely attached to the remaining 3-foot blade sections.

Landing Gear

A standard undamaged UH-1D landing gear was installed on the repaired fuselage. The landing gear was not modified.

Crew Seat and Anthropomorphic Dummy

A repaired UH-1D armored crew seat was installed in the pilot's position on the right side of the crew compartment. An instrumented Alderson F95 anthropomorphic dummy (205 pounds) was positioned in the pilot's seat, and the shoulder harness and the lap belt were secured. A close-up of the dummy and seat is presented in Figure 48.

No other seats were installed in the test vehicle.

Figure 48. Anthropomorphic Dummy and Crew Seat Installation.

Ancillary Equipment

Several items of ancillary equipment were tested to determine their mounting and/or tiedown adequacy.

First-Aid Kits

Four aircraft first-aid kits (FSN 6545-919-6650) were chosen as representative of on-board first-aid kits. Each was installed on the existing snap mounts. One was located at the rear of the cargo area, two on the left doorpost, and one on the right doorpost. Figure 49 illustrates a typical first-aid-kit installation.

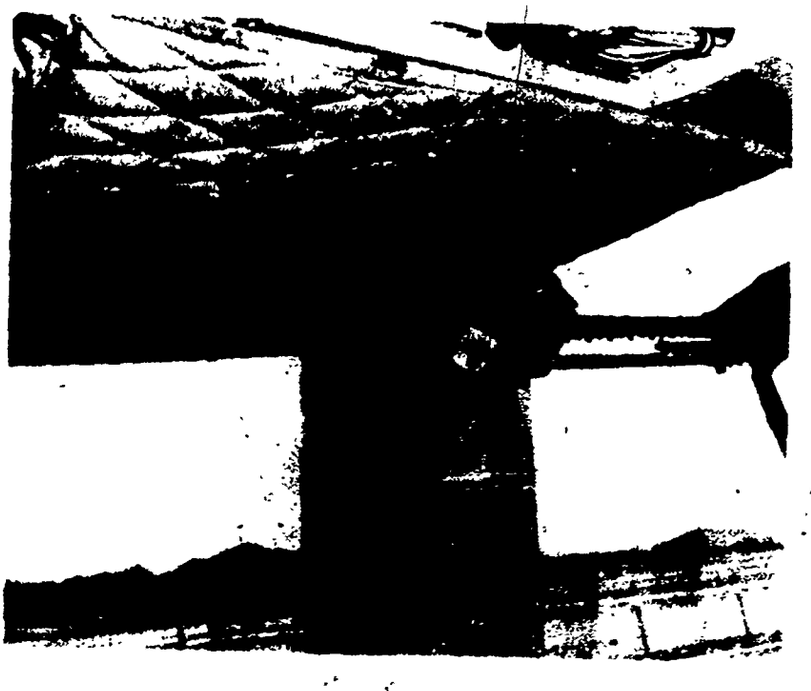

Figure 49. Typical First-Aid Kit Installation.

Fire Extinguisher

One 2-3/4-pound-capacity fire extinguisher (FSN 4210-555-8837) was installed in the existing mount bracket below and to the right of the pilot's seat (Figure 50).

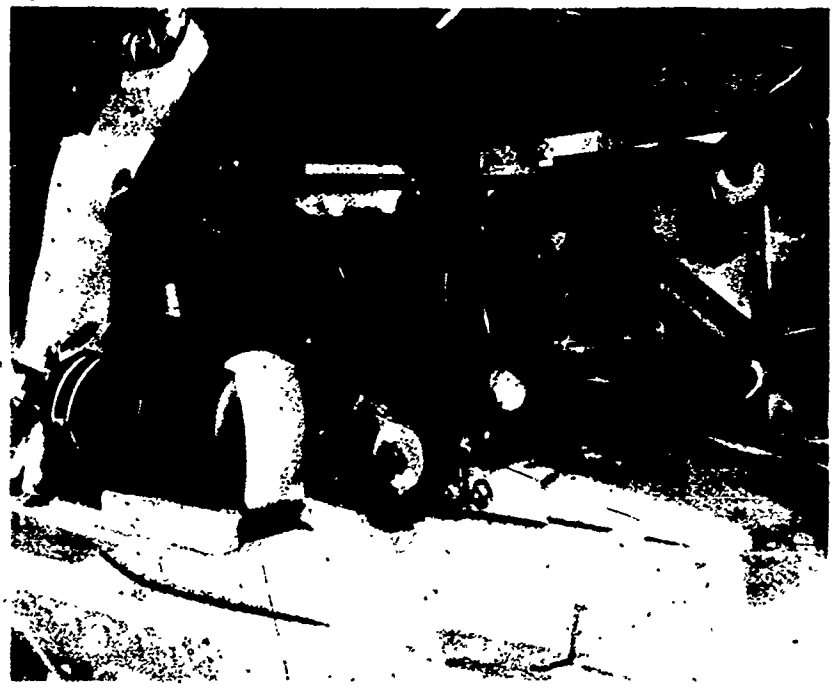

Figure 50. Fire Extinguisher Installation.

Toolbox

An aviation mechanics toolbox was chosen because of its weight (45 pounds) and potential for inflicting injuries on crew members and passengers. A survey of combat-experienced maintenance technicians revealed that the toolbox is normally stowed well forward in the aircraft near the control console between the pilot and copilot. This survey also revealed that the toolbox is usually not tied down.

The toolbox was positioned in the test vehicle behind the copilot's seat position. It was not placed directly behind the center console, since that space was used as an accelerometer position. The toolbox, shown in Figure 51, was not restrained from movement in the drop test.

Breakaway Self-Sealing Quick-Disconnect Valves

A ratchet-type breakaway self-sealing valve was mounted in the fuel supply line in place of the quick-disconnect at the

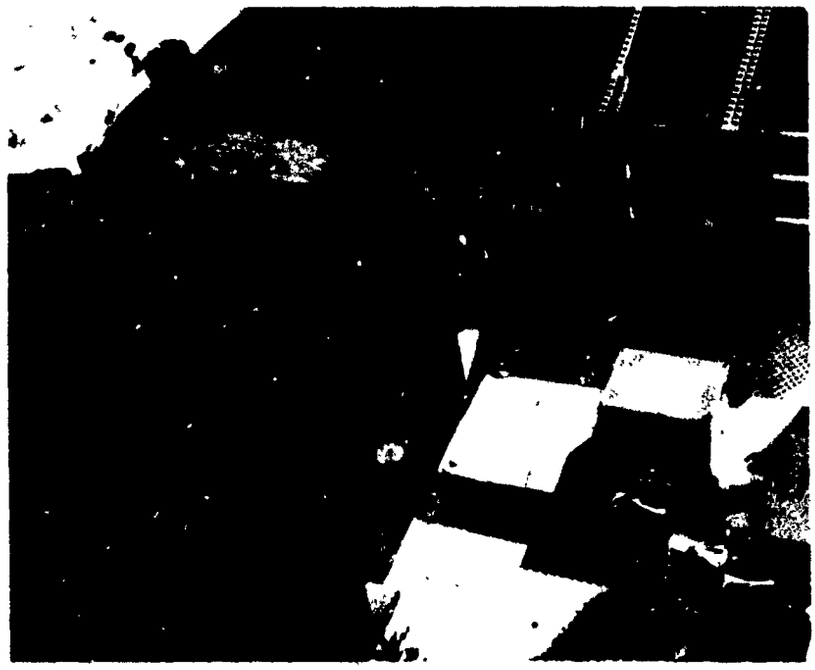

Figure 51. Mechanic's Toolbox Location.

attachment of the fuel supply line to the fuel filter (Figure 52). The centerline of the valve mounted in this manner would be perpendicular to the crash forces so that the mass of the valve half and the attached hose would act on the valve frangible section during the crash pulse. Since the breakaway self-sealing valve was designed to release only when acted upon by a tensile, bending, or direct impact force, it was not expected to actuate during this test drop.

Exterior Painting and Identification

The entire exterior of the test vehicle was painted a flat white. The assigned test identification number (T-34) was placed on the nose and on each side of the helicopter. At least one of the identifying numbers was in the field of view of each camera.

Weight and Balance

The total weight of the test vehicle was obtained after all components, equipment, simulated fuel, and instrumentation had

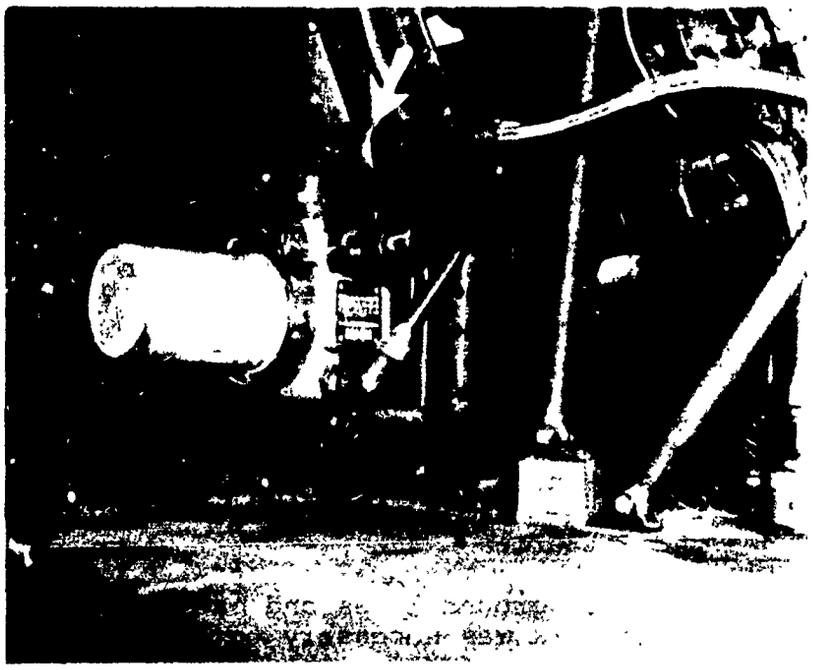

Figure 52. Fuel Filter and Breakaway Valve Installation.

been added. The test vehicle weighed 5,400 pounds, which was 3,600 pounds below the 9,000-pound desired gross weight at time of drop. Ballast was added to bring the gross weight up to the desired amount. This ballast was positioned throughout the cabin area with a maximum load distribution of 100 psi, which is within the design limits of the floor panels.

After the ballast was added and the proper drop weight was obtained, a check was made of the location of the helicopter center of gravity. The position of the ballast was then adjusted to move the center of gravity to a point near the forward limit.

The simulated fuel was then removed, following confirmation that no leakage existed.

FACILITY PREPARATION

Impact Pad

A 15-foot x 25-foot x 1-foot reinforced concrete pad was prepared as the impact surface for the test vehicle. This impact

surface was chosen to more closely represent the infinitely rigid impact surface used in the computer simulation.

Stadia Poles

Six stadia poles, marked off in 1-foot segments, were positioned on the concrete pad. These poles provided a dimensional reference for three ground-mounted high-speed cameras at time of impact. The stadia poles and impact pad are shown in Figure 46.

Camera Stands

Camera stands were erected at eight selected locations around the impact area to provide mounts for the high-speed cameras during the drop sequence.

Ground Lines and Batteries

The wiring network of ground lines and batteries was put into position. This network was necessary to insure the proper sequencing and operation of all eight high-speed cameras.

Stabilizing Ropes

Two 1/4-inch nylon ropes were attached to the tail boom skid of the test vehicle. These ropes were necessary to insure against lateral movement of the test vehicle prior to and during hook release.

Release Mechanism

An air-actuated release mechanism was used on this drop test. This hook release mechanism had been used successfully on numerous full-scale and component test drops.

INSTRUMENTATION

On-Board Data Acquisition System

Accelerations at various locations were to be recorded during the impact sequence. The relative locations of the sensing instruments are shown in Figure 53. All accelerometers, other than those installed in the anthropomorphic dummy, were housed in metal cases. A typical installation is shown in Figure 51.

The outputs of the accelerometers were fed individually to a central junction box mounted at the rear of the test vehicle cargo area.

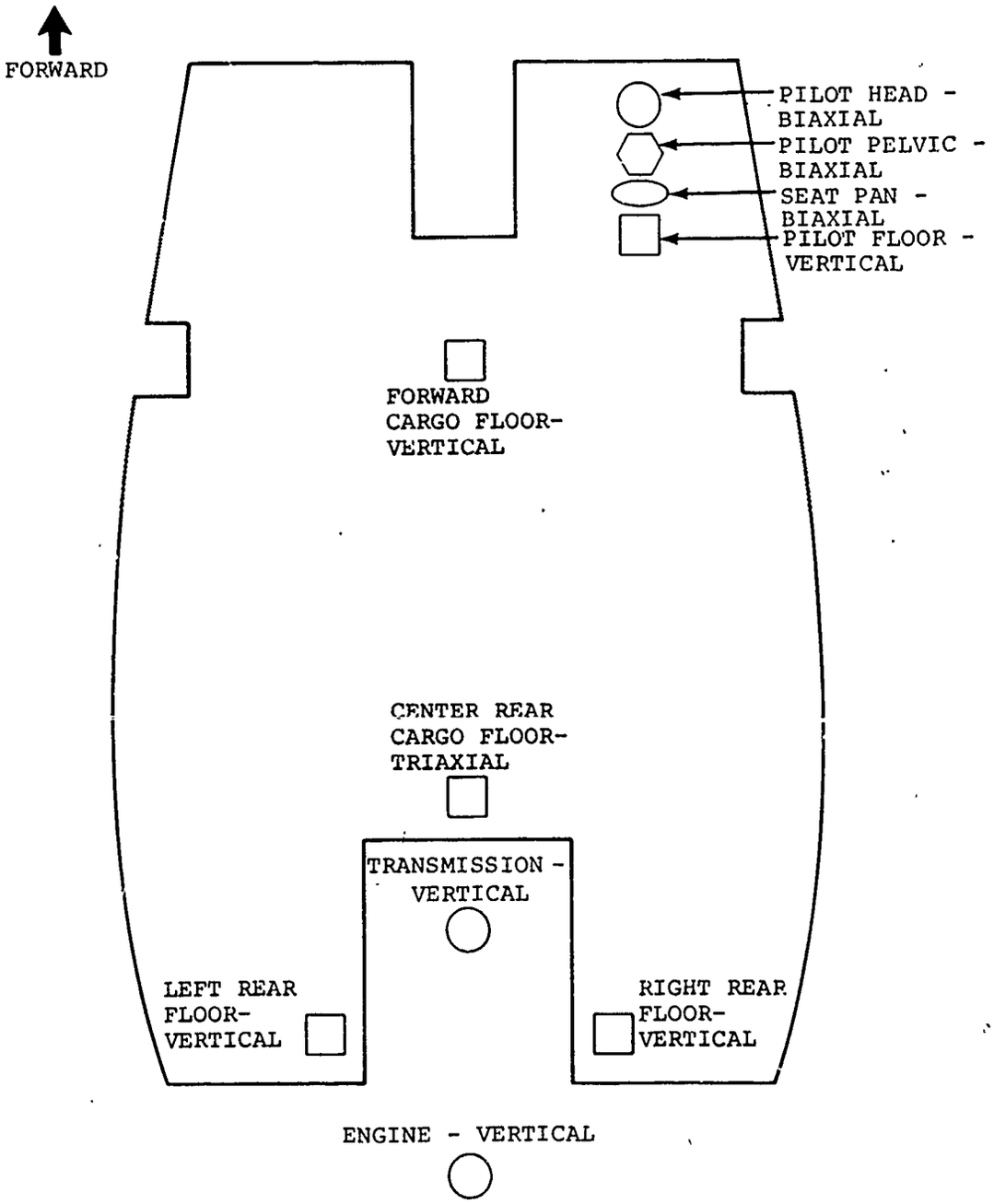

Figure 53. Accelerometer Locations.

Impact-Sensitive Switch and Correlation Lights

An impact-sensitive switch was mounted near the forward end of the right landing skid. Upon impact, this switch completed an electrical circuit that fired four flashbulbs for camera correlation and provided an electrical signal to correlate the data that was recorded on the FM tape recorder. Figure 54 shows the impact switch installation.

Figure 54. Impact-Sensitive Switch Installation.

Acceleration-Sensitive Switch

An acceleration-sensitive switch is being considered for use in helicopters as an electrical system inerting device. This switch (and its independent circuitry) was included in the test to obtain performance evaluation data. It was mounted directly on top of the engine accelerometer (Figure 55). This switch was designed to trip when subjected to a vertical acceleration in excess of 4G for a pulse duration of over 0.03 second. An electrical signal was fed through the switch, permitting the functioning of the switch to be recorded by the data acquisition system.

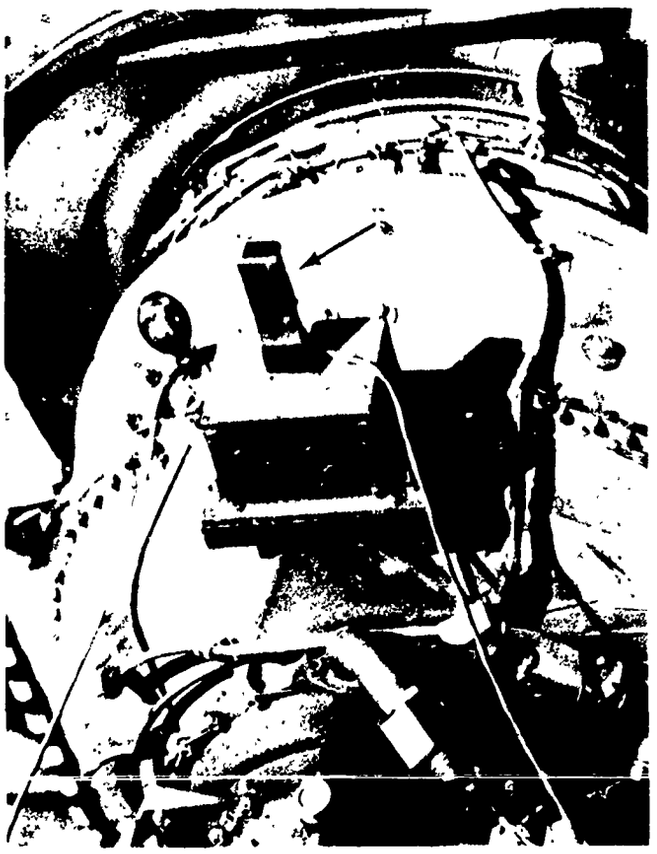

Figure 55. Acceleration-Sensitive Switch Installation.

Release Signal

A loop of small-diameter wire that completed an electrical circuit was mounted on the top of the rotor assembly. The loop portion of this circuit was placed on the lifting hook of the crane immediately prior to hoisting of the helicopter. The breaking of this circuit upon release of the helicopter was recorded to provide a means of measuring the time required for the aircraft to fall, from which impact velocity could be computed.

Umbilical Cable

A 50-foot-long umbilical cable fed the output of all instrumentation to the signal conditioning equipment located in an instrumentation trailer.

Signal Conditioning and Recording Equipment

The outputs from the accelerometers were fed into signal conditioning equipment that provided for the balancing and the controlling of the outputs. This conditioned signal was fed into individual voltage controlled oscillators. This voltage varied the frequency of the oscillators in proportion to the G-forces acting on the accelerometers. The output of the voltage controlled oscillators was amplified and recorded on the magnetic tape.

A Gensco Model 10-110(12012) FM tape recorder operating at a tape speed of 60 ips and capable of handling up to 25 channels of data was used to record the signals from the instrumentation.

FM Tape Playback

A CEC Model GR-2800 data tape equipped with filters and discriminators was used to reproduce the analog data from the test tape.

PHOTOGRAPHY

Motion Photographic Coverage

High-speed (1000 pictures-per-second) color film coverage of the helicopter drop sequence was provided to record the kinematics of the test items in the time interval between hook release and for several seconds following the completion of action after impact.

Eight high-speed cameras were used, positioned as shown in Figure 56.

Color documentary coverage at 24 pictures-per-second of the drop sequence was also provided.

Still Photographic Coverage

Black and white 4- x 5-inch photographs were taken of the test vehicle prior to the drop sequence. These included general overall views of the helicopter and test site as well as detailed close-ups of test articles and installations.

Black and white 4- x 5-inch photographs and colored 35mm slides were taken of the wreckage following the drop. These photographs included overall views, damaged areas, close-ups of individual components, and damaged items or areas following disassembly.

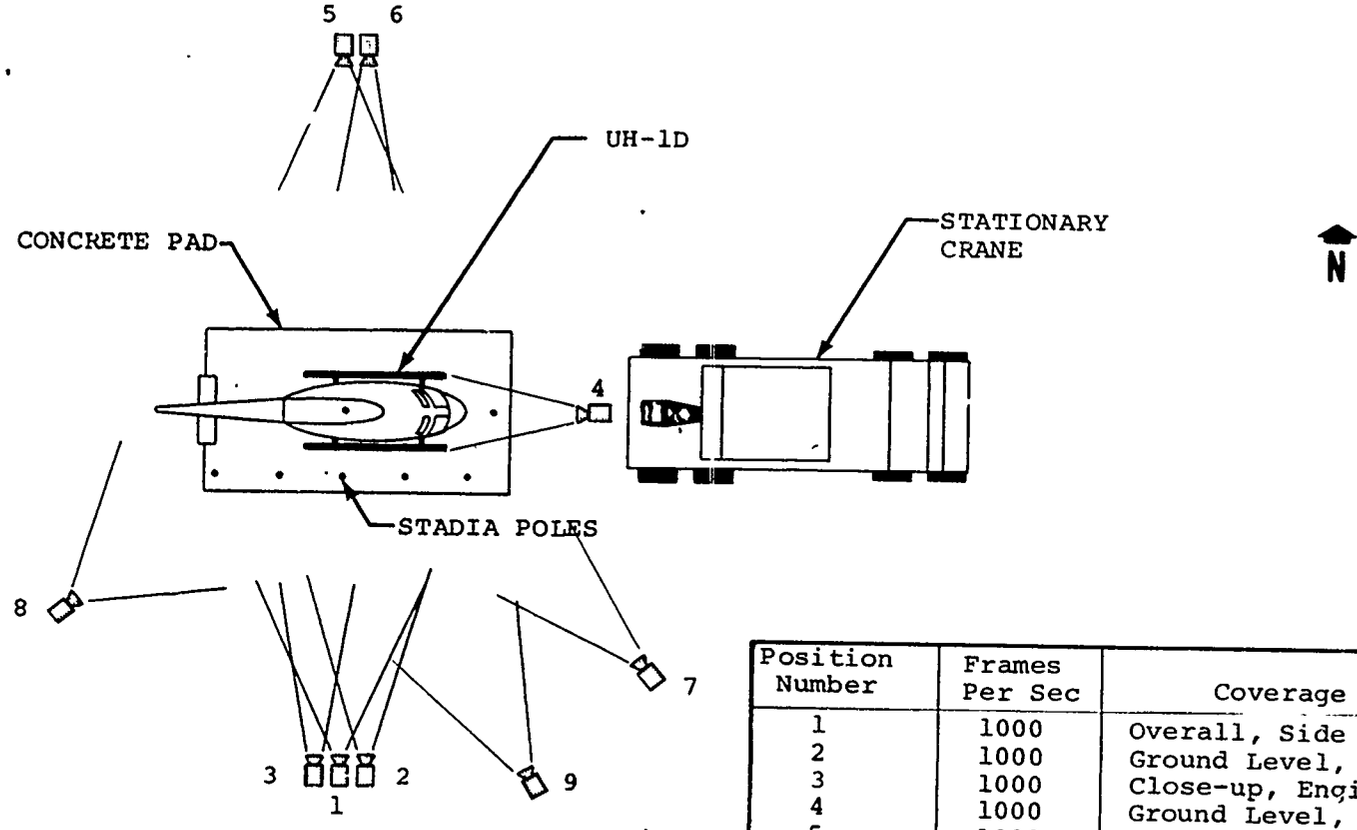

Position Number	Frames Per Sec	Coverage
1	1000	Overall, Side
2	1000	Ground Level, Gear
3	1000	Close-up, Engine
4	1000	Ground Level, Front
5	1000	Overall, Side
6	1000	Ground Level, Gear
7	1000	Overall, Front Quarter
8	1000	Overall, Rear Quarter
9	24	Tracking
Cameras 1 through 8, Photosonics 1B; Camera 9, Bolex.		

Figure 56. Camera Locations.

DROP TEST

General

The test vehicle was prepared and instrumented as described previously. The target crash conditions at impact were as follows:

- Drop Height - 14 ft
- Vertical Velocity - 30 fps
- Longitudinal Velocity - 0 fps
- Lateral Velocity - 0 fps
- Flight Path Angle - 90°
- Resultant Flight Path Velocity - 30 fps
- Pitch Angle - ±3°
- Roll Angle - ±3°
- Yaw Angle - ±3°
- Test Weight - 9,000 lb

Final Preparations

The test vehicle was moved to the impact area and positioned on the drop pad. The fuel tanks were filled with 173 gallons of colored water to simulate the weight of a UH-1D's normal servicing of 220 gallons of JP-4 fuel.

The high-speed cameras and associated wiring were placed in position. The umbilical cable was attached to the test vehicle, and the instrumentation was made ready.

A motorized crane equipped with a 70-foot boom was used to lift the helicopter. Prior to lifting, a 0- to 10,000-pound load cell was installed between the crane hook and the attachment point on the test vehicle. Final ballast adjustments were then made to obtain a gross drop weight of 9,000 pounds. The test vehicle was then lowered onto three load cells, and weight and balance calculation was again verified. The center of gravity was calculated to be at fuselage station 132.2. The allowable c.g. range for a gross weight of 9,000 pounds is from fuselage station 131.8 to 143.6.

The static pitch and roll angles were then checked and found to be -1-1/2 and 0 degree, respectively.

The test vehicle was lowered to the pad, and pretest photographs were taken.

The stadia poles were placed in position and the wire loop used to indicate hook release was installed. Final instrumentation and camera adjustments were made. After a final check-out of all systems, the test vehicle was raised to a height of 14 feet and released.

TEST RESULTS

General

Posttest examination of the high-speed film revealed that the helicopter impacted in a 1/2-degree nose-down attitude while yawed 2 degrees to the right and level laterally. The velocity at impact was 29.9 fps, as calculated from the recorded data.

With the exception of one high-speed camera and two accelerometers, all cameras and instrumentation functioned properly. Camera No. 6 (Figure 56) did not run at its programmed speed, but fluctuated widely, rendering the film valueless. The vertical accelerometers in the seat pan and dummy pelvis (Figure 53) malfunctioned on impact, causing loss of this data.

Those traces considered most pertinent to the mathematical simulation are presented and discussed in the section dealing with the correlation of the simulator with the test data.

An overall posttest view of the test vehicle is presented in Figure 57.

Landing Gear

The landing gear cross tubes distorted outward and upward, permitting the fuselage to contact the concrete pad. The cross tubes did not fail but were permanently distorted, permitting the fuselage to rest on the concrete pad (Figure 58). The fuselage remained within 1 inch of the pad after all simulated fuel was drained from the tanks. The lowest point of the loaded fuselage prior to the drop was slightly over 14 inches.

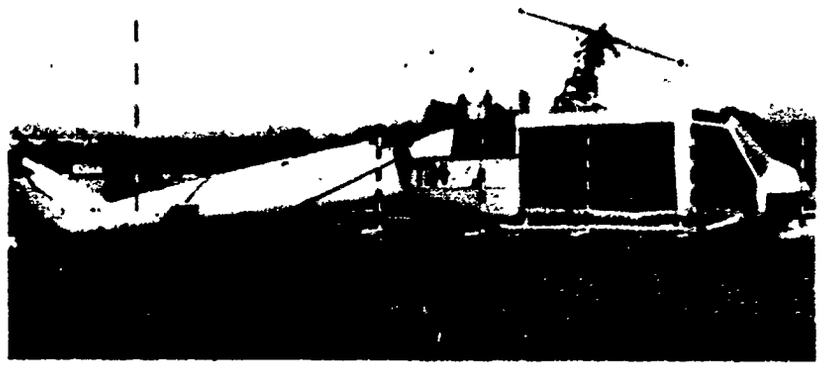

Figure 57. Overall Posttest View.

Figure 58. Three-Quarter Posttest View.

Fuselage Structure

The entire lower portion of the fuselage contacted the concrete pad following the collapse of the landing gear. The jack pad lugs on the bottom of the fuselage made indentations in the concrete averaging 7/16 inch in depth.

The deformation of the lower fuselage structure and the fluid in the under-floor tanks forced the cargo floor panels at each side of the lower pylon area (island) upward. Scratch marks on the pylon sides indicate that the inboard edge of the floor panels above the fuel tanks buckled upward as high as 8-1/2 inches for the right panel and 10-1/4 inches for the left panel prior to tank rupture. The aft portion of the inboard edge of the right floor panel remained 6 inches above the normal position, and the aft portion of the inboard edge of the left panel remained 5 inches above the normal position (Figure 59).

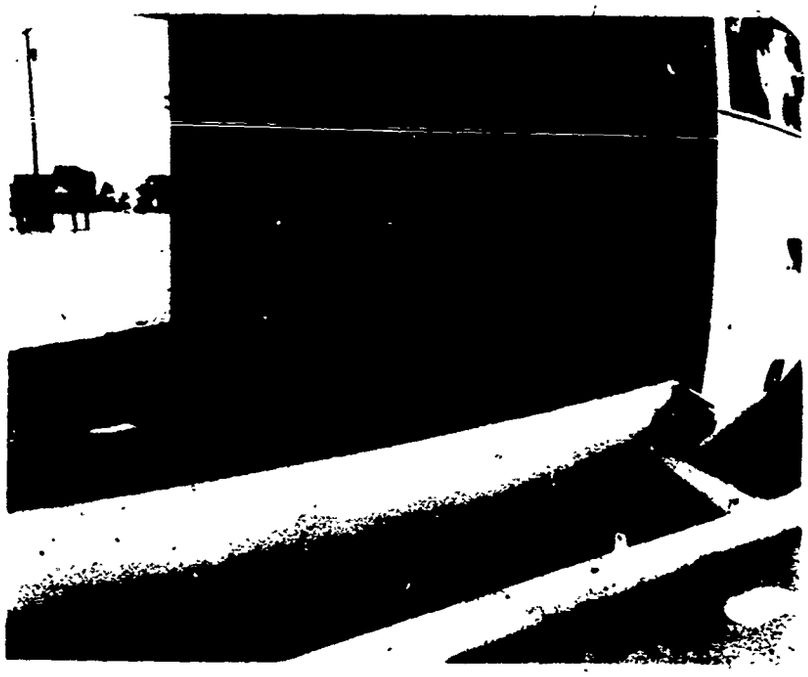

Figure 59. Cargo Floor Distortion.

The floor separation at fuselage station 129.0 was almost 2-3/4 inches on the right side (Figure 60) and 1-3/4 inches on the left side (Figure 61).

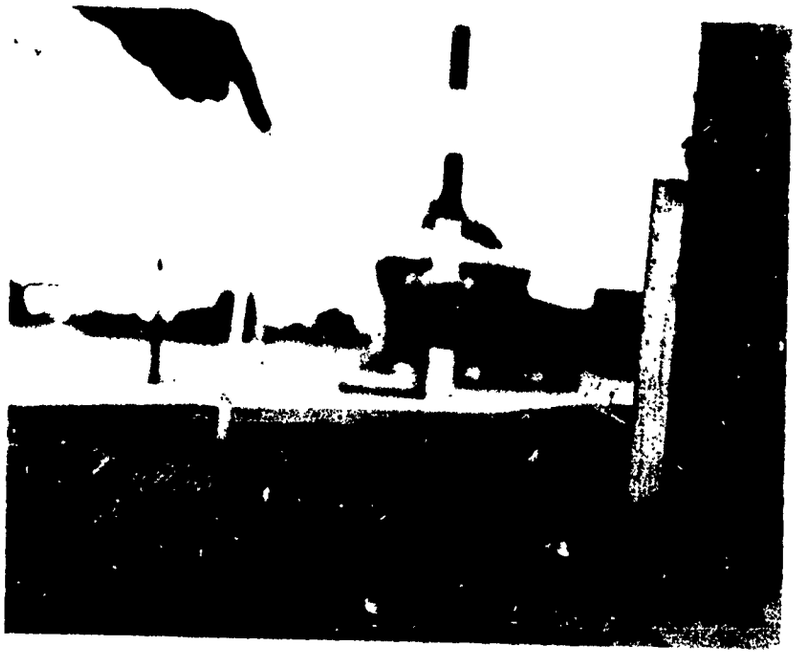

Figure 60. Close-up of Right Cargo Floor Distortion Inboard of Fuel Cell.

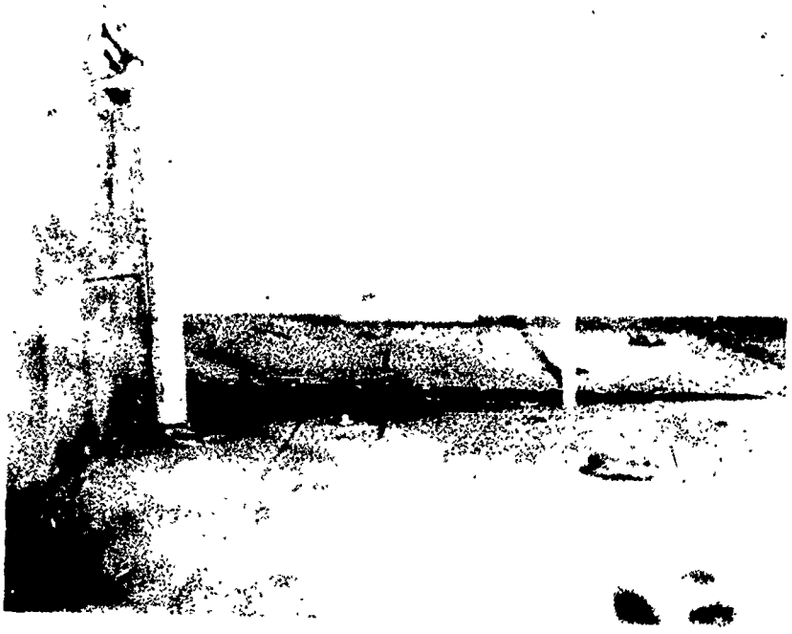

Figure 61. Close-up of Left Cargo Floor Distortion Inboard of Fuel Cell.

The landing gear cross tubes deflected upward into the fuselage structure, as shown in Figures 62, 63, 64, and 65, causing the structure above them to fail in several locations.

The fuselage keel sections and bulkhead panels surrounding the under-floor fuel tanks were badly crushed (Figures 66, 67, and 68). The fuselage shell was permanently distorted, as shown in the posttest photographs presented herein. The nose of the helicopter deflected downward, forward of the front landing gear cross tube.

Tail Boom

After the lower portion of the fuselage contacted the concrete pad, the tail boom continued downward, applying a moment to the fuselage. This tended to raise the front of the helicopter. The upper two tail boom attachment bolts then failed, permitting the tail boom to pivot about the lower attachment points. The end of the tail boom came to rest on the ground approximately 1 foot below the concrete surface (Figure 69).

Cargo Floor and Ballast

The floor panels of the cargo compartment were loaded with ballast, as shown in Figure 70, a posttest view. The load distribution did not exceed the recommended 100 psi. All ballast stayed in position except the 200-pound weight to the right of the pylon and the 100-pound weight to the left of the pylon. These two weights were thrown free when their restraining straps failed during rebound.

The most severe floor deformation occurred at the rear of the cargo area on each side of the island. The deformation of the floor in the forward portion of the cargo area measured 2 inches, as shown in Figure 71.

The support post (part number 205-001-302-1) for the tube and lever assembly of the flight control system was forced upward through the floor panel at fuselage station 90 and butt line 12. Further penetration was prevented by the ballast on the floor above the support post. Figure 72 shows the damaged support post after the removal of the damaged floor panel.

Fuel System

General

All simulated fuel was lost from the fuel system. Posttest investigation revealed that the fuel system was damaged in seven locations.

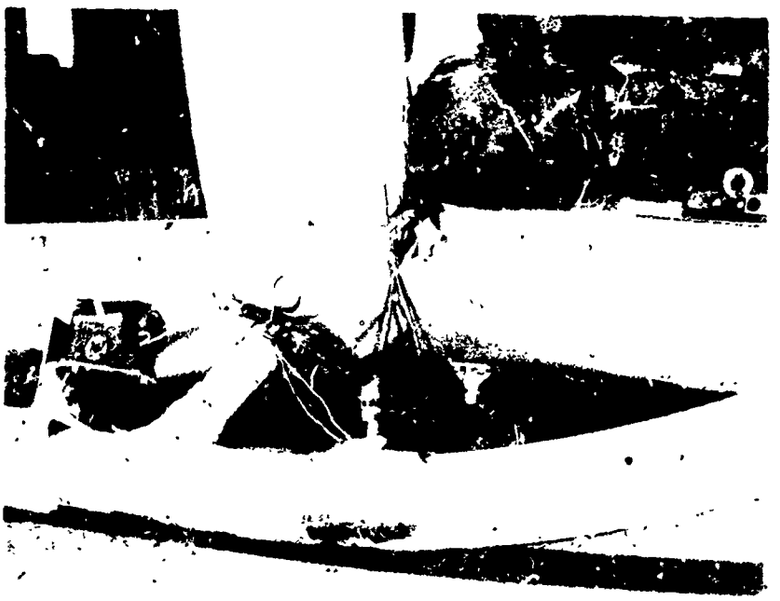

Figure 62. Fuselage Damage at Right Front Cross Tube.

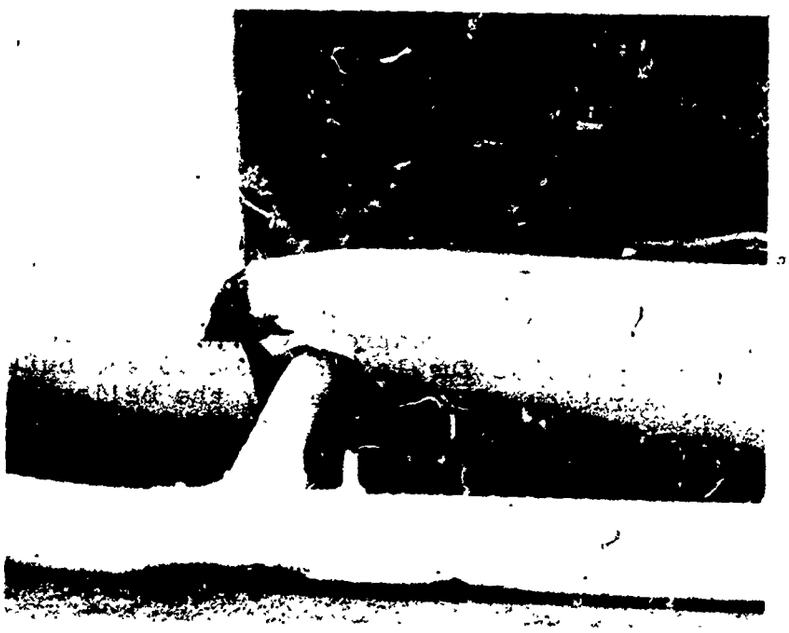

Figure 63. Fuselage Damage at Right Rear Cross Tube.

Figure 64. Fuselage Damage at Left Front Cross Tube.

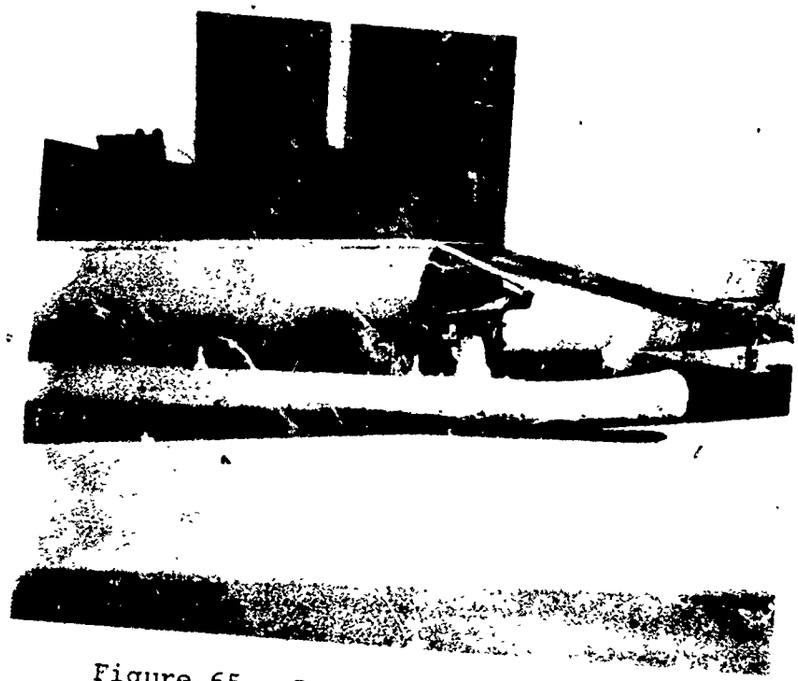

Figure 65. Fuselage Damage at Left Rear Cross Tube.

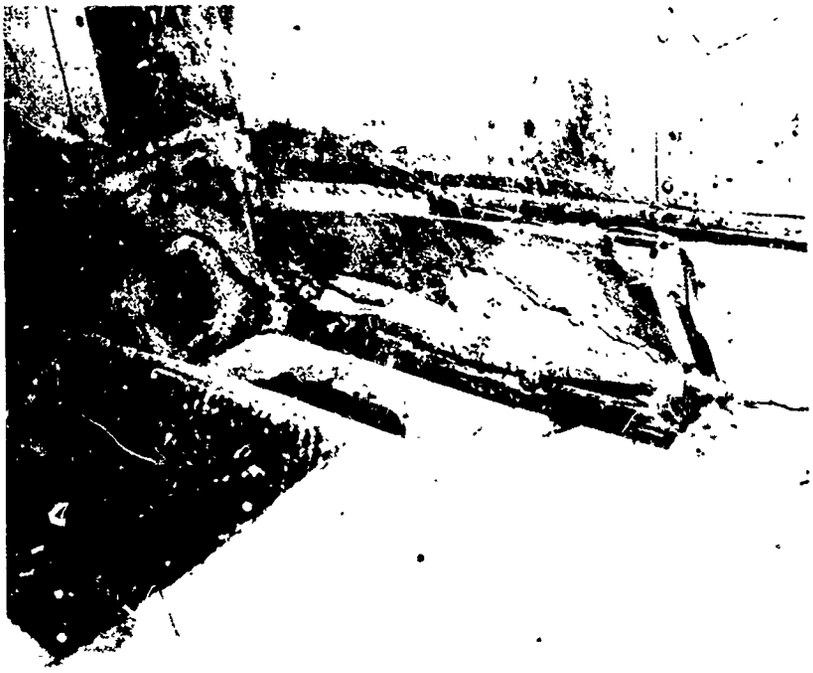

Figure 66. Fuselage Damage Around Right Under-Floor Fuel Tank Cavity, Looking Aft.

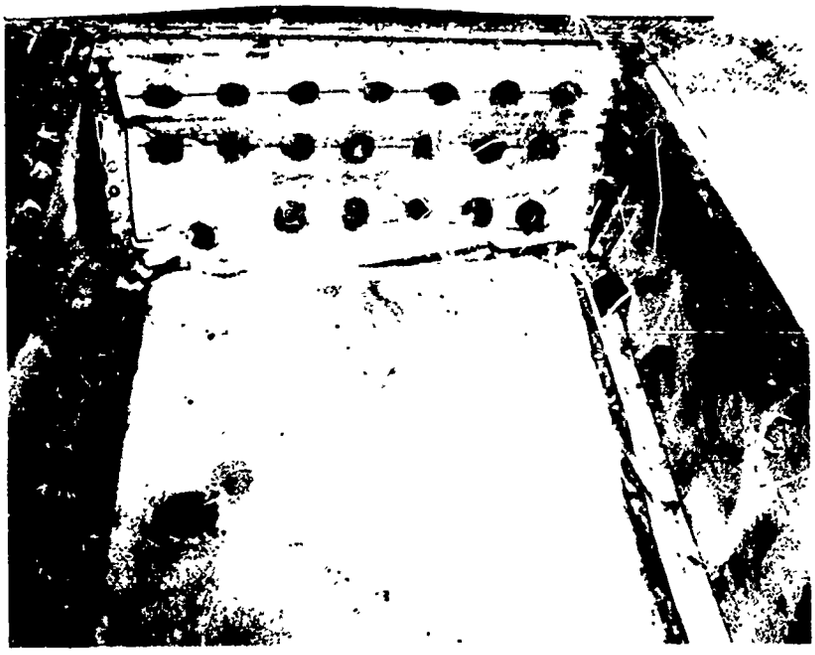

Figure 67. Fuselage Damage Around Right Under-Floor Fuel Tank Cavity, Looking Forward.

Figure 68. Fuselage Damage Around Left Under-Floor Fuel Tank Cavity, Looking Aft.

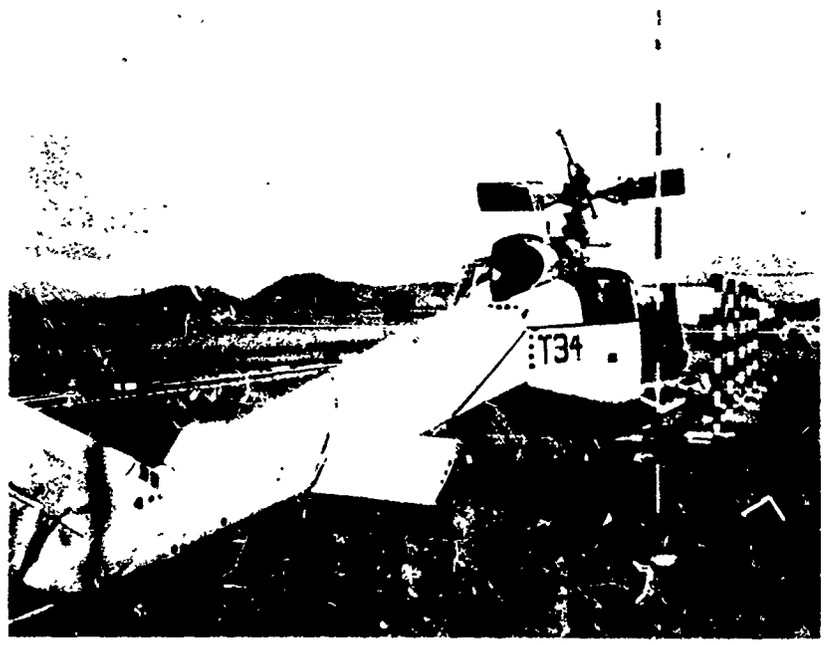

Figure 69. Final Position of Tail Boom.

Figure 70. Posttest View of Ballast in Cargo Compartment.

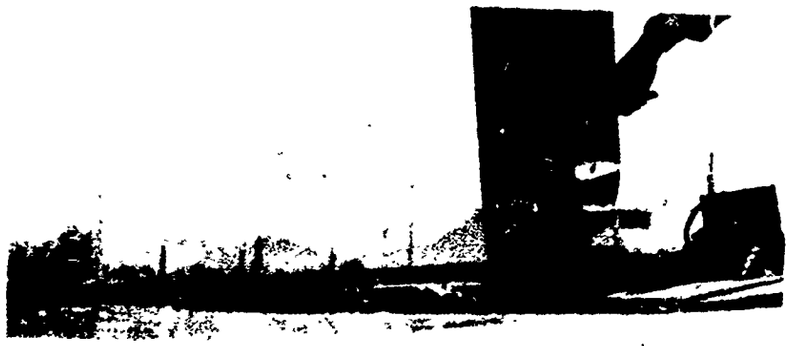

Figure 71. Deformation of Forward Cargo Floor.

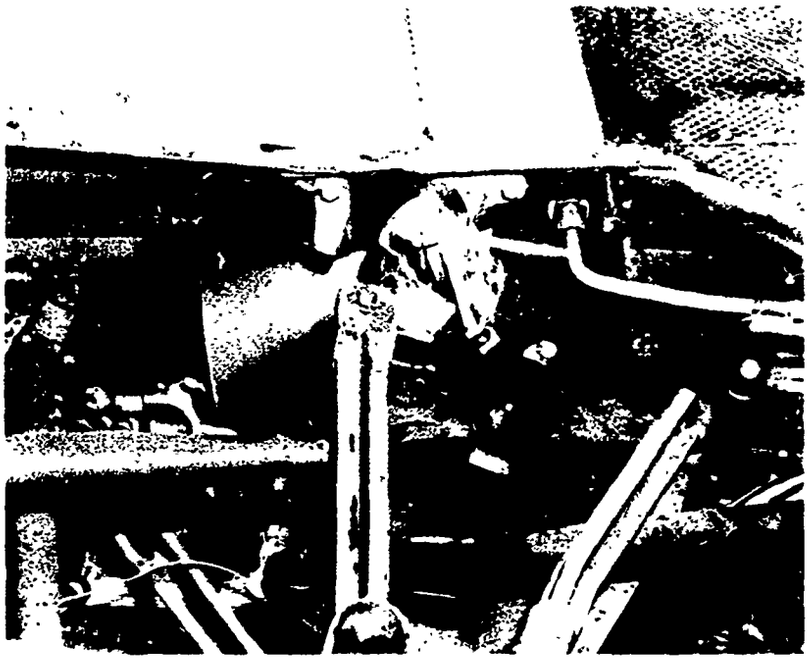

Figure 72. Damaged Support Post (P/N 205-001-302-1).

Right Under-Floor Tank

Fuel escaped from the right under-floor tank in two locations. Immediately following impact, the tank material failed inboard of the long narrow access plate that was located in the top of the tank. This tear was 19 inches long and apparently resulted from the pressure build-up in the fuel tank immediately following impact (Figure 73). Fuel escaping from this opening sprayed through the floor separation forward of the pylon area (Figure 74) and into the cabin area and ceiling.

The sump assembly plate was distorted as a result of the lower fuselage deformation. This permitted fuel to escape past the O-ring seal, thus draining the entire tank.

Left Under-Floor Tank

The left under-floor tank was damaged in two locations. The access plate tore free from the surrounding tank material along one 18-inch side and across both 2-inch

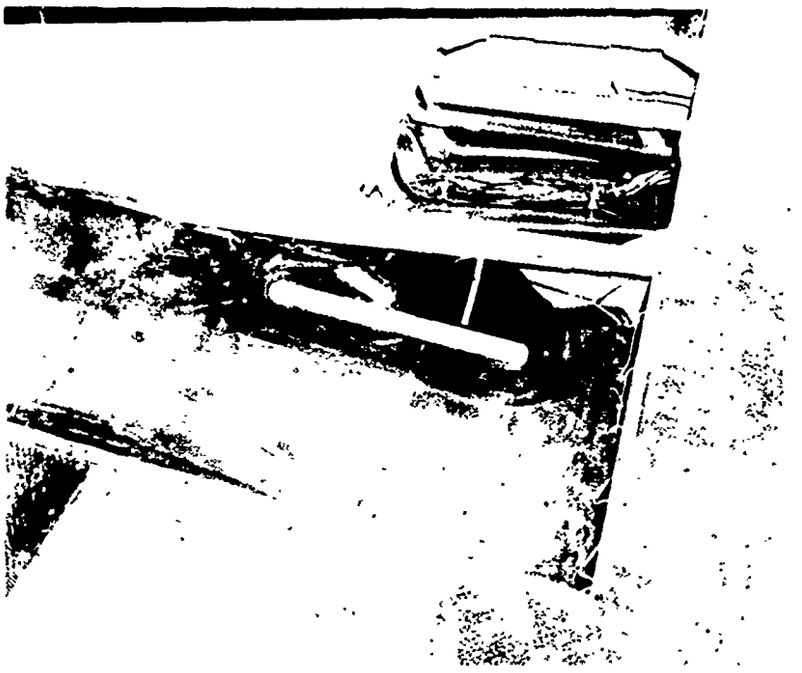

Figure 73. Damage to Right Under-Floor Fuel Tank.

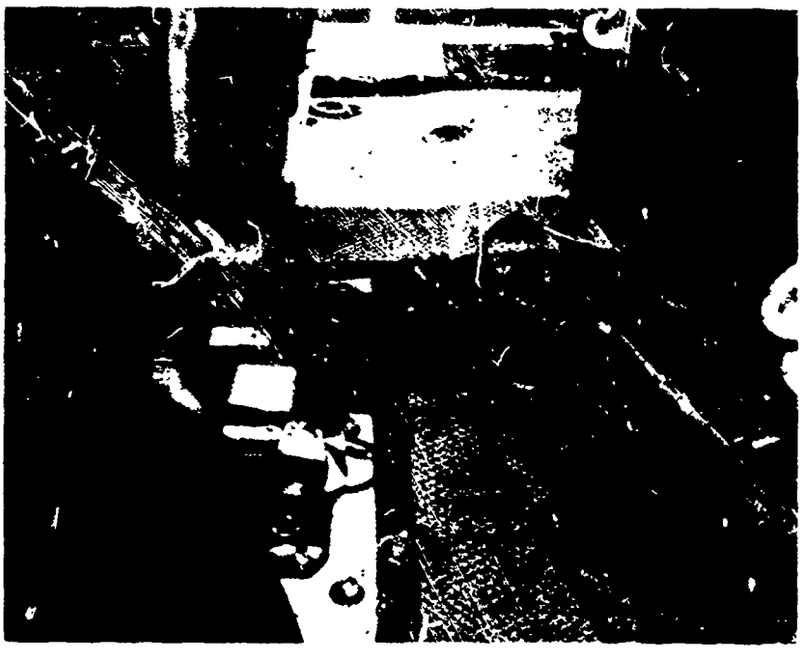

Figure 74. Floor Separation Inboard of Right Under-Floor Fuel Tank.

ends (Arrow A, Figure 75). The vent attachment fitting, midway back along the upper inboard edge of the tank, tore the tank material adjacent to it along two sides for a total tear length of 7 inches (Arrow B, Figure 75). Fluid escaped from both of the e openings when they were ruptured as a result of the pressure buildup on impact. Figure 75 also shows the failed quantity indicator in the center foreground following removal from the right tank.

Figure 75. Damaged Under-Floor Fuel Tanks Following Removal From Test Aircraft.

The quick drain located in the sump assembly plate was depressed by contact with the concrete pad after the collapse of the landing gear. Continued contact with the concrete pad permitted the drain to be held open, resulting in the loss of all fluid in the tank.

Aft Tanks

The bottom of the center aft tank was punctured by a portion of the fuselage structure that was forced upward

through the honeycomb panel and into the tank material. The resulting three-corner tear in the tank material measured 3/16 inch by 3/8 inch. The protrusion into the tank cavity is shown in Figure 76.

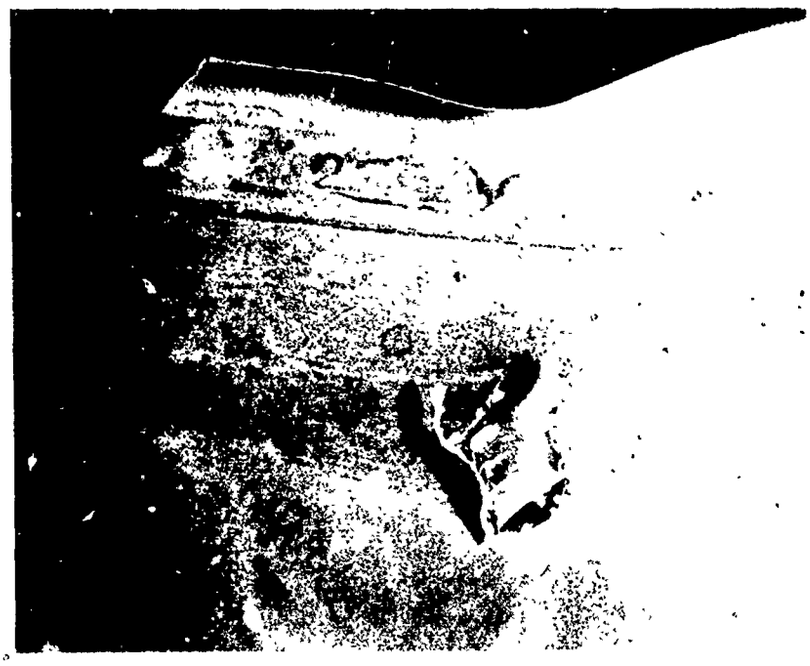

Figure 76. Puncture in Center Aft Fuel Tank.

The smaller two aft tanks located on each side of the center tank received no damage. However, the fluid in the tanks was lost both through the opening in the interconnected center tank and through the openings in the lower tanks and line.

Fuel Lines

The fuel lines that connect the five tanks in the UH-1D fuel system were distorted as a result of the upward movement of the rear cross-tube and the collapsing of the lower-fuselage structure. No fluid was lost from the fluid lines except in the crossover assembly, which permits the center aft tank to drain into he crossover

between the right aft tank and the right under-floor tank. This crossover line received a 1/2-inch cut perpendicular to the flow direction at the point where the line passes through the right keel below the center tank (shown by the arrow in Figure 77.

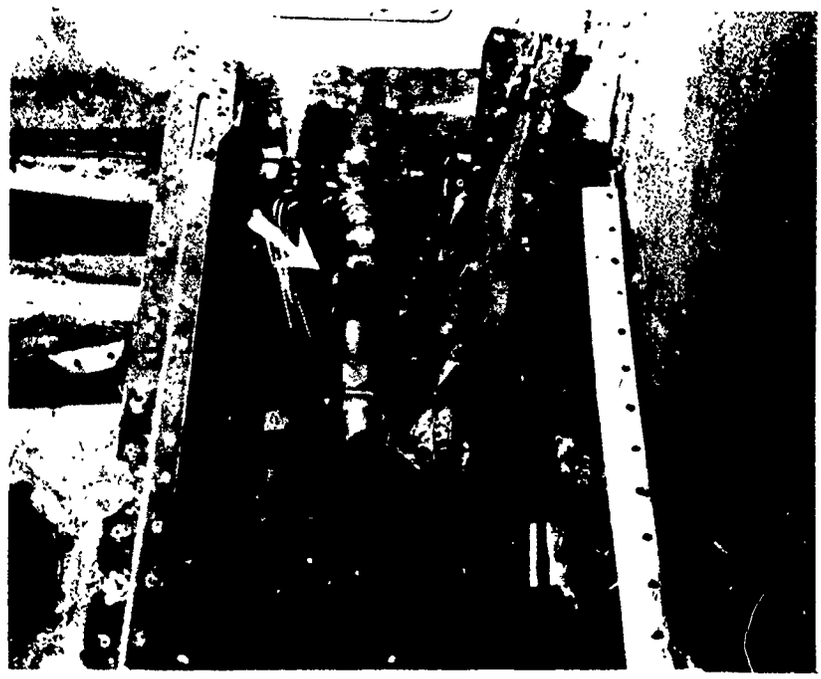

Figure 77. Fluid Loss From Failed Cross-over Line Aft of Right Under-Floor Tank.

Oil System

The oil system remained intact throughout the impact sequence, and no oil loss occurred. The displacement of the engine did remove all slack and apply a load to the 3/4-inch oil breather line attached to the upper boss at the rear of the oil tank. This loading did not fail the elbow end fitting, but it did deflect the boss on the oil tank downward, as shown by the arrow in Figure 78.

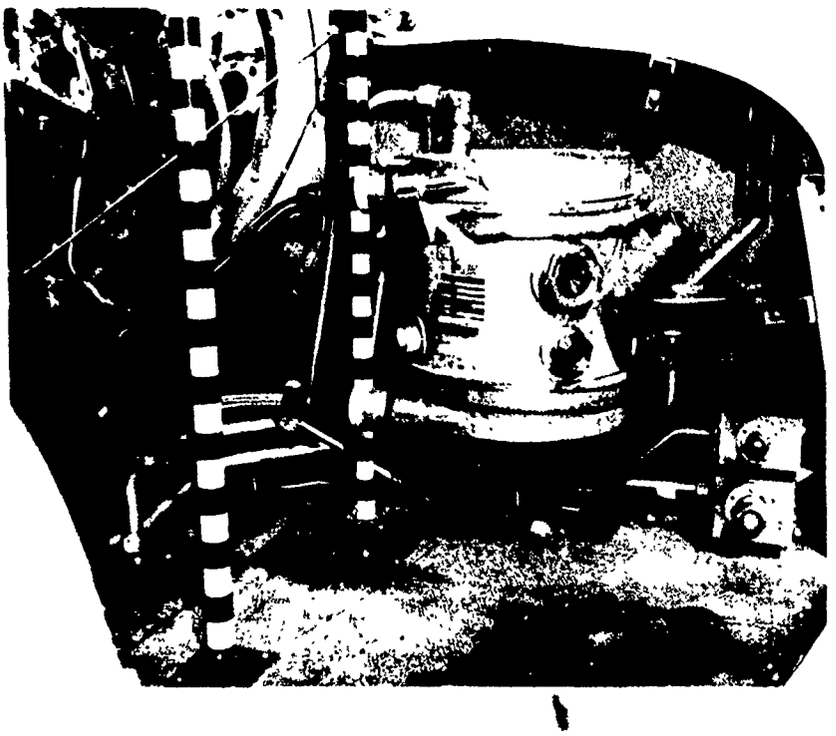

Figure 78. Bent Oil Breather Line Boss on Oil Tank.

Power Plant

The engine moved downward and to the right when subjected to the impact load. All 6 tubes of the engine mount assemblies received some damage. Both legs of the bipod mount on the right side buckled, as shown in Figure 79. The single tube at the left front of the engine buckled, while the legs of the tripod support of the left mount were only slightly bowed (Figure 80). The high-speed film indicates that the right mount trunnion bearing deflected downward 7 inches during impact and remained 5 inches below its original position.

Acceleration-Sensitive Switch

The acceleration-sensitive switch mounted on the engine accelerometer box functioned during the impact.

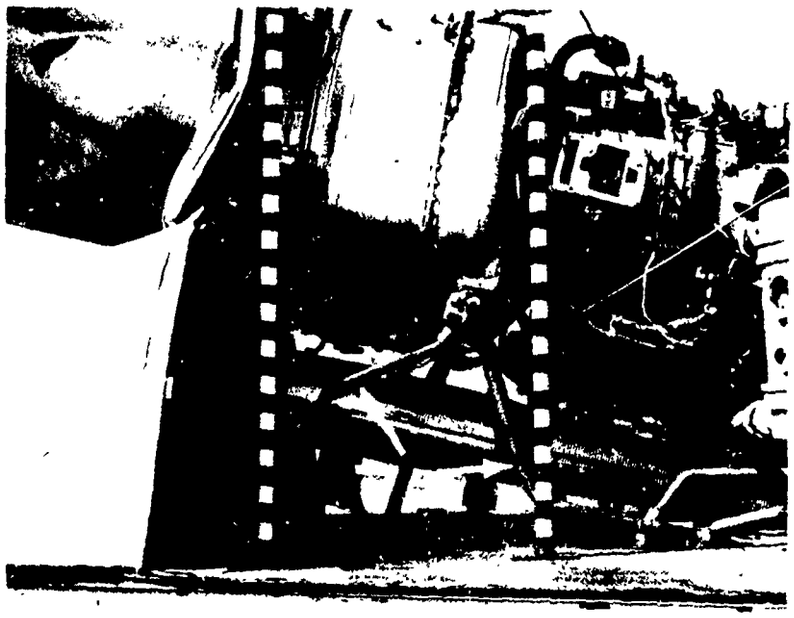

Figure 79.. Damage to Right Engine Mount.

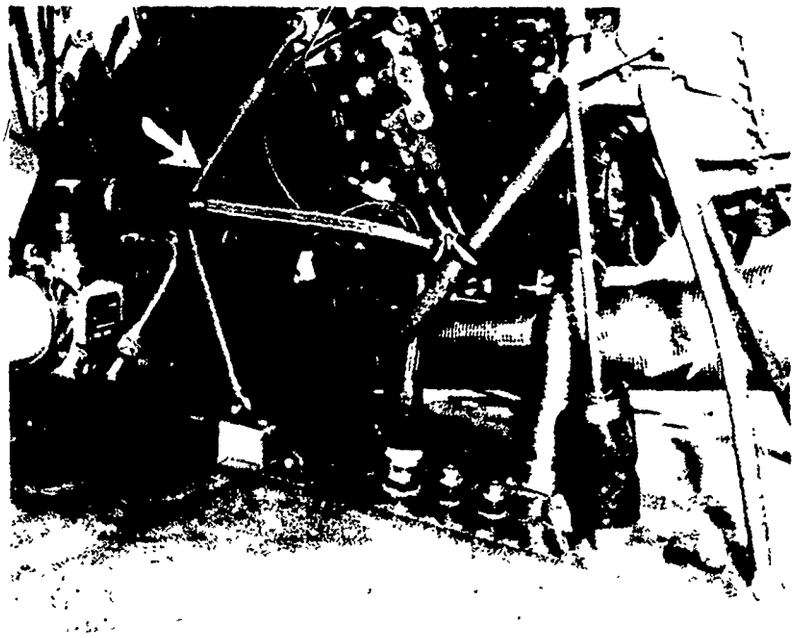

Figure 80. Damage to Left Engine Mount.

Transmission and Rotor Assembly

The impact load placed upon the transmission assembly resulted in failure of all four legs of the transmission support base. Two of these legs are shown in Figure 81. The stability link at the bottom of the transmission also failed. The transmission and rotor mast then rotated forward approximately 18 degrees against the top of the cabin roof.

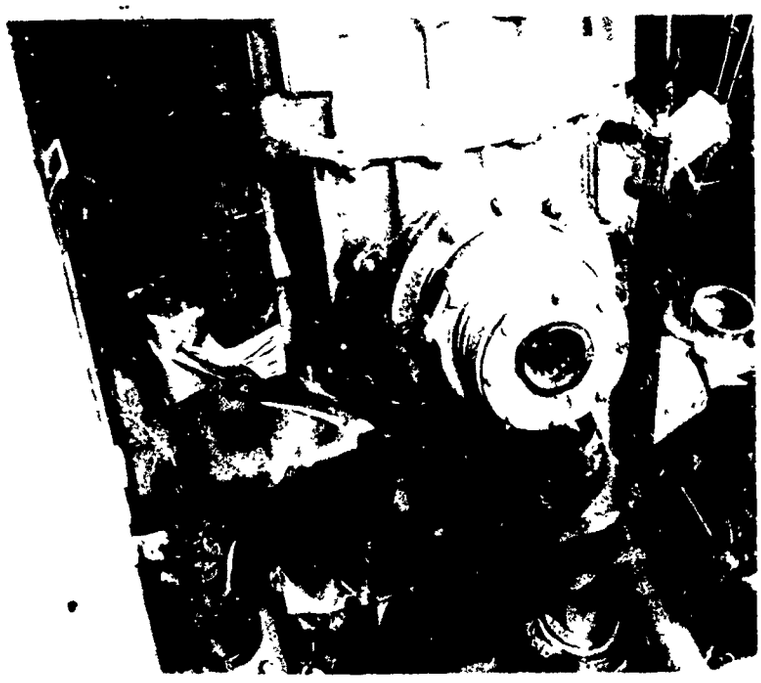

Figure 81. Damage to Transmission Support Base.

Crew Seat and Anthropomorpic Dummy

Minor damage was noted to the crew seat installed in the pilot compartment. The seat remained in place and provided restraint for the occupant. A posttest view of the seat and occupant is shown in Figure 82.

The front of the seat pan deflected downward during impact, due to bending of the rear support columns. This seat had been fitted with modified rear support columns that are stronger

Figure 82. Posttest View of Crew Seat and Anthropomorphic Dummy.

than the standard columns, and so fared better than a standard crew seat would have. The downward movement of the pan caused the occupant's upper torso to pitch forward and contact the glare shield on the instrument panel with his head. This pitching was aggravated by slack in the restraint harness resulting from the failure of the net seat liner that allowed the occupant to move down in the seat.

Analysis of the high-speed film showed violent flailing of the occupant's head and extremities.

Ancillary Equipment

The four aircraft first-aid kits (FSN 6545-919-6650) that were installed in the existing snap mounts did not fall free during the impact sequence. However, only the one installed on the right doorpost near the pilot's head was still retained by all four attachment snaps following the impact. The first-aid kit installed in a similar position on the left doorpost was retained by only the two top snaps following impact (Figure 83). All snaps of the kit installed on the left doorpost held except one (Figure 84). The kit installed at the rear of the

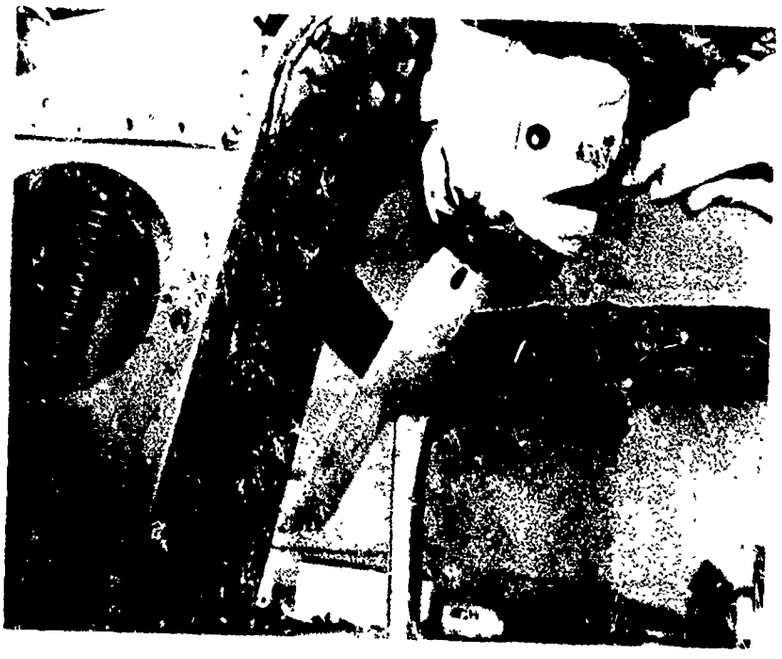

Figure 83. Posttest View of First-Aid Kit on Left Doorpost Overhead.

Figure 84. Posttest View of First-Aid Kit Installed Low on Left Doorpost.

cargo area was held by only the two lower snaps following t: impact (Figure 85; the two arrows indicate the two upper sna mount posts).

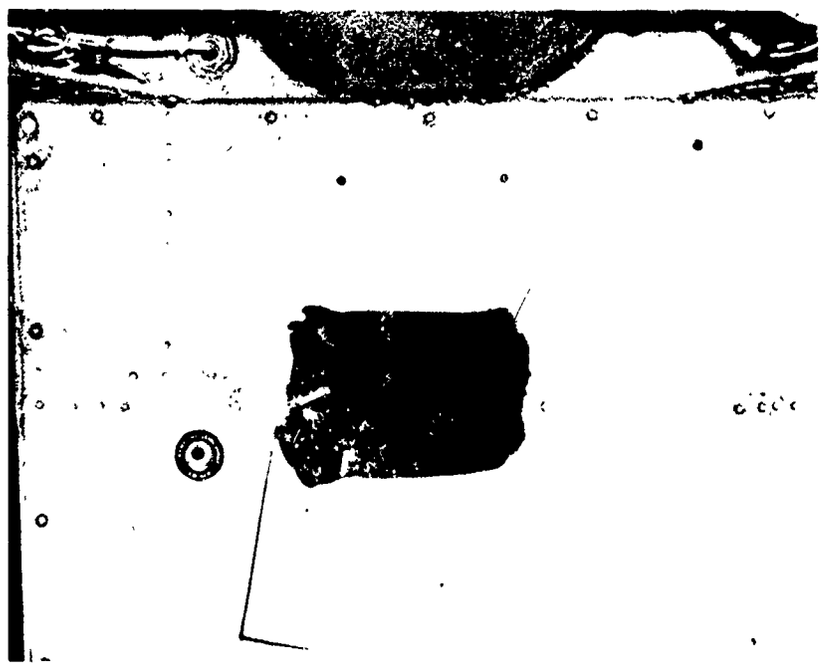

Figure 85. Posttest View of First-Aid Kit Installed in Rear of Cargo Compartment.

The 2-3/4-pound fire extinguisher (FSN 4210-555-8837) that was installed in the mount bracket below and to the right of the pilot's seat was not affected by the crash impulse and remained secure in its mount (Figure 82).

The aviation mechanic's toolbox (weight 45 pounds) was displaced 1-7/8 inches to the right and 1-1/4 inches to the rear by the impact (Figure 86).

CORRELATION OF THE FULL-SCALE TEST WITH THE MATHEMATICAL SIMULATION

The correlation between the test results and the analytical predictions of the mathematical model is focused around four major areas:

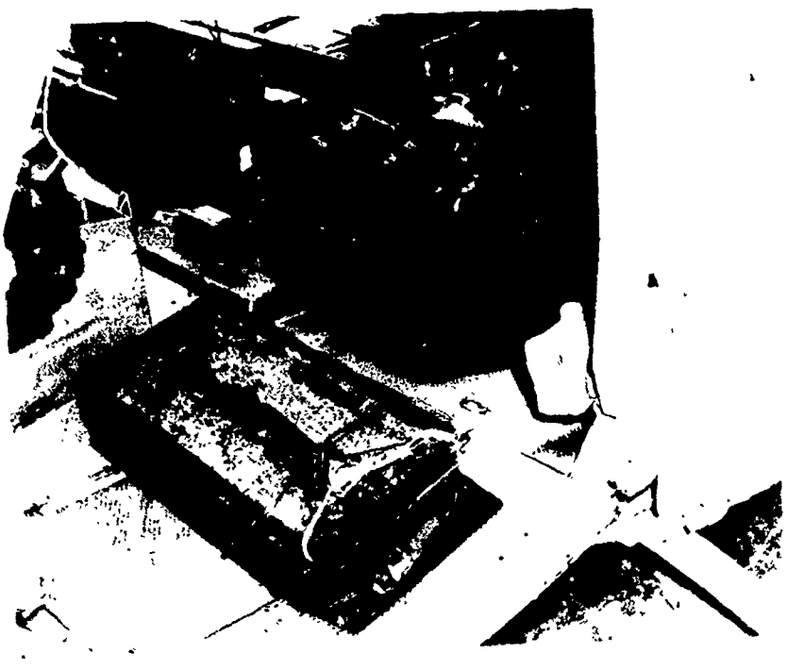

Figure 86. Posttest View of Mechanic's Toolbox.

1. Correlation of general deformation.
2. Correlation of general acceleration levels.
3. Correlation of more specific relative deformation, such as the engine, transmission, and belly of the aircraft.
4. Correlation of the general shape of the acceleration response curves and time.

General Deformation

The general deformation of the postcrash configuration agreed reasonably well with the mathematical simulation. The mathematical model indicated the total collapse of the landing skids and their inability to support the weight of the airframe after impact, as shown in Figures 57 and 58. The tail boom failed and formed the plastic hinge as shown in Figure 57; however, the plastic hinge in the computer simulation was somewhat stiffer, allowing the boom to rotate only 10 degrees.

An interesting point of correlation of the model is the assumed location of the forward plastic hinge point. A plastic hinge was formed at fuselage station 110, which agrees with the modeling configuration of Figure 20 (compare Figures 20 and 21 with Figure 57). However, an additional hinge formed just forward of the front skid attachment point (a deformation pattern which the program is unable to correlate since it has only two possible plastic hinge locations).

Careful review of the high-speed films showed, however, that the formation of the plastic hinge at fuselage station 70 occurred during the secondary impact following rebound. This explains the apparent inconsistency in the angular deformation of the forward fuselage section of Table VII. The model indicated a -0.026 radian angular deformation or approximately a 2-degree nose-up condition. Analysis of the high-speed films indicated that this was the condition of the airframe immediately after the primary impact.

The validity of the model is further reinforced by the close agreement between measured and predicted floor acceleration at the pilot's location. The inability of the simulator to produce the drooping nose in the postcrash condition is not considered serious since the more severe conditions occur earlier in the impact.

Acceleration Levels

The peak accelerations at several locations in the aircraft are compared for the simulator and test results in Table VIII.

TABLE VIII. COMPARATIVE ACCELERATION DATA

Location	Acceleration (G) Test T-34	Simulator
*Forward Floor	-110	-116
**Rear Floor	-72	-74
Engine	-90	-64
Transmission	-70 +110	-43

*Average of 2 locations
**Average of 3 locations

The acceleration levels shown for the model simulation are obtained from Figures 30 and 31 and Table VII. Measured acceleration-time histories are shown in Figures 87, 88, and 89.

The extremely close correlation of floor accelerations (Figures 31, 87, and 88) indicates that the model was accurately simulating the actual landing skid and fuselage structure load-deflection characteristics. The comparison of the engine acceleration levels produced by the simulator and the test indicates that a minor adjustment to the simulated load-deflection characteristics for the engine support system is necessary. The adjustment is minor because the relative deformation was accurately predicted.

The area of least satisfactory correlation is the transmission. Figure 89 shows the acceleration-time history of the transmission. Failure of the front supports occurred at 0.13 second, causing the entire system to pivot forward about the rear supports and control linkage. This flailing action produced the usual acceleration response shown in Figure 89 - a delayed positive acceleration pulse occurs at approximately .240 second. The rotor support system programmed into the model was an approximate 8G vertical strength system, which did not permit the rotation and flailing action that occurred in the test. The computer simulation produced a total failure of the rotor support system, permitting the transmission and rotor to move vertically into the box structure of the aircraft fuselage. This total failure permitted increased deformation, and, consequently, a lower negative acceleration level of 43G compared to the test results of 70G. The nature of the failure of this rotor support system accounts for the large inconsistency of the test results and computer simulation.

The actual rotor support system is apparently stronger than the programmed 8G level. The load-deflection characteristic of the rotor support system in the simulator would have to be changed to compensate for this discrepancy. The transmission on the drop test failed in an undesirable manner; i.e., it tended to rotate the rotor system forward and down into the crew compartment. This deformation trend is serious because the rotating blades are inclined toward the angle required to intersect the pilot and copilot stations.

Relative Deformation

Analysis of the high-speed 16mm motion film indicated a maximum deformation of 2-3 inches for the crushable belly of the fuselage upon impact. Approximately 1 inch of the deformation was recovered by elastic rebound. Computer simulation results summarized in Table VII yielded a 2.5-inch average value for

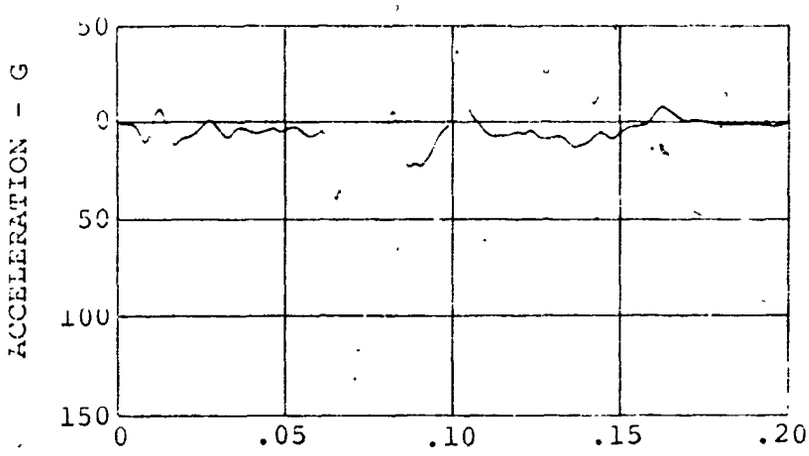

PILOT FLOOR

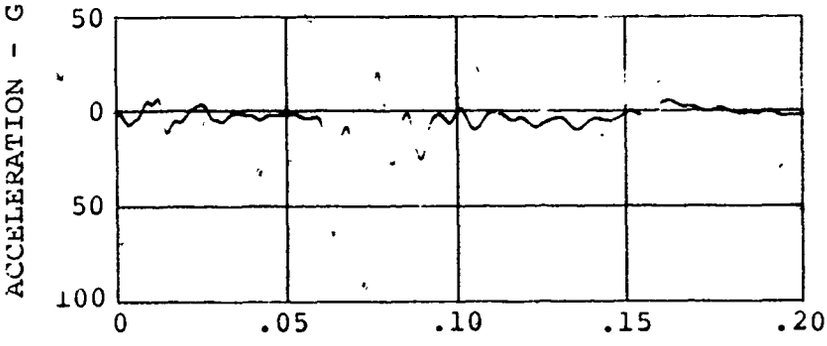

FORWARD CARGO FLOOR

Figure 87. Acceleration-Time Histories - Forward Floor.

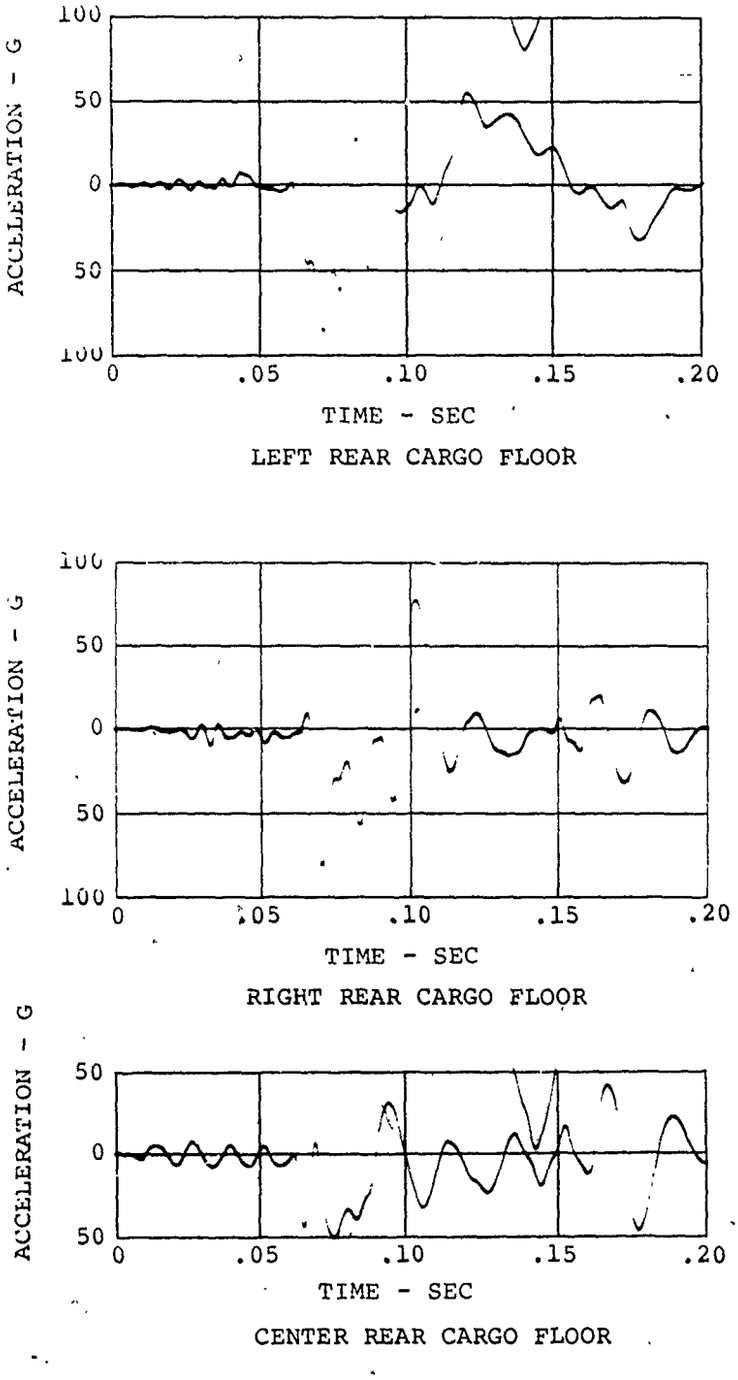

Figure 88. Acceleration-Time Histories - Rear Floor.

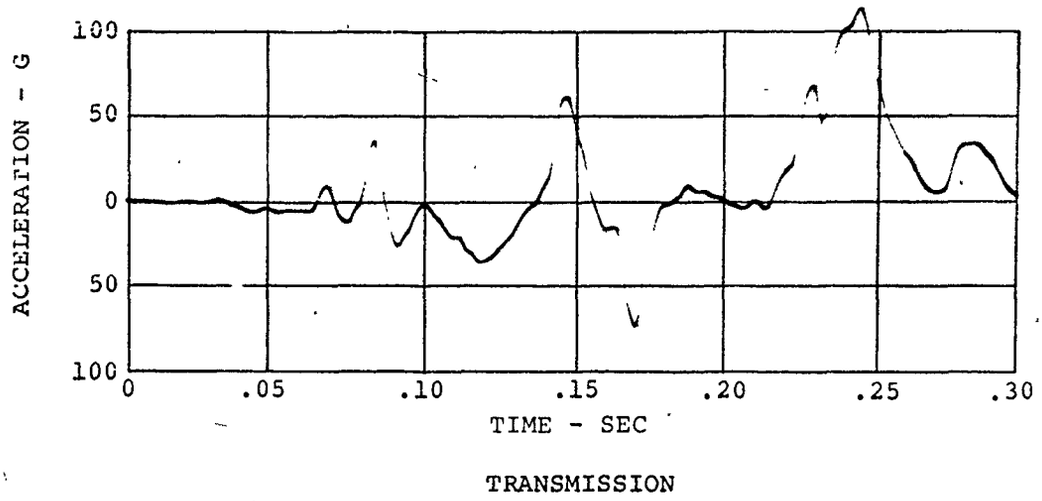

TRANSMISSION

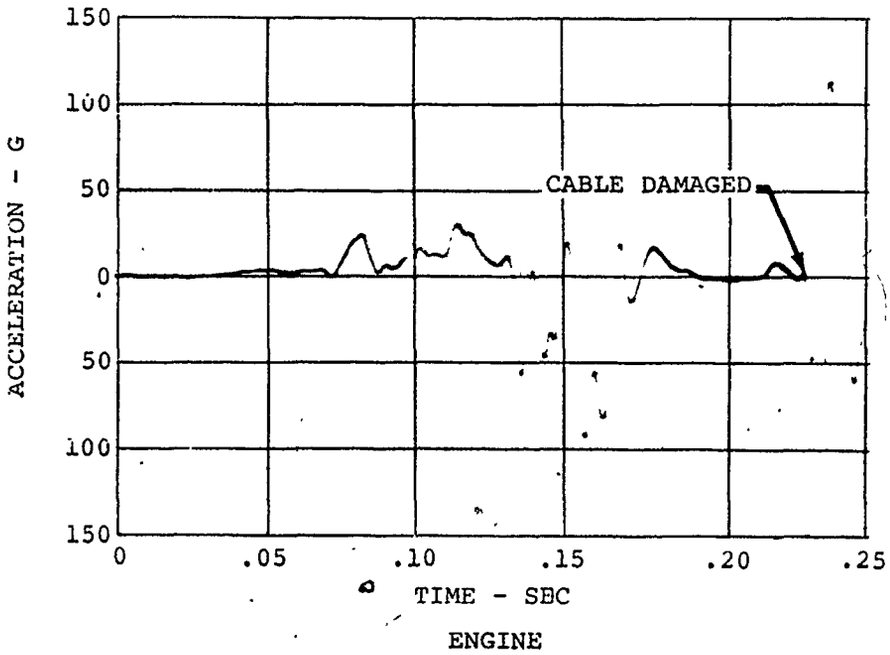

ENGINE

Figure 89. Acceleration-Time Histories - Transmission and Engine.

forward and rear floor relative deformation. This close correlation is not surprising, since the acceleration level agreed so well.

The relative deformation of the engine was determined from film analysis to be approximately 5 to 5-1/2 inches. The model supplied a 4.95-inch relative deformation. However, rotor and transmission results do not agree because the model's transmission broke loose completely from its mounts and moved vertically approximately 8.7 inches relative to the fuselage top surface. Actual test results, however, yielded only a 2-3-inch vertical movement of the transmission. The larger value from the model resulted from an underestimated strength of the support system.

This illustrates one deficiency of the computer simulator: the lack of a rotational degree of freedom for the transmission system that would permit this type of postcrash configuration. The load-deflection characteristics for the transmission could be adjusted to obtain closer correlation; however, the rotational tendency of that component of the aircraft cannot be simulated by this model.

The relative deformations of these major components are shown in Table IX.

TABLE IX. MAJOR COMPONENT DEFORMATION

Item	Deformation (inches) Test	Simulation
Floor	2-3	2.5
Engine	5-5.5	4.95
Transmission	2.5-3.0	8.74

Acceleration-Response-Time History

The test aircraft and the simulation model agreed in gross weight, weight distribution, and input conditions. There was one area, however, in which the two did not agree. The lowest point of the test aircraft's fuselage was approximately 14.5 inches above the ground when the helicopter was supporting its own weight. The mathematical simulation used a corresponding dimension of only 9.5 inches. To understand the effect of

this difference, see Figure 36. Notice that floor accelerations are unaffected by available stroke for the UH-1D/H landing gear strength of 4G. This fact is illustrated by the very accurate correlation obtained for floor acceleration.

The effect upon the engine and transmission is shown in the same figure. One would have expected the measured accelerations to be slightly lower than predicted if the load-deflection properties of the supporting system were exactly correct. This would serve as a guide in estimating the increase in engine and transmission strength required to more closely correlate with the test.

The effect of the additional 5 inches of landing gear stroke (14.5 actual, less 9.5 simulated) would tend to shift the time scale of the acceleration-response-time history of the test data. This 5-inch difference in gear stroke would produce a time shift of approximately 15 milliseconds. Comparison of these acceleration responses in Figures 30 and 31 and Figures 87 and 88 shows the general nature of these responses to be quite similar. The response of the model's floor oscillated more than the actual test, indicating that the mathematical model was slightly underdamped in this area. The engine and rotor support system, however, appeared to be slightly overdamped.

The times at which peak accelerations occurred are summarized in Table X. The time for the test results has been shifted .015 second to account for the difference in available landing gear stroke.

TABLE X. TIME TO PEAK FOR KEY ACCELERATION EVENTS

Item	Maximum Acceleration Time (milliseconds)	
	Test	Simulation
Floor (pilot)	55	40
Floor (rear)	55	30-40
Engine	145	50
Transmission	175	60

Correlation of the response curve and time of peak acceleration for the floor can be considered good. Poor correlation of the transmission is due to the mode of transmission support failure.

The relatively poor correlation of the time at which the engine acceleration peaks is more difficult to explain; however, two important factors strongly affect the engine. Engine support strength for the model was overestimated by approximately 20 percent, and damping characteristics were overestimated by some unknown amount. A second iteration of the input data in this area would be required to understand the difference.

DISCUSSION OF PROGRAM RESULTS

The ability of the mathematical model to simulate the general crash deformation characteristics is acceptable. The generality of the mathematical model permitted a reasonable lumped-mass representation of the major structural components of the test aircraft.

The ability of the mathematical model to predict acceleration levels and relative deformations of particular areas of the aircraft has been proven. In the comparison between model and test results, the correlation of acceleration levels and deformation characteristics for the pilot's station was excellent; the correlation of rear floor and cargo compartment data was very good; the correlation for the engine response, as indicated by the acceleration data, was fair to good; while comparison of transmission response was poor.

The ability of the model to correlate with any particular test is completely dependent on the accuracy of the input data in describing the structural properties of the airframe. The input data for the simulator results presented here were obtained by some analytical work, reinforced by intuitive engineering thought about the crash dynamics expected, based upon past experience in this area. A second iterative pass on the input, adjusting structural properties, based upon accurate information for this particular helicopter, could eliminate the weak points of correlation. It is strongly felt that the prediction of transmission acceleration could be adjusted to within acceptable engineering accuracy, and that the time correlation for the entire test could be improved.

The results of this test should be used to further improve the ability of the model to simulate the crash conditions. For example, the correlation of test results and model response indicates the following initial structural adjustments to the model are necessary:

1. Extend the available landing gear stroke from 9.5 to 14.5 inches.

2. Slightly increase the damping for the crushable fuselage belly.

3. Adjust the characteristic of the boom-fuselage plastic spring to permit total failure and ground impact.

4. Decrease the engine strength level approximately 20 percent, and the damping factor slightly.

5. Increase the transmission strength level approximately 10 to 20 percent. Damping appears acceptable.

Even if these improvements were not applied to the model, the computed floor acceleration as a function of time can still be used to evaluate the effect of the crash on the passenger.

The test illustrated the insignificant amount of energy-absorbing capability in the landing support system.

Although it is a check of only one point, and therefore not capable of being interpreted statistically, the parametric study helped to check the effect of the additional 5 inches of available gear stroke on measured acceleration. It was concluded that additional available landing gear stroke in conjunction with an increase in strength of the gear would help attenuate floor acceleration.

CONCLUSIONS

Based upon the accident survey, computer simulation, and test T-34 results, the following conclusions are presented:

1. The sideward (lateral) impact is a significant crash condition, because more than half of the accidents studied resulted in significant lateral force.

2. The fuselage structural design features needing greatest improvement in this particular type of helicopter are listed in order of priority:

   a. Structural integrity and energy-absorbing mechanisms to keep personnel in place with a livable volume in sideward (lateral) impacts.

   b. Energy-absorbing mechanisms to prevent excessive upward decelerative forces on seated occupants in severe vertical impacts.

   c. Fuselage strength and continuity to provide a livable volume in sideward and forward "roll-over" accidents.

   d. Transmission retention strength sufficient to prevent penetration of the troop compartment.

3. The lumped-mass modeling technique can adequately simulate the vertical crash condition for a general rotary-wing aircraft.

4. The floor accelerations for an aircraft similar to the UH-1D/H may be reduced as much as 65 percent by energy-absorbing techniques in the landing gear system and the belly of the fuselage.

5. Inability of the mathematical model to predict the transmission response sheds serious doubts upon the validity of the parametric study in this area and indicates that further study is required.

6. Test results can be used to effect modification of the mathematical model and the input required.

RECOMMENDATIONS

On the basis of the foregoing conclusions, it is recommended that the following areas of structural crashworthiness be investigated in accordance with the listed priority:

1. Conduct research and development to improve the design configuration and energy-absorbing capability for sideward (lateral) impacts.

2. Conduct research and development to improve the capability of the airframe to absorb the energy of high rate vertically downward impacts without transmitting excessive decelerative forces to the floor.

3. Conduct additional research and development to clarify the requirements necessary for the retention of transmissions and rotor masts when the blades strike trees or other obstacles.

4. Conduct research to evaluate the affects on other systems, e.g.; the fuel system, of designing the structure to the crashworthy requirements of this study.

5. Conduct a second iteration on the input data for the mathematical model to more closely correlate test data and improve the model itself for the UH-1D/H aircraft.

6. Conduct research on passenger response by adding a passenger and restraint system as an integral part of the mathematical model.

7. Conduct research and create a mathematical model to simulate the longitudinal impact, with provision for lateral roll-over. The model will then be capable of analyzing dynamic response to impacts which involve both longitudinal and vertical velocity changes.

8. Investigate the applicability of the mathematical model to other helicopters presently in the U. S. Army inventory. Use the model in conjunction with crash tests to determine additional areas of crashworthiness improvement.

UNCLASSIFIED

Security Classification

DOCUMENT CONTROL DATA - R & D

(Security classification of title, body of abstract and indexing annotation must be entered when the overall report is classified)

1. ORIGINATING ACTIVITY (Corporate author) Dynamic Science (The AvSER Facility) A Division of Marshall Industries Phoenix, Arizona	2a. REPORT SECURITY CLASSIFICATION Unclassified 2b. GROUP

3. REPORT TITLE

ANALYSIS OF HELICOPTER STRUCTURAL CRASHWORTHINESS
VOL. I. MATHEMATICAL SIMULATION AND EXPERIMENTAL VERIFICATION FOR HELICOPTER CRASHWORTHINESS

4. DESCRIPTIVE NOTES (Type of report and inclusive dates)

Final Report

5. AUTHOR(S) (First name, middle initial, last name)

Clifford I. Gatlin
Donald E. Goebel
Stuart E. Larsen

6. REPORT DATE	7a. TOTAL NO OF PAGES	7b. NO OF REFS
January 1971	159	One

8a. CONTRACT OR GRANT NO.	9a. ORIGINATOR'S REPORT NUMBER(S)
DAAJ02-69-C-0030 b. PROJECT NO. 1F162203A529 c. d.	USAAVLABS Technical Report 70-71A 9b. OTHER REPORT NO(S) (Any other numbers that may be assigned this report) AvSER Report 1520-70-30

10. DISTRIBUTION STATEMENT This document is subject to special export controls, and each transmittal to foreign governments or foreign nationals may be made only with prior approval of Eustis Directorate, U. S. Army Air Mobility Research and Development Laboratory, Fort Eustis, Virginia 23604.

11. SUPPLEMENTARY NOTES	12. SPONSORING MILITARY ACTIVITY
Volume I of a 2-volume report	Eustis Directorate, U. S. Army Air Mobility Research and Development Laboratory, Fort Eustis, Virginia

13. ABSTRACT

This report describes the development of a mathematical model that will simulate the response of a UH-1D/H helicopter airframe to vertical crash loading and the full-scale test performed to verify the validity of the model.

In the initial phase of the model development, a study was made of 43 major accidents involving the UH-1D/H aircraft to determine what types of structural failure were contributing to injuries in helicopter accidents.

Based on the results of this accident study, a nonlinear lumped-mass model of 23 degrees of freedom was developed and programmed for computer solution. This model was then used in a parametric study of the UH-1D/H to evaluate potential areas of crashworthiness improvement.

At the conclusion of the parametric study, a full-scale, instrumented drop test of a UH-1D/H airframe was conducted. The data generated in this test were correlated with the model data to determine the ability of the model to predict airframe accelerations and deflections under crash conditions.

The results of this program indicate that:

- The structural weaknesses contributing to most impact injuries in UH-1D/H helicopter accidents are lack of resistance to failure in lateral roll-over and lack of energy-absorbing capability to reduce vertical accelerations.
- The mathematical model is capable of accurately predicting the floor and engine accelerations and deflections.
- In its present form, the model does not accurately predict the transmission accelerations and deflections.

Further research in the field of mathematical modeling for structural crashworthiness is recommended.

DD FORM 1 NOV 68 1473

UNCLASSIFIED

Security Classification

14 KEY WORDS	LINK A		LINK B		LINK C	
	ROLE	WT	ROLE	WT	ROLE	WT
Structural Crashworthiness Study Helicopter Airframe Crashworthiness Mathematical Simulation Dynamic Test Verification						